

Tectonic controls on basin physiography and sediment dispersal: the Vana Sub-basin, northern North Sea

Jarle Thorsen Haugland

Master thesis in Basin and Reservoir studies



Department of Earth Science

University of Bergen

June 2018

Abstract

A number of studies have investigated the controls on syn-rift sedimentation patterns and shift in syn-rift depocentres in rift-basins. However, few studies are focusing on how the change in tectonic regime that comes with the transition from syn-rift to post-rift has implications for the way depocentres are formed and how sedimentary systems respond to basin physiography.

This study includes a 3D seismic survey covering the Vana Sub-basin, located in the northern North Sea. The seismic survey is used for seismic interpretation of stratigraphic intervals of Upper Jurassic to early Upper Cretaceous age. These intervals are used in order to construct chronostratigraphic Wheeler diagrams.

Generation of TWTT thickness maps based on two interpreted horizons displays the interval's depocentre location. Based on a series of interpreted stratigraphic intervals a history of shifts in depocentre location is revealed. A comparison of generated TWTT structure-, TWTT thickness maps, and constructed Wheeler diagrams are conducted to explain shifts in location of depocentres through time.

An analysis of the depocentre shifts through time in the Vana Sub-basin shows that the downthrown VSCF hanging wall topography was not filled in before the deposition of the Mid Aptian-Albian Rødby+Sola formations. The analysis also shows that the Upper Jurassic structural configuration was influencing the sediment distribution until the deposition of the Upper Cenomanian – Lower Turonian Blodøks formation.

Acknowledgement

First of all I would like to thank my main supervisor Dr. Gijs Allard Henstra for constructive feedback and great supervision for the two past years. A special thanks goes to ConocoPhillips for providing the seismic data, and to Peter Bormann for providing a challenging and interesting thesis, in addition to providing valuable guidance and ideas the past year.

I would like to thank Schlumberger for licensing Petrel to the University of Bergen.

Thanks to Prof. Rob Gawthorpe and Prof. Atle Rotevatn for having me in the Syn-Rift Systems Project. Thanks to the sponsors of the project: The National Research Council Norway, Faroe Petroleum, ConocoPhillips, AkerBP, Equinor and VNG Norge for funding the project.

I would like to express my gratitude to my fellow students for the past years, especially Sander Hofker Berg, Max Osen Osnes, Anders Hågenvik, Mads André Meland and the rest of the Grotten crew for all academic discussions and input these past years.

Jarle Thorsen Haugland

June 2018

Contents

Contents

1.	Introduction.....	1
1.1	Rationale.....	1
1.2	Aim and objectives	1
2.	Background theory	3
2.1	Seismic stratigraphy	3
2.2	Chronostratigraphy	4
2.3	Sequence stratigraphy in deep-water siliciclastic settings.....	5
2.4	Normal fault growth and its sedimentary implications.....	7
2.5	Deep-water submarine fans.....	8
2.6	Basin-fill architecture	9
3.	Geological setting	11
3.1	Tectonostratigraphic evolution	11
3.1.1	Permian–Triassic.....	11
3.1.2	Jurassic.....	12
3.1.3	Cretaceous.....	13
3.2	Structural framework of the study area.....	14
3.2.1	Vana Sub-basin	15
3.2.2	Gudrun- and Heimdal terraces.....	15
3.2.3	Utsira High	15
3.3	Stratigraphy of the study area.....	16
3.3.1	Heather formation.....	16
3.3.2	Draupne formation.....	16
3.3.3	Åsgard formation.....	16
3.3.4	Sola formation	16
3.3.5	Rødby formation.....	17
3.3.6	Svarte formation.....	17
3.3.7	Blodøks formation	17
4.	Data and Methods	18
4.1	Seismic reflection data	18
4.2	Well data	18
4.3	Software	18
4.4	Seismic resolution	19

4.5 Seismic interpretation	20
4.5.1 Horizons.....	20
4.5.2 Seismic attributes	22
4.6 Thickness maps.....	22
4.7 Workflow Wheeler diagrams	23
4.8 Uncertainties and sources of errors	24
5. Results	25
5.1 Time structure maps	26
5.1.1 Top Hugin TWTT structure map	27
5.1.2 Top Heather TWTT structure map.....	29
5.1.3 Intra Draupne TWTT structure map	31
5.1.4 Base Cretaceous Unconformity TWTT structure map.....	33
5.1.5 Internal Åsgard TWTT structure map	35
5.1.6 Top Åsgard TWTT structure map.....	37
5.1.7 Top Rødby TWTT structure map.....	39
5.1.8 Top Svarte TWTT structure map.....	41
5.1.9 Top Blodøks TWTT structure map	43
5.1.10 Internal Draupne RMS-amplitude map	45
5.1.11 Top Upper Draupne sst RMS-amplitude map	47
5.2 Time interval maps.....	50
5.2.1 Heather TWTT thickness map	52
5.2.2 Lower Draupne TWTT thickness map.....	56
5.2.3 Upper Jurassic Wedge TWTT thickness map.....	60
5.2.4 Upper Draupne TWTT thickness map.....	62
5.2.5 Lower Åsgard TWTT thickness map.....	65
5.2.6 Upper Åsgard TWTT thickness map.....	68
5.2.7 Rødby + Sola TWTT thickness map.....	71
5.2.8 Svarte TWTT thickness map	74
5.2.9 Blodøks TWTT thickness map.....	77
5.3 Wheeler diagrams	81
5.3.1 Diagram 1	81
5.3.2 Diagram 2	84
5.3.3 Diagram 3	87
6. Discussion	90
6.1 Shift in location of depocentres through time	90
6.2 Reservoir characteristics	97

7. Conclusion	101
7.1 Main conclusions.....	101
References:.....	102

1. Introduction

1.1 Rationale

Tectonics is considered a significant controlling factor on the spatial and geographic evolution of depositional systems in active-margin rift-basins (Prosser, 1993; Ravnås & Steel, 1997; Gawthorpe & Leeder, 2000; Ravnås et al. 2000). Evolution and growth of normal fault arrays have implications on the basin-scale architecture and control the erosional potential and the rate of sediment flux (Gawthorpe & Leeder, 2000).

A number of studies have investigated the controls on syn-rift sedimentation patterns, and shift in syn-rift depocentres in rift basins (Gupta et al. 1998; Dawers & Underhill, 2000; Cowie et al. 2000; Sharp & Gawthorpe, 2000; Ravnås et al. 2000). However, few studies are focusing on how the change in tectonic regime that comes with the transition from syn-rift to post-rift has implications for the way depocentres are formed and how sedimentary systems respond to basin physiography. Upper Jurassic, syn-rift, deep-water sandstones form reservoirs. These reservoirs are underexplored in the Norwegian sector of the South Viking Graben because of difficulties in predicting the reservoir distribution and the configuration of structural traps in this area (Jackson et al. 2010).

1.2 Aim and objectives

The aim of this thesis is to understand how a change in tectonic regime from syn-rift to post-rift has implications on the formation of depocentres, and to investigate the distribution of Upper Jurassic reservoir rocks in the study area. This has been done by using 3D seismic reflection data and wells. The Late Jurassic to early Late Cretaceous tectono-stratigraphic evolution of the Vana sub-basin will be established by comparing thickness variations across the study area at eight intervals. Based on interpretation of stratigraphic architecture of every interval and plotting the strata against time, a subsequent transformation of the data into the chronostratigraphic domain is conducted. Interpretation of stratigraphic data into the chronostratigraphic domain enables the identification of significant geological features, especially erosional and non-depositional features that are not directly visible in the original seismic domain (Amosu & Sun, 2017).

The chronostratigraphic approach of this study is visualized in a series of Wheeler diagrams.

The specific objectives are:

- Interpreting horizons on the available 3D seismic dataset based on well picks
- Generation of TWTT structure-, thickness-, and RMS-amplitude maps in Petrel
- Analyze fault activity and its influence on the depositional distribution
- Convert every interval into the chronostratigraphic domain by interpreting stratigraphic architecture with respect to time
- Compare and discuss generated TWTT structure-, TWTT thickness maps and Wheeler diagrams to explain shifts in location of depocentres
- Discuss reservoir character based on results and conceptual models

2. Background theory

2.1 Seismic stratigraphy

Seismic stratigraphy is the basis of stratigraphy and depositional facies studies interpreted from seismic data (Mitchum et al. 1977). Analysis of seismic sequences subdivide the seismic section into packages of concordant reflections, separated by surfaces defined by systematic reflection termination. Reflection terminations include onlap, downlap, toplap and erosional truncation (Fig. 2.1) (Mitchum et al. 1977).

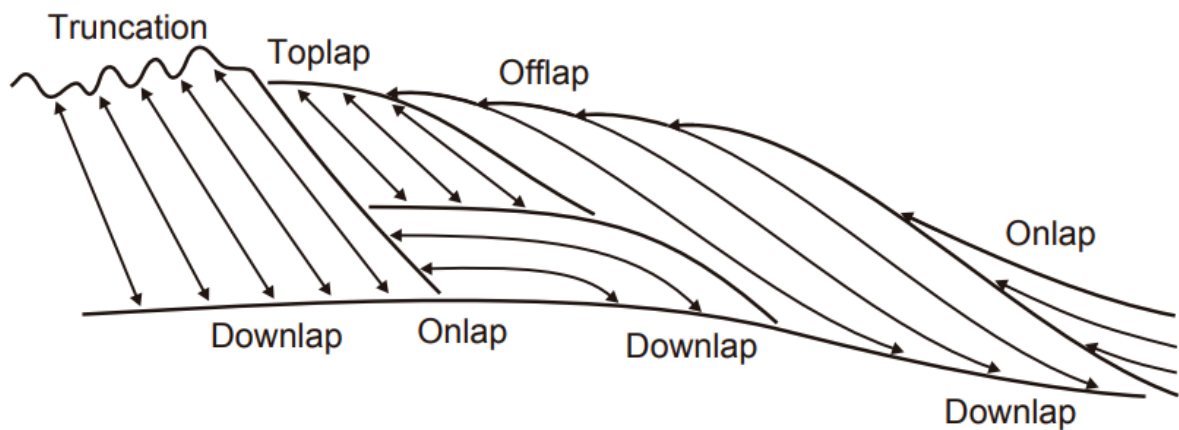


Figure 2.1: Types of stratal terminations (modified by Catuneanu, 2006 from Emery et al., 1996).

Seismic facies analysis is the interpretation of environmental setting and lithofacies from the seismic data. The seismic facies are seismic reflection groups based on parameters as, amplitude, frequency, continuity, reflector configuration and interval velocity (Mitchum et al. 1977). The main groups of reflection configurations include divergent, parallel, subparallel, chaotic (hummocky), sigmoidal, and oblique patterns (Fig. 2.2).

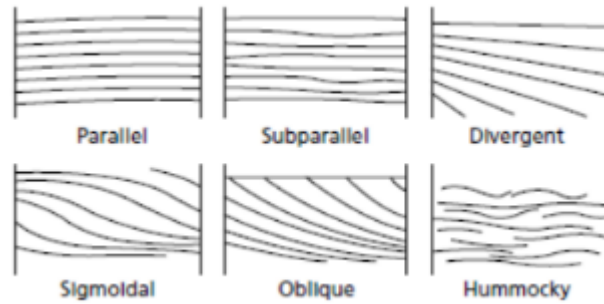


Figure 2.2: Selection of internal reflector configuration that typifies different seismic facies within sedimentary sequences on seismic section (Sheriff, 1980)

2.2 Chronostratigraphy

Chronostratigraphic charts, or Wheeler diagrams display horizontal distribution of a sedimentary sequence, including missing stratigraphy. This time-stratigraphic concept was initially formalized by Wheeler (1958). Wheeler diagrams are constructed by mapping stratigraphic successions. They are used to show time relationships of different sedimentary sequences and their relationship to erosional and non-depositional surfaces (Emery et al., 1996) (Fig. 2.3). The building blocks of the charts are “chronosomes” (Schultz, 1982), which are horizontal ribbons representing a body of rock, bounded by time planes. The horizontal axis in the Wheeler diagrams represent the horizontal dimension of the chosen seismic section, and the vertical axis represent time.

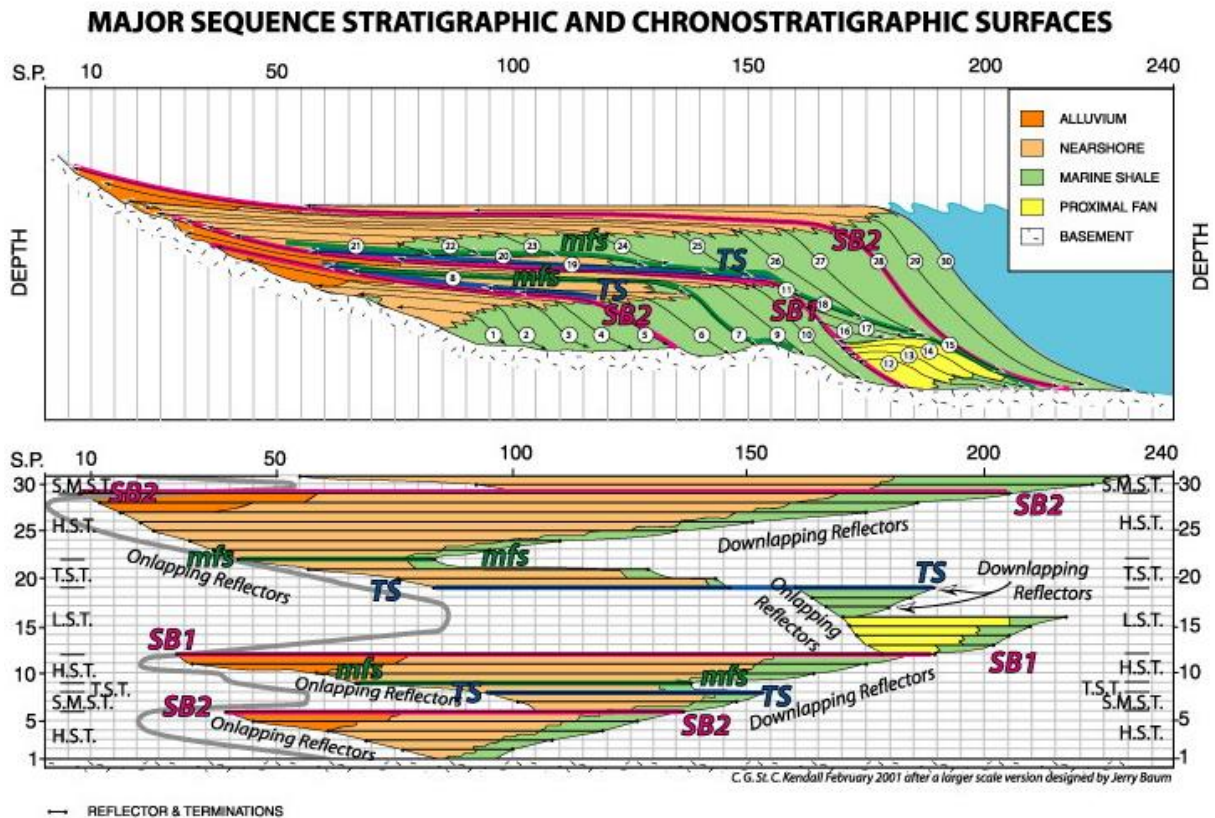


Figure 2.3: The figure shows a chronostratigraphic chart (lower) of a sequence stratigraphic cross-section (upper). The chronostratigraphic chart (Wheeler diagram) displays periods of non-deposition and erosion, and lateral deposition related to time (Kendall, 2001).

2.3 Sequence stratigraphy in deep-water siliciclastic settings

The use of 3D seismic data compensates for the difficulties with observing deep-water processes in a basin (e.g., Posamentier & Walker 2006; Weimer & Slatt 2007). The application of sequence stratigraphy in a deep-water setting is challenging because of several uncertainties, listed by (Catuneanu et al., 2011). (1) Physical disconnection between the deep-water portion of sequences, and shallow-water equivalents is possible. This is often a result of non-deposition or erosion and sediment instability in upper slope areas and the shelf-edge shelf-edge to upper slope areas. (2) Time control in correlation between the shallow-water and the deep-water portions of a sequence is often poor. (3) The depositional processes in a deep-water setting is primarily controlled by gravity flows and mass transport, which may favor lateral stacking of depositional elements and systems tracts, rather than vertical. (4) Evidence of relative sea-level change is not as prominent in

deep-water settings as in shallow-water settings. A deep-water sequence includes equivalents of shallow-water forced regressive, lowstand normal regressive, transgressive and highstand normal regressive deposits. (Catuneanu et al., 2011). These systems tracts are generalized trends that describe cyclicity of deep-water sedimentation (Fig. 2.4). Deviation from this model may occur related to sediment supply, patterns of sediment transport and shelf width (e.g., Porebski & Steel 2006; Covault et al. 2007; Catuneanu et al. 2011), but the effects of tectonics on base-level may override these controls in an active rift setting.

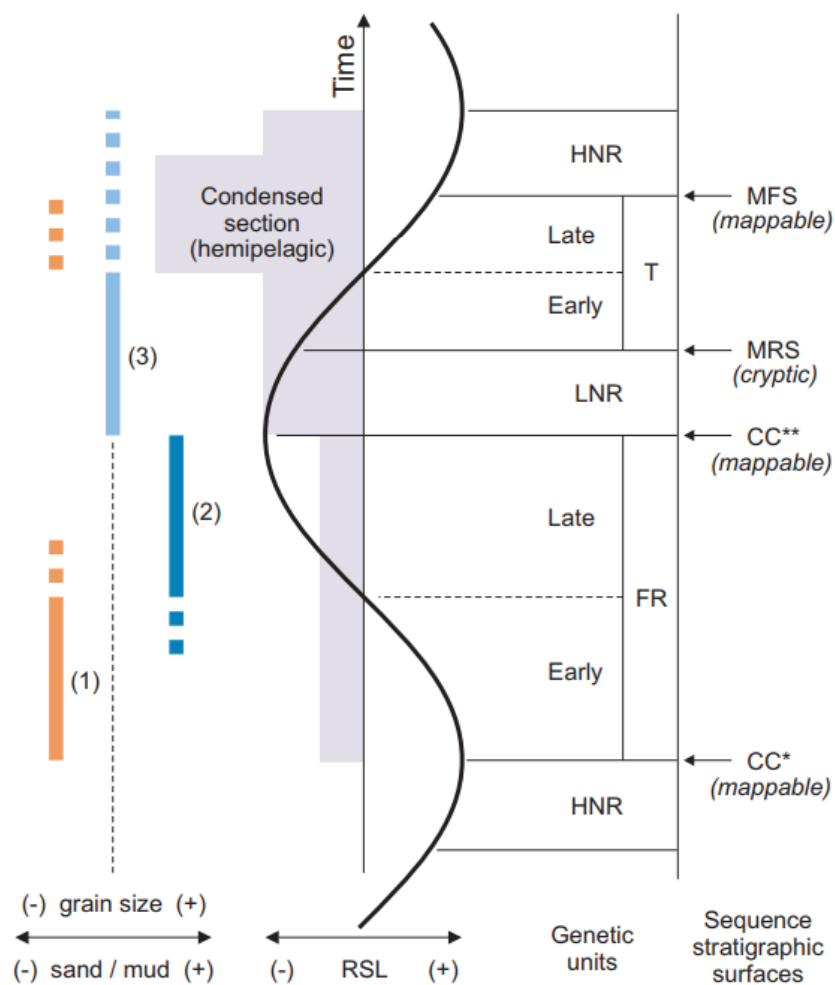


Figure 2.4: (1) mudflow deposits; (2) high-density turbidites and/or grain-flow deposits; (3) low-density turbidites are the dominant types of gravity-flow deposits forming submarine fan complexes in deep-water settings (modified by Catuneanu et al. 2011, from Posamentier & Kolla 2003; Catuneanu 2006). Abbreviations: HNR: highstand normal regressive deposits; FR: forced regressive deposits; LNR: lowstand normal regressive deposits; T: transgressive deposits; CC*: correlative conformity (Posamentier & Allen, 1999); CC**: correlative conformity (Hunt & Tucker 1992); MRS: maximum regressive surface; MFS: maximum flooding; RSL: relative sea level

2.4 Normal fault growth and its sedimentary implications

The evolution history of a normal fault array, is based on work by Gawthorpe & Leeder (2000), divided into three stages (Fig. 2.5). Starting with an initiation stage characterized by many faults with small displacement, the normal fault array evolves into the through-going fault zone stage with fewer, but longer faults with larger displacements. This evolution has because of responding surface uplift and subsidence, implications on the sediment distribution in a rift basin (Gawthorpe & Leeder, 2000). Occurring features are drainage reversals due to fault-block tilting (Leeder & Gawthorpe 1987; Steel 1993; Ravnås & Steel 2000; Gawthorpe & Leeder 2000), development of relay ramps which influence drainage, erosion and sedimentation (Morley et al., 1990; Gawthorpe and Hurst, 1993; Peacock and Sanderson, 1994), and stratal thickness changes in hanging wall depocentres (Gupta et al., 1998; Sharp et al. 2000a). A numerical model of fault growth conducted by Gupta et al. (1998) indicates that fault interactions during the development of linked fault systems show a major impact on fault displacement rate, and rates of hanging wall subsidence.

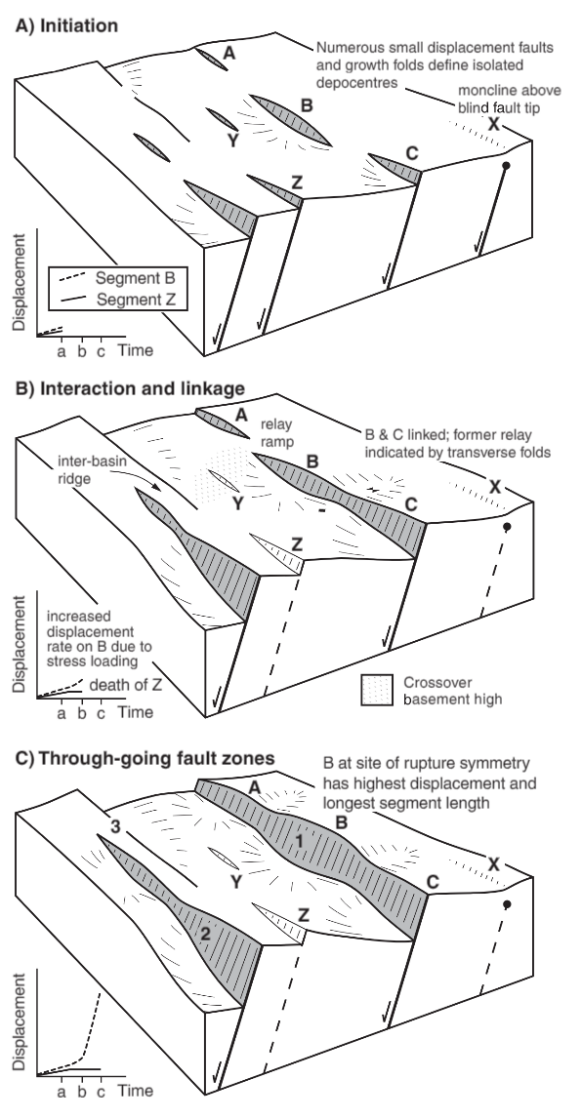


Figure 2.5: Schematic 3D evolution of a normal fault array. The graphs illustrate the displacement history of fault segments B and Z, where segment B links with segments A and C, and segment Z becomes inactive (Gawthorpe & Leeder, 2000).

2.5 Deep-water submarine fans

In the UK sector of the South Viking Graben, Upper Jurassic deep-water sandstones form important reservoirs (e.g. T-Block, Brae, Miller and Kingfisher) (Branther 2003; Fletcher 2003a, b; Fraser et al. 2003; Gambaro & Donagemma 2003; Rooksby 2003; Spence & Kreutz 2003). The equivalent Upper Jurassic reservoirs in the Norwegian sector are underexplored, mainly because of difficulties in predicting the configuration of structural traps and reservoir distribution (Fraser et al. 2003). Based on the evolution of submarine fans in relation to fault-scarp activity in the South Viking Graben, two main types are recognized: slope-apron fans (Fig. 2.6a), and basin-floor fans (Fig. 2.6b) (Fraser et al. 2003). Both types display a rapid lateral facies change both parallel and perpendicular to the fault scarp (Fig. 2.6).

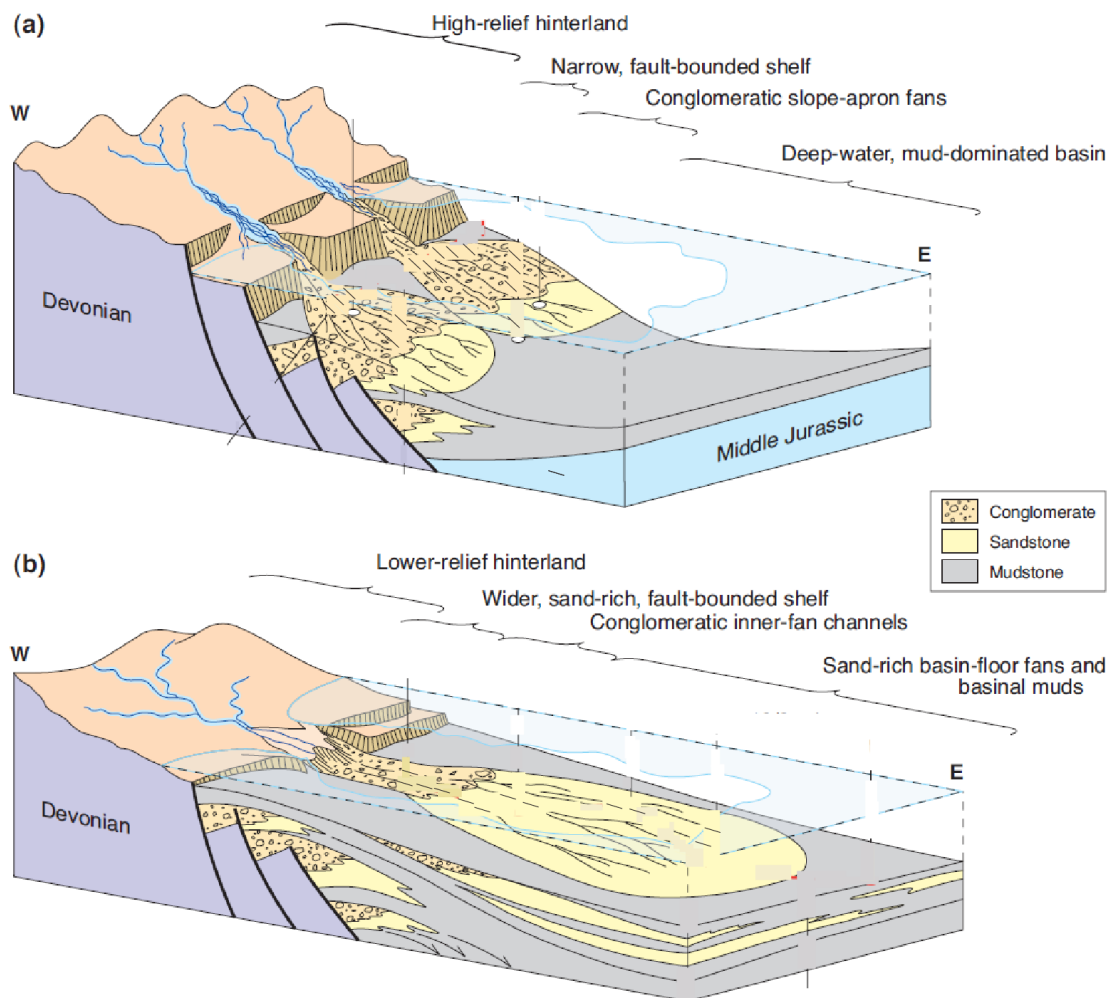


Figure 2.6: Illustration of evolution of submarine fans in the South Viking Graben in relation to fault-scarp activity. a) Slope-apron fan, b) Basin-floor fan (Fraser et al. 2003)

The slope-apron fans (e.g. Brae, Tiffany, Tony and Thelma reservoirs) are characterized by a small radius, and a wide range of facies types formed by a range of different sediment gravity-

flow processes (Fraser et al. 2003). The proximal area adjacent to the fault scarp are characterized by thick intervals of conglomerates, with a rapidly fining trend basinwards through turbiditic sandstones and basinal mudstones (Stow et al., 1982; Stow, 1983; Turner et al., 1987; Fraser et al., 2003).

The basin-floor fans (e.g. Miller, Kingfisher and East Brae reservoirs), are characterized by a relatively large radius compared to the slope-apron fans. They show greater basinward extent, a relatively minor conglomeratic component and a higher proportion of sandstone (Fraser et al. 2003). Every identified major basin-floor fans in the UK-sector of the South Viking Graben are deposited later than the slope-apron fans. This suggest that slope-apron fans are deposited in initial conditions, with gravel-rich fans, reflecting a steep and active fault margin with high stream gradients (Fraser et al. 2003). The relative age and the lithological record of basin-floor fans indicate later conditions with reduced fault-scarp topography, lower stream gradients and an increase in sand proportion (Fraser et al. 2003).

2.6 Basin-fill architecture

Tectonics are considered to be a significant control on the spatial and geographic evolution of depositional systems in active-margin rift-basins (Prosser, 1993; Ravnås et al. 2000). Movement of basin-bounding faults and stage of basin development have a controlling factor on the potential for erosion and the rate of sediment flux (Ravnås and Steel, 1997). Prosser (1993) has proposed a four-fold division of the basin infill stratigraphy based on the internal stratigraphic architecture. These are related to the rift initiation, rift climax, immediate post-rift and late post-rift stages of basin evolution (Fig. 2.7).

In the rift initiation stage the first increment of fault movement causes a depression in the surface of the crust with the activation of gravity-driven sedimentary systems (Prosser, 1993).

The rift climax stage reflects the time of maximum rate of fault displacement. Sedimentation is likely to be outpaced by subsidence at this stage, with a creation of differential relief across the fault scarp (Prosser, 1993).

The immediate post-rift stage is related to the period where active tectonism and basin-bounding fault displacement ends. The cessation of these controls has two implications

for the systems tract characteristics. (1) Tilting of the hanging wall and the fault plane differential subsidence ceases. (2) Regional subsidence rate will decrease, but subsidence will stay active because of lithospheric cooling effects (Prosser, 1993). The late post-rift stage is characterized by gradual degradation of rift-related topography. This is an event that may take millions of years, but is still regarded as a sedimentary response to a rifting event (Prosser, 1993).

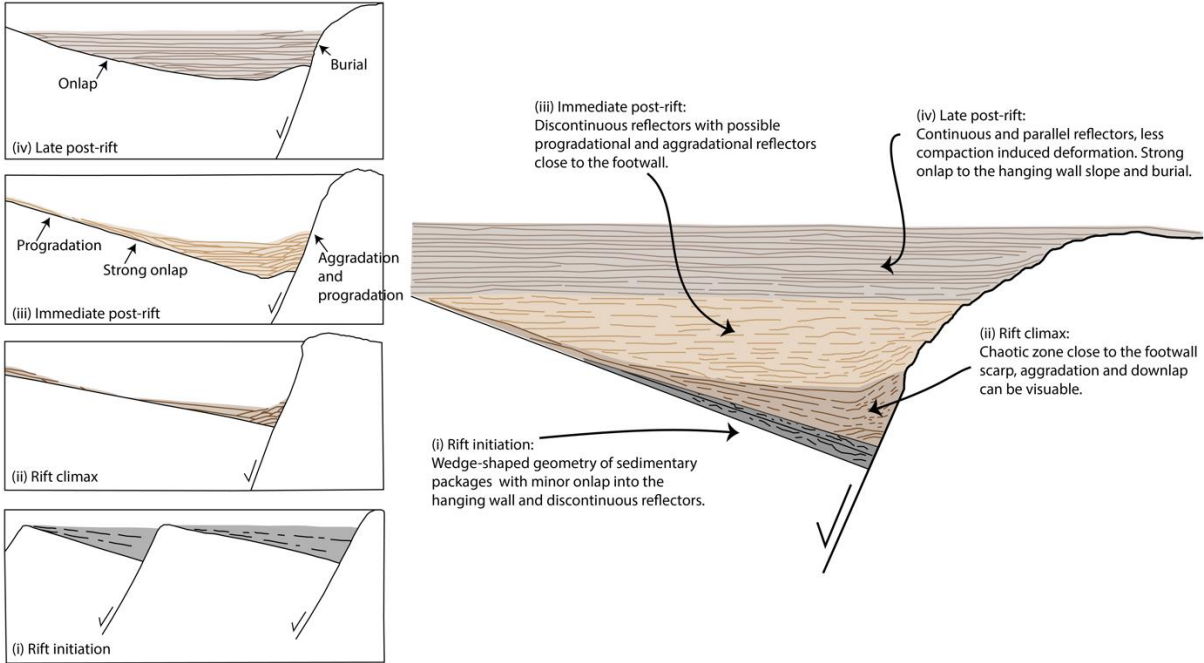


Figure 2.7: Illustration of an idealized four-fold basin fill, with summaries of characteristic seismic expression in the annotation for every rift-stage (modified by Ordemann (2016), from Prosser (1993)).

3. Geological setting

Chapter 3 provides an overview of the geological setting in the study area. This chapter is subdivided into three parts. Section 3.1 gives an introduction to the main tectonic events, developing the northern North Sea. Section 3.2 presents the main structural elements in the study area, the Vana-sub basin, Gudrun Terrace, Heimdal Terrace and the Utsira High. In the last section (3.3), the stratigraphy of the study area is presented. The formations interpreted in the thesis are the main focus of the description of the stratigraphy.

3.1 Tectonostratigraphic evolution

3.1.1 Permian–Triassic

The South Viking Graben initiated in Late Permian to Early Triassic times in response to crustal extension (e.g. Pegrum & Ljones, 1984; Glennie, 1990; Coward, 1995; Roberts et al., 1995). During this event the South Viking Graben was situated along the northern margin of the Northern Permian Salt Basin, where a NE-SW-trending fault-bounded embayment was formed (Ziegler, 1990). Thick evaporite-rich strata of the Zechstein Group were deposited in axial parts of the South Viking Graben during the Permian-Triassic rift event. The units of the Zechstein Group passed northwards and eastwards into more carbonate-rich evaporite facies towards the basin margins (e.g. Glennie, 1990; Ziegler, 1990; Hodgson et al., 1992). A period of extension during the Late Triassic occurred, but it is scientifically agreed that the magnitude of extension and subsidence was relatively minor compared with the Permo-Triassic and the prominent late Jurassic rift phase (Thomas & Coward, 1996). The Triassic deposition in the area occurred initially in a marginal lacustrine environment (Smith Bank Formation), before the establishment of alluvial fans to alluvial plain environments (Skagerrak Formation) in the Late Triassic (Fischer & Mudge, 1998) (Fig. 3.1).

3.1.2 Jurassic

A mantle plume at the base of the lithosphere led to uplift of the South Viking Graben and the formation of the Mid-North Sea Dome during the Early Jurassic (Ziegler, 1990; Underhill and Partington, 1993, 1994). This event resulted in erosion of Triassic and Lower Jurassic strata, which during early Middle Jurassic fed the northwards prograding Brent delta. The eroded material largely bypassed the South Viking Graben, before being deposited in the North Viking Graben (Helland-Hansen et al. 1992). During Bajocian-Bathonian age, the Mid-North Sea Dome collapsed and extensional faults in the western margin of the basin were reactivated, which lead to transgression of the South Viking Graben (Thomas & Coward, 1996). This transgression is recorded by shallow marine deposits of the Hugin Formation that overly fluvial deposits of the Sleipner Formation (Harris & Fowler, 1987). Towards the latest Jurassic eustatic sea-level rise accompanied with continued fault-driven subsidence, led to further deepening of the South Viking Graben basin (Fraser et al., 2003). Rotation of fault blocks was caused by basin marginal compressional inversion in the southern Viking Graben (Coward et al., 2003; Jackson & Larsen, 2009). Erosion of uplifted fault blocks provided deposition of the shelfal Heather formation and the deep-marine Draupne formation. These formations were deposited during a period of eustatic sea-level rise (Fraser et al., 2003; Jackson & Larsen 2009). The Draupne formation is in general organic rich, but in addition, it shows bodies of sandstone deposited in deep-water environments (NPD, 2018). These sand bodies could act as a good reservoir, and will be studied in this thesis. Ongoing activity on the western boundary fault of the South Viking Graben resulted in westward rotation of the hanging wall and gravity sliding of the Triassic-Middle Jurassic strata overlying evaporite-dominated units of the Permian Zechstein Group (Thomas & Coward, 1996; Jackson & Larsen, 2008). Faulting during this period has influenced the thickness of the Upper Jurassic syn-rift deposits and possibly been a factor in controlling local facies variations (Harris & Fowler, 1987; Jackson & Larsen, 2009).

3.1.3 Cretaceous

Most of the rift-related normal faults became inactive during the latest Jurassic-Early Cretaceous, although the western boundary fault of the South Viking Graben continued to be active (Cherry, 1993). Ongoing eustatic sea-level rise led to continued deepening of the basin, and resulted in marl deposits in structural lows and marl-limestone cycles on intrabasinal structural highs (Copestake et al., 2003). Towards the termination of the period with basin extension the South Viking Graben experienced a period of compression, which developed a series of anticlines expressed in the Late Jurassic to Early Cretaceous strata (Pegrum & Ljones, 1984). The formation of these compressional structures is suggested to be the result of reverse reactivation of former extensional faults, and potential reactivation of NW-SE trending strike-slip, basement-involved shear zones (Thomas & Coward, 1996).

System	Series	Group	Formation	Mapped seismic events & approximate ages	Structural and/or stratigraphic significance
Cretaceous	Upr.	Shetland		Maastrichtian (65 Ma)	syn-inversion post-inversion post-rift
			Blodøks	E. Turonian (93 Ma)	
		Cromer Knoll	Rødby	L. Albian (100 Ma)	
	Sola		E. Albian (106 Ma)		
	Åsgard		L. Aptian (121 Ma)		
	Lwr.		Draupne	L. Ryazanian (138 Ma)	
Jurassic	Upr.	Viking	Heather	E. Volgian (148 Ma)	
	Mid.	Brent	Hugin	M. Callovian (162 Ma)	
			Sleipner		
Triassic		Hegre	Skagerrak	pre-rift riffs	
			Smith Bank		
Permian	Upr.	Zechstein		mechanically-weak detachment	
	Lwr.	Rörligendes	Auk		

Figure 3.1: Stratigraphic column through Permian and Mesozoic stratigraphy of the South Viking Graben showing the stratigraphic position, approximate ages of formations and their relative to the rift-event (Jackson et al., 2009).

3.2 Structural framework of the study area

The study area is located in the South Viking Graben in between the axial part of the Viking Graben in the west and the Utsira High in the east. The main structural elements of the study area are the Vana Sub-basin, the northern Gudrun Terrace, the southern Heimdal Terrace and the northwestern flank of the Utsira High. (Fig. 3.2).

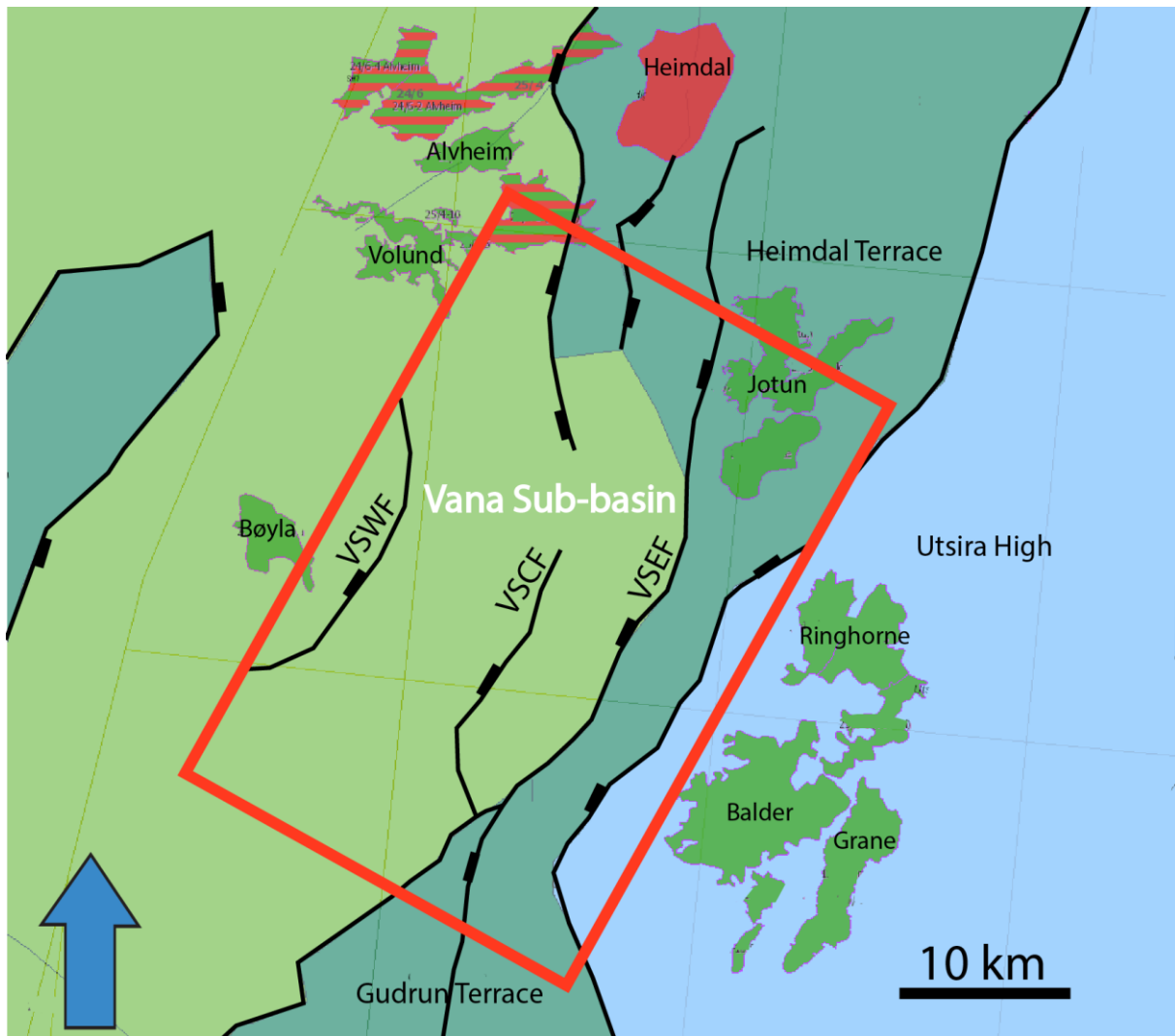


Figure 3.2: Study area. Structural elements: Vana Sub-basin, Heimdal terrace, Gudrun Terrace, Utsira High. Faults: VSWF (Vana Sub-basin western fault), VSCF (Vana Sub-basin central fault), VSEF (Vana Sub-basin eastern fault).

3.2.1 Vana Sub-basin

The Vana Sub-basin is located between the Heimdal terrace in the northeast, the Gudrun terrace in the southeast, and the axial part of the South Viking Graben in the west. The Vana Sub-basin is heavily faulted, and the basic fault pattern shows two discrete fault trends, which intersect, and overprint in the middle of the study area. The dominant fault trend in the northern part is N-S to NNW-SSE, while a NNE-SSW trend is dominant in the south. At a large scale, the Vana Sub-basin consists of three large-offset faults. A fault at the western boundary of the study area and the 25/7 block, bounds the Vana Sub-basin to the axial part of the South Viking Graben (VSWF). A central fault (VSCF) bounds the deeper part of the Vana Sub-basin from a proximal terrace area. In the east, a third large fault (VSEF) is located bounding the proximal terrace area to the southern part of the Heimdal Terrace, in the hanging wall to the Utsira High boundary fault (NPD,2018).

3.2.2 Gudrun- and Heimdal terraces

The Gudrun- and Heimdal terraces are bounded by the Utsira High boundary fault in the east, and towards deeper sub-basins, including the Vana Sub-basin, in the west. The shallow terrace area in block 25/7 (2.2.1) bounds the Heimdal Terrace in the north to the Gudrun Terrace in the south.

3.2.3 Utsira High

The Utsira High is located within the quadrants 15, 16, 24 and 25 in the North Sea. The structure is bounded to the west by the Gudrun- and Heimdal terraces, and to the east by the Stord Basin. In the Triassic the Utsira High was likely to be a topographic high (Steel & Ryseth, 1990). The Triassic strata underwent crustal thinning and erosion in the Jurassic to Early Cretaceous, resulting in thinning of the high towards the east (Færseth, 1996). The present structural configuration is a result of extension that occurred in the Late Paleozoic and Mesozoic (Isaksen & Ledje, 2001).

3.3 Stratigraphy of the study area

3.3.1 Heather formation

The Heather formation consists mainly of silty claystones with thin streaks of limestone, deposited in an open marine environment during the Bathonian to Kimmeridgian (Vollset & Doré, 1984). The formation can be observed over large parts of the northern North Sea north of 58° N and east of the boundary faults of the East Shetland Platform (Vollset & Doré, 1984).

3.3.2 Draupne formation

The Draupne formation consists mainly of dark grey-brown to black carbonaceous claystone, deposited in a marine environment with restricted bottom circulation, during the Oxfordian to Ryazanian (Vollset & Doré, 1984). It has a very high radioactivity, because of its organic carbon content. The Draupne formation is together with the Heather formation the most important source rock in the northern North Sea. Along the flanks of the Viking Graben several Intra-Draupne sandstone bodies are found, acting as reservoirs for hydrocarbons. The formation is found in the East Shetland Basin, the Viking Graben and over the Horda Platform (NPD, 2018).

3.3.3 Åsgard formation

The Åsgard formation consists of a combination of calcareous claystones, marlstones and stringers of limestone, deposited in an open marine, low-energy shelf environment from Late Ryazanian to Late Hauterivian (Isaksen & Tonstad, 1989). The formation is widespread in the North Sea, and is only absent over the highest parts of structural highs and locally over salt pillows and diapirs (Vollset & Doré, 1984).

3.3.4 Sola formation

The Sola formation consists of shales interbedded with marlstone- and limestone stringers. It shows an in general lower carbonate content than the underlying Åsgard formation and the overlying Rødby formation (Isaksen & Tonstad, 1989). The Sola formation was deposited in a marine environment with alternating anoxic and oxic bottom conditions, during Mid Aptian to Early Albian. The formation is covering the entire North Sea, apart from on different structural highs and over salt-induced structures (Isaksen & Tonstad, 1989).

3.3.5 Rødby formation

The Rødby formation consists mainly of red-brown marlstones, deposited in an open marine with a general limited supply of clastics during the Albian (Isaksen & Tonstad, 1989). The formation is widespread in the North Sea, but is absent on the Utsira High and Horda Platform (Isaksen & Tonstad, 1989).

3.3.6 Svarte formation

The Svarte formation consists mainly of mudstones interbedded with limestones. The content of limestone relative to mudstone is higher in the southern part of the Viking Graben compared to the northern Viking Graben (Isaksen & Tonstad, 1989). The formation was deposited in an open marine environment during the Cenomanian (Isaksen & Tonstad, 1989).

3.3.7 Blodøks formation

The Blodøks formation consists of calcareous shales and mudstones, deposited during a period with anoxic bottom conditions in Latest Cenomanian to Early Turonian (Isaksen & Tonstad, 1989). The formation is widespread in the North Sea, only absent on local highs like the Utsira High (Isaksen & Tonstad, 1989).

4. Data and Methods

This chapter provides information on the available data and methods used in this study. Section 4.1-4.3 give an overview of the seismic reflection data (4.1), well data (4.2), and software (4.3) that is used during this work. The seismic resolution of seismic data is described and calculated in chapter 4.4. Chapter 4.5 gives an overview on how the seismic interpretation was performed. In chapter 4.6 (Thickness maps) and 4.7 (Wheeler diagrams), the main tools to generate the results of this thesis are described. Chapter 4.8 elucidate uncertainties, and possible sources of errors related to the use of seismic reflection data.

4.1 Seismic reflection data

One 3D-seismic survey acquired by PGS, and provided by ConocoPhillips is used in this study. The seismic is not depth converted.

Survey	Type	Phase	Area (km²)	Line Orientation	Line Spacing (m)
CP15M01	3D	Zero	1750	Inline= NW-SE	IL:12.5 XL:12.5

4.2 Well data

One well (25/7-2) was used. The study area in general lacks sufficient well-control, leaving only one well (25/7-2) useful for this thesis' interpretations. Several wells within block 25/8 on the southern Heimdal Terrace, and wells within block 25/10 on the northern Gudrun Terrace are located in the survey, but they show in general missing Upper Mesozoic stratigraphy (NPD,2018).

4.3 Software

The University of Bergen license for Schlumbergers Petrel E&P Software Platform (version 2016) was used for all interpretations and generation of maps for this thesis.

4.4 Seismic resolution

Vertical and horizontal resolution of the seismic data is important in terms of how small visible features in the seismic can be. The vertical resolution depends on the velocity (V) and frequency (f) of the seismic signal, which are solved using the equation (Brown, 1996);

$$\lambda = V/4f \quad (4.1)$$

To find the vertical resolution of the seismic the dominating frequency and velocity within the area of interest need to be determined. The dominating frequency is derived with a statistical extraction using the wavelet toolbox in Petrel. Within the area of interest in well 25/7-2 the dominating frequency is around 20 Hz (Fig. 4.1).

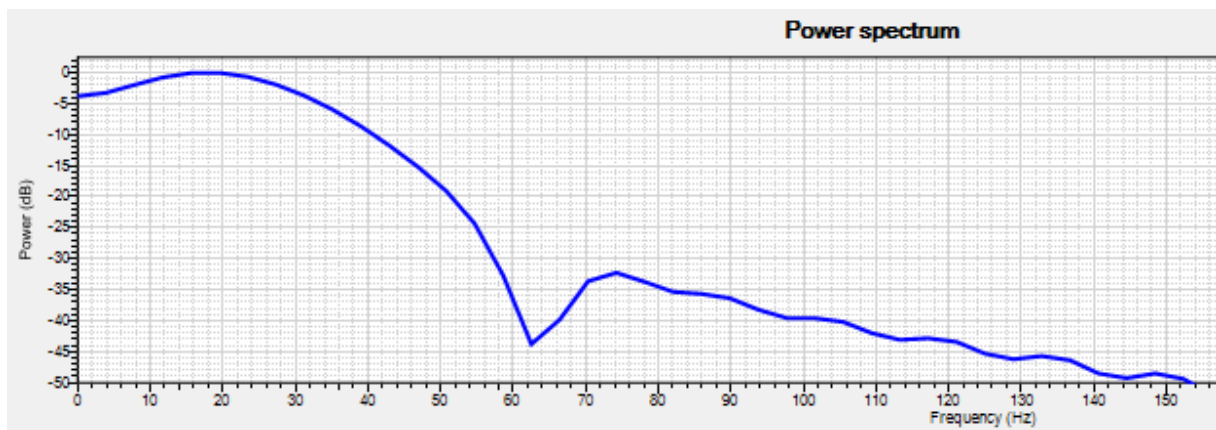


Figure 4.1: Power spectrum of frequency in the interval 2800 ms-3500 ms in well 25/7-2 derived from use of wavelet toolbox in Petrel.

The velocity is calculated from analysis of the interval velocity using the sonic log in well 25/7-2. The sonic log shows a large range of P-sonic values (50-90 $\mu\text{s}/\text{ft}$) in the interval of interest, but with an approximate main value (75 $\mu\text{s}/\text{ft}$), the average velocity of the interval is set to be 2350 m/s. By solving equation 4.1, the vertical resolution is calculated to be approximately 29 meters. This is a relatively high resolution, but the widespread power spectrum (Fig. 4.1), the large range of P-sonic values in the large depth interval of interest (2800-3500 ms), suggests large uncertainties.

4.5 Seismic interpretation

The seismic data is zero phase, where a red peak is representing an increase in acoustic impedance, and a blue trough is representing a decrease in acoustic impedance (Fig. 4.2). Seismic horizons can be interpreted on peaks, troughs or zero-crossings, where only peaks and troughs are interpreted in this thesis. Selection of which part of the wavetrain, depended on where the reference well top (well 25/7-2) intersects with the reflector, and the continuity of the reflector.

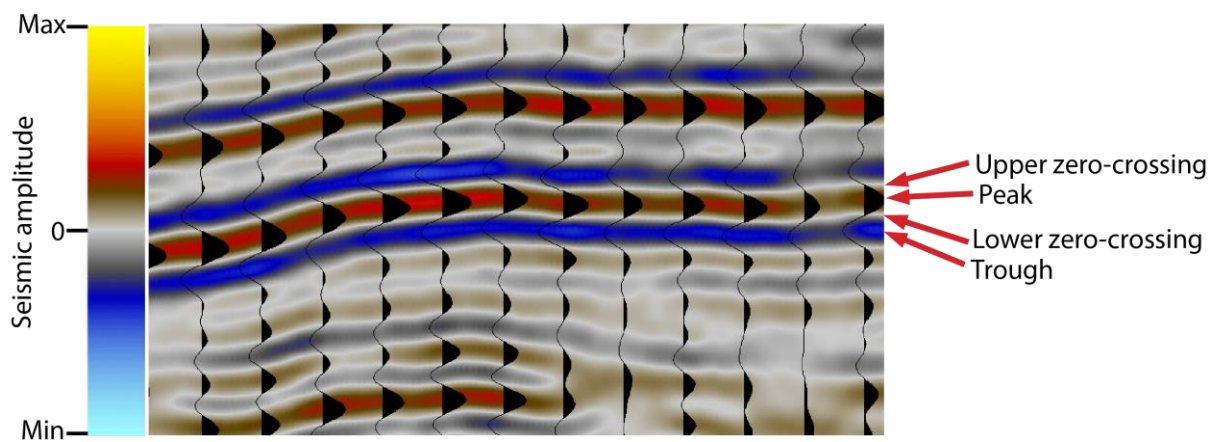
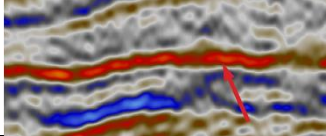
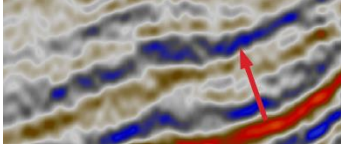
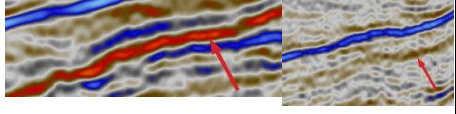
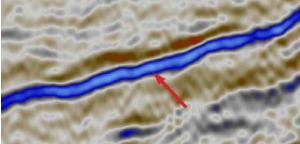
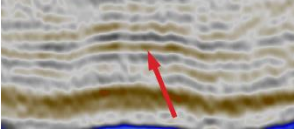
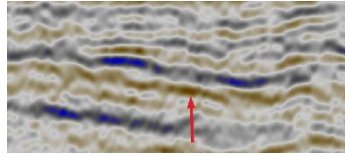
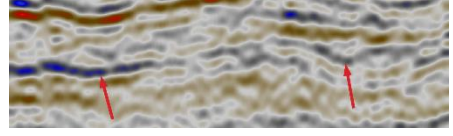
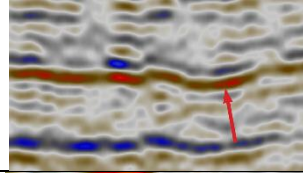
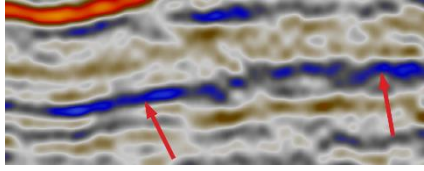


Figure 4.2: An entire wavetrain including peak, trough and zero-crossings. Positive amplitude is a red peak, and negative amplitude is a blue trough.

4.5.1 Horizons

Seismic interpretation was mainly performed on inlines with a 16-64 line increment on the seismic data. Crosslines were used where reflectors on inlines were subject to lack of continuity. The majority of the horizons were manually interpreted with the use of very low tolerance guided autotracking interpreted with the use of 2D and 3D autotracking. The use of manual interpretation increased gradually towards the southwestern part of the survey, because of increased reflector discontinuity. The southwestern part of the survey is subject to poor seismic resolution.

Horizon	Phase	Characteristics	Example
Top Hugin	AI increase (peak)	High amplitude, continuous	
Top Heather	AI decrease (trough)	High to medium amplitude, continuous to discontinuous in certain areas	
Internal Draupne	AI increase (peak)	High to medium amplitude, continuous to discontinuous in certain areas	
BCU	AI decrease (trough)	High amplitude, continuous	
Internal Åsgard	AI increase (peak)	Medium to low amplitude, continuous to discontinuous in certain areas	
Top Åsgard	AI increase (peak)	Medium amplitude, continuous to discontinuous in certain areas	
Top Rødby	AI decrease (trough)	High to medium amplitude, continuous to discontinuous in certain areas	
Top Svarte	AI increase (peak)	High to medium amplitude, continuous	
Top Blodøks	AI decrease (trough)	High to medium amplitude, continuous	

4.5.2 Seismic attributes

RMS (root mean square) amplitude maps are generated in this study. This is a post-stack attribute that calculates the square root of the sum of squared amplitudes within a specified search window, that is divided into a certain number of samples. With the RMS-amplitude attribute, a reflectivity measurement can be conducted in order to map indicators of hydrocarbons in areas of interest. A RMS attribute can also indicate lithology, fractures and seismic tuning effects. The RMS attribute is sensitive to noise as it squares every value within the search window. RMS-amplitude maps (Fig. 4.11, 4.13) in this study are generated with a search window of 20 ms above and below the reference horizons.

4.6 Thickness maps

The two-way time thickness maps in the study are made from isochron maps between two interpreted surfaces. The seismic data is not depth converted, meaning that the thickness of the maps are in milliseconds two-way travel-time. The Petrel software is used to generate the maps from calculations based on two interpreted surfaces. Variations in thicknesses are helpful in the analysis of fault activity in the study area.

4.7 Workflow Wheeler diagrams

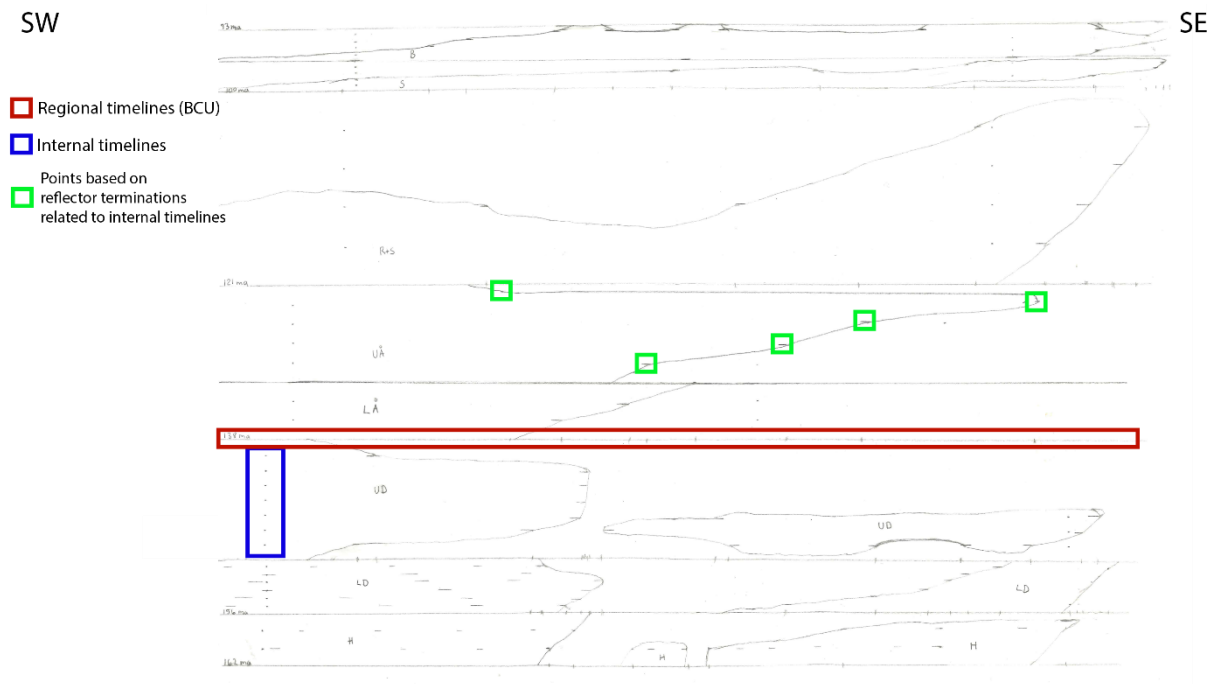


Figure 4.3: The figure shows the sketch of the generated Wheeler diagram 2 (Fig. 5.38).

The workflow used for generating the three Wheeler diagrams in the thesis is summarized in six steps:

1. Select a seismic line (or create a composite line) which includes areas and features of interest, and rescale the y-axis to fit the entire Petrel window.
2. Interpret every seismic peak in the chosen seismic line (shown as stippled lines in Fig. 4.35) within each interval to find and determine reflector terminations.
3. Draw timelines of every interval on a transparent A3-sheet (regional ages for the Norwegian sector of the northern part of the South Viking Graben) (Fig. 3.3).
4. Subdivide every interval in y-direction into internal timelines based on the number of traceable peaks in the thickest part of the interval (Fig. 3.33).
5. Stick the transparent paper to the screen and plot points based on reflector terminations related to the internal timelines (Fig. 3.3).
6. Draw lines between the points, to form bodies of preserved deposits.

4.8 Uncertainties and sources of errors

There are many sources of error when studying seismic data. To constrain all details within a large survey is difficult. For instance, the vertical resolution determines whether certain small geomorphological objects are imaged on seismic. If these fall below seismic resolution, in our case c. 30 meters, they remain hidden from observation. The seismic data is not depth-converted, which means that there could be a mismatch between true and apparent distance between interpreted surfaces. This is a consequence of a velocity change for the different stratigraphic groups.

Without any well-ties to the western part of the study area, the westward interpretation of the horizons are uncertain, especially horizons of medium to low amplitude, and lack of continuity. Well 25/7-2 is located in the immediate hanging wall of VSEF, which is close to the eastern edge of the mapped surfaces in this study. This lack of usable wells in the study area is another source of interpreting errors.

Reflectors used for generating Wheeler diagrams can show apparent termination in the seismic, could for instance be a result of thinning and fading below seismic resolution. Interpreted erosional truncations could be misinterpreted toplaps, which would define a non-existent erosional period in the Wheeler diagram. Three separate Wheeler diagrams are generated in this study. The maximum visible number of peaks in every time interval from the three cross-sections, is used as reference for a time interval with continuous deposition. With a larger number of generated Wheeler diagrams, a generally larger portion of the time intervals would be marked as periods of erosion or non-deposition.

5. Results

This chapter presents results from interpreting seismic reflection data from the 3D survey CP15M01. Upper Jurassic to early Upper Cretaceous stratigraphy in the study area were studied. The chapter is sub-divided into three parts. The first section 5.1 addresses time structure maps of selected formation tops, including two RMS-amplitude maps. Section 5.2 describes time thickness maps generated from interpreted time structure maps, to portray thickness variation within every interval. In the last section, 5.3, three Wheeler diagrams generated from the time interval maps and their stratigraphic architecture are presented.

5.1 Time structure maps

The foundation of this study is based on the interpretation of nine formation tops, where every formation top is described by a time structure map. Well-tops from the 25/7-2 well are used as reference for the interpretation. The nine formation tops are Top Hugin, Top Heather, Internal Draupne, Base Cretaceous Unconformity, Internal Åsgard, Top Åsgard, Top Rødby, Top Svarte and Top Blodøks arranged in upward stratigraphic succession.

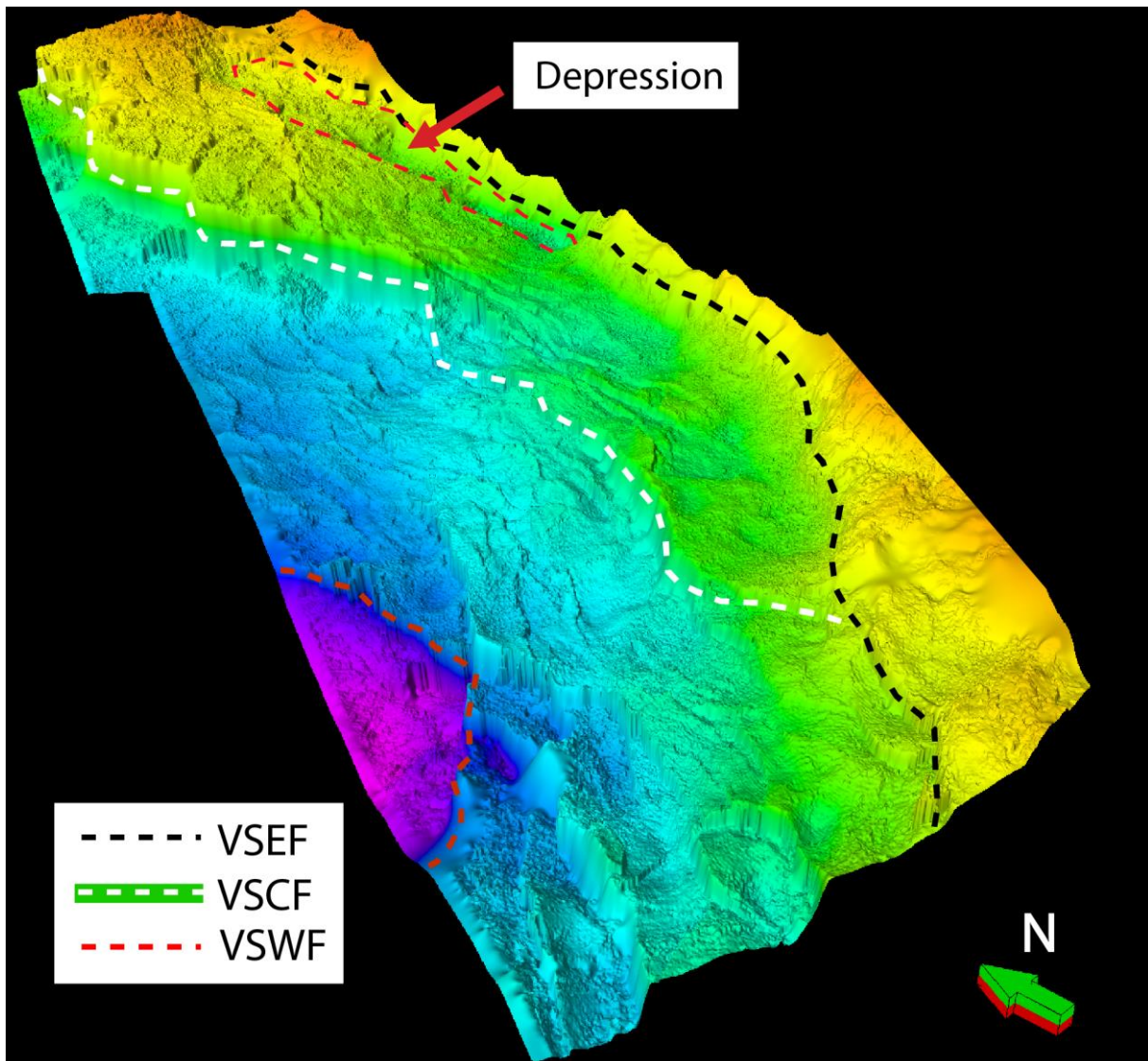


Figure 5.1: 3D-illustration of the generated Top Hugin TWTT structure map. The strike of the Vana Sub-basin western- (VSWF), central- (VSCF) and eastern fault (VSEF) are marked with stippled lines.

5.1.1 Top Hugin TWTT structure map

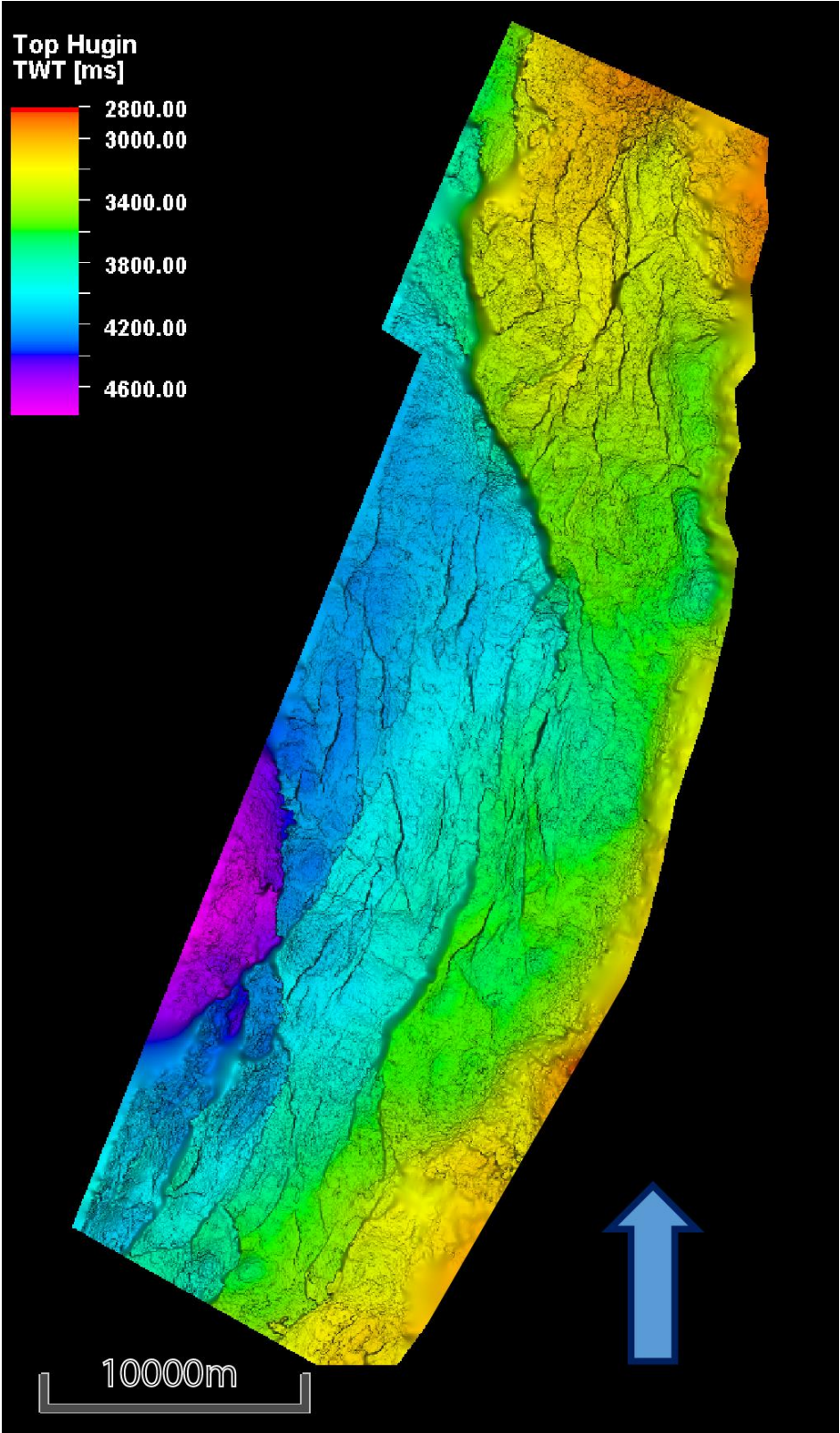


Figure 5.2: Illustration of the generated Top Hugin TWTT structure map. The VSEF is located along the eastern edge of the map, while the VSCF with a general N-S trend is located in the central part of the map.

Description

The TWTT structure map of the Top Hugin shows the stratigraphically deepest formation top in this study. The structure map shows two distinct faults that extend across the whole study area, where the Vana Sub-basin eastern fault (VSEF) is the easternmost, and the Vana Sub-basin central fault (VSCF) is located further west (Fig. 5.2). They have an overall similar south-north strike with different smaller segments of varying strike and displacement. The structure map shows a deepening trend towards the southwest. Two abrupt deepening trends are observed from the footwall to hanging wall of the VSCF ($\approx 3400\text{-}3600$ ms to ≈ 4000 ms), and from the footwall to the hanging wall of the VSWF (≈ 4200 ms to >4600 ms), respectively. The trend is gradual in a southwestern direction in the rest of the structure map. A depression in the hanging wall to the VSEF is observed in the northeastern part of the map.

Interpretation

The Top Hugin structure map is full of sharp elevation contrasts, where the contrasts correspond to fault offset. The elevation contrast across the central segment of the VSCF is minor compared to the southern and northern segment, suggesting a complex nature of the VSCF. The depression observed in the immediate hanging wall to the VSEF, shows a similar orientation as the strike of the VSEF, suggesting that the depression is fault-controlled (Fig. 5.1, 5.2).

5.1.2 Top Heather TWTT structure map

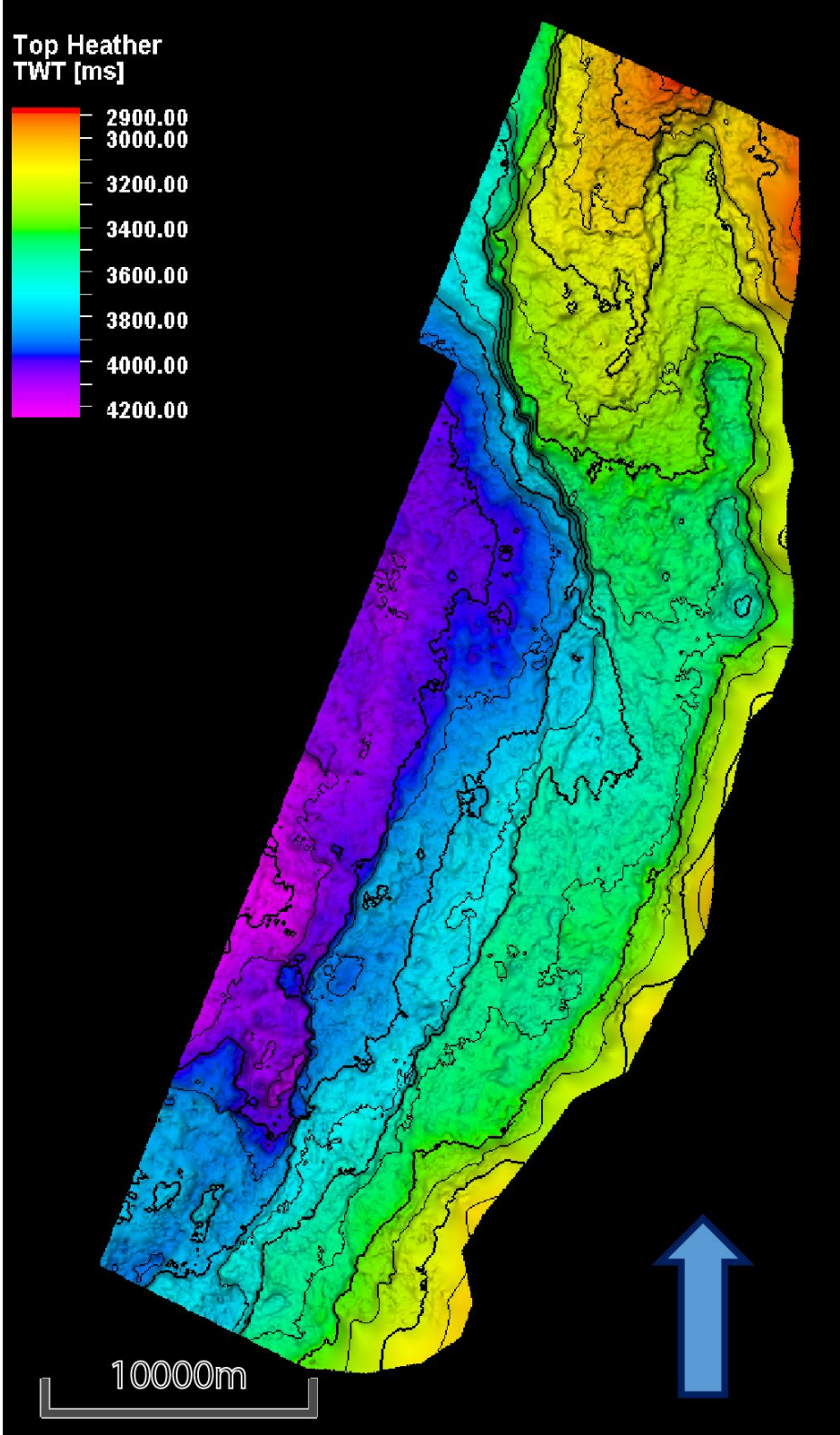


Figure 5.3: Illustration of the generated Top Heather TWTT structure map. The contour lines have an increment of 100 ms decreasing from a value of 4200 ms, where every second contour line is bold.

Description

The Top Heather TWTT structure map shows a generally increasing elevation time in a southwesterly direction (Fig. 5.3). The VSCF is observed striking north-south on the structure map, with a displacement towards the west across the southern and central segment of 100-200 ms. The elevation time increase is more abrupt across the northern segment of the VSCF with a difference of 300-400 ms. A depression of increased elevation time (3200-3600 ms) is observed in the hanging wall to the northern segment of the VSEF.

Interpretation

The northern segment of the VSCF exhibits a large displacement of the Top Heather surface, as observed in the Top Hugin surface. However, the central and southern segment do not show a displacement of similar magnitude that may be related to deposition of sediments across the fault. The VSWF exhibits less displacement in the southwest in the Top Heather structure map (100-200 ms), than the Top Hugin structure map illustrated (≈ 400 ms). The northwestern depression is bounded to surrounding elevated areas, suggesting it to be a result of downfaulting and increased erosion. These observations indicates that the Top Heather surface is heavily fault-influenced.

5.1.3 Intra Draupne TWTT structure map

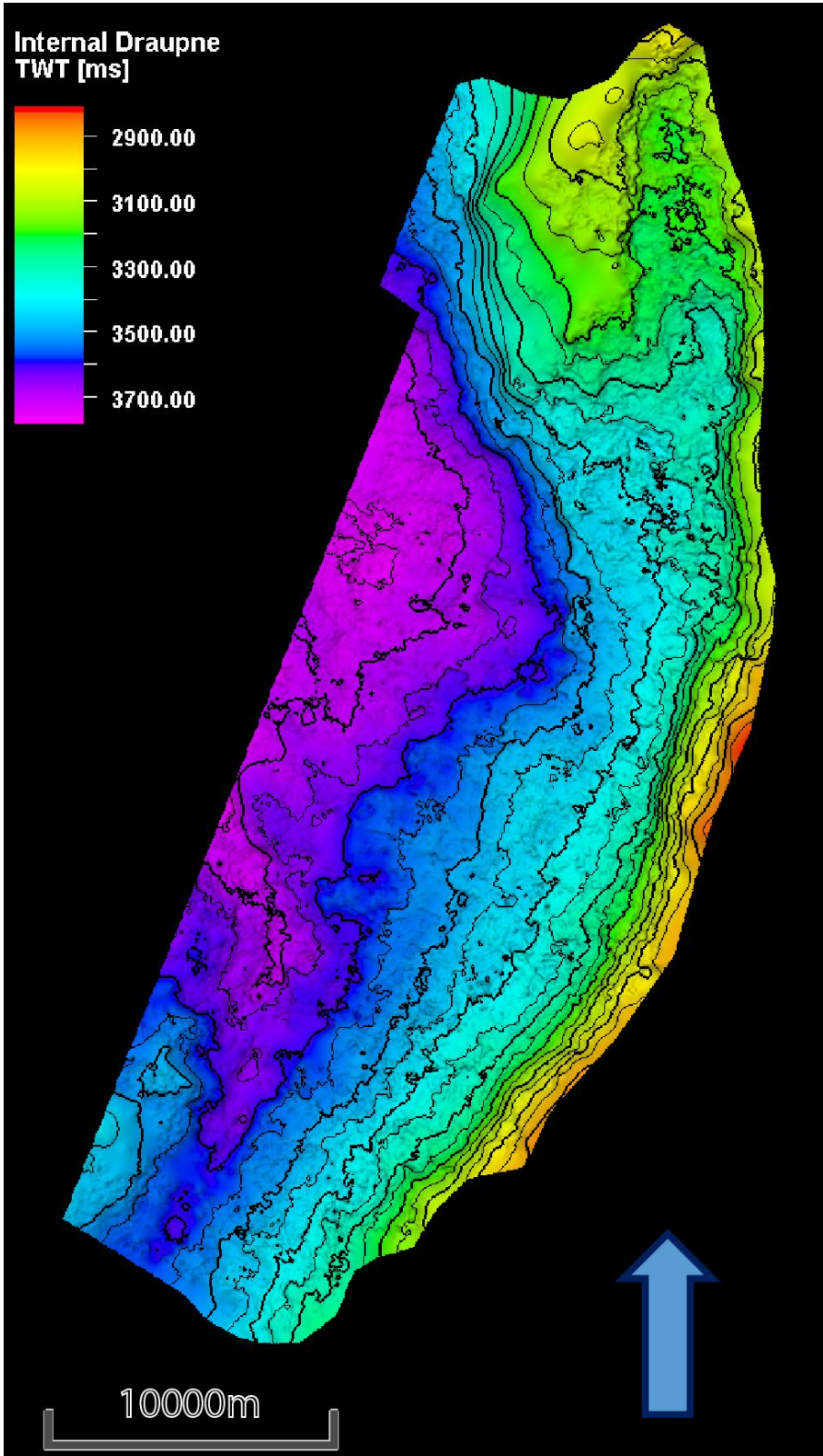


Figure 5.4: Illustration of the generated Internal Draupne TWTT structure map. The contour lines have an increment of 50 ms decreasing from a value of 3750 ms, where every second contour line is bold.

Description

The Intra Draupne TWTT structure map (Fig. 5.4) shows a general increase in elevation time towards the west. This trend is not covering the description of the southern part of the structure map, where an area of decreased elevation time (3450-3600 ms) is observed in the southwestern edge of the map. The western deepening trend is more gradual in the central part of the map, compared to the northern and the southern part. In the northeastern part of the map, a north-trending depression of increased elevation time (3150-3300 ms) is observed.

Interpretation

Figure 5.4 shows a map of similar trends as the Top Hugin map (Fig. 5.2) and the Top Heather map (Fig. 5.3), with an elevation time increase towards the west. The depression in the northwest is observed in all three structure maps, though the depression is shallower in the Intra Draupne surface. In the Intra Draupne TWTT structure map, the depression exhibits an elevation time difference of <200 ms from minimum to maximum, while it exhibits a difference of >400 ms in the Top Heather TWTT structure map (Fig 5.3). This suggests that Lower Draupne deposits have filled a large part of the relief. The variation in the western deepening trend exhibits the nature of the VSCF, with the central area coinciding with the low-displacement central segment of the VSCF. The more pronounced hanging wall depressions towards the south and the north coincide with the relatively high-displacement northern and southern segments. This area along the underlying VSCF resembles as a monocline. The elevated area (3450-3600 ms) in the southwest creates a NW-SE syncline. This feature is not observed in the Top Heather surface (Fig. 5.3), and it suggests a syn-depositional uplift resulting in the northwestern limb of the syncline. Accumulated Lower Draupne deposits sourced from the west is another possible cause of the elevated area, but a comparison with TWTT thickness map of the same stratigraphic level needs to be conducted to provide a more accurate interpretation.

5.1.4 Base Cretaceous Unconformity TWTT structure map

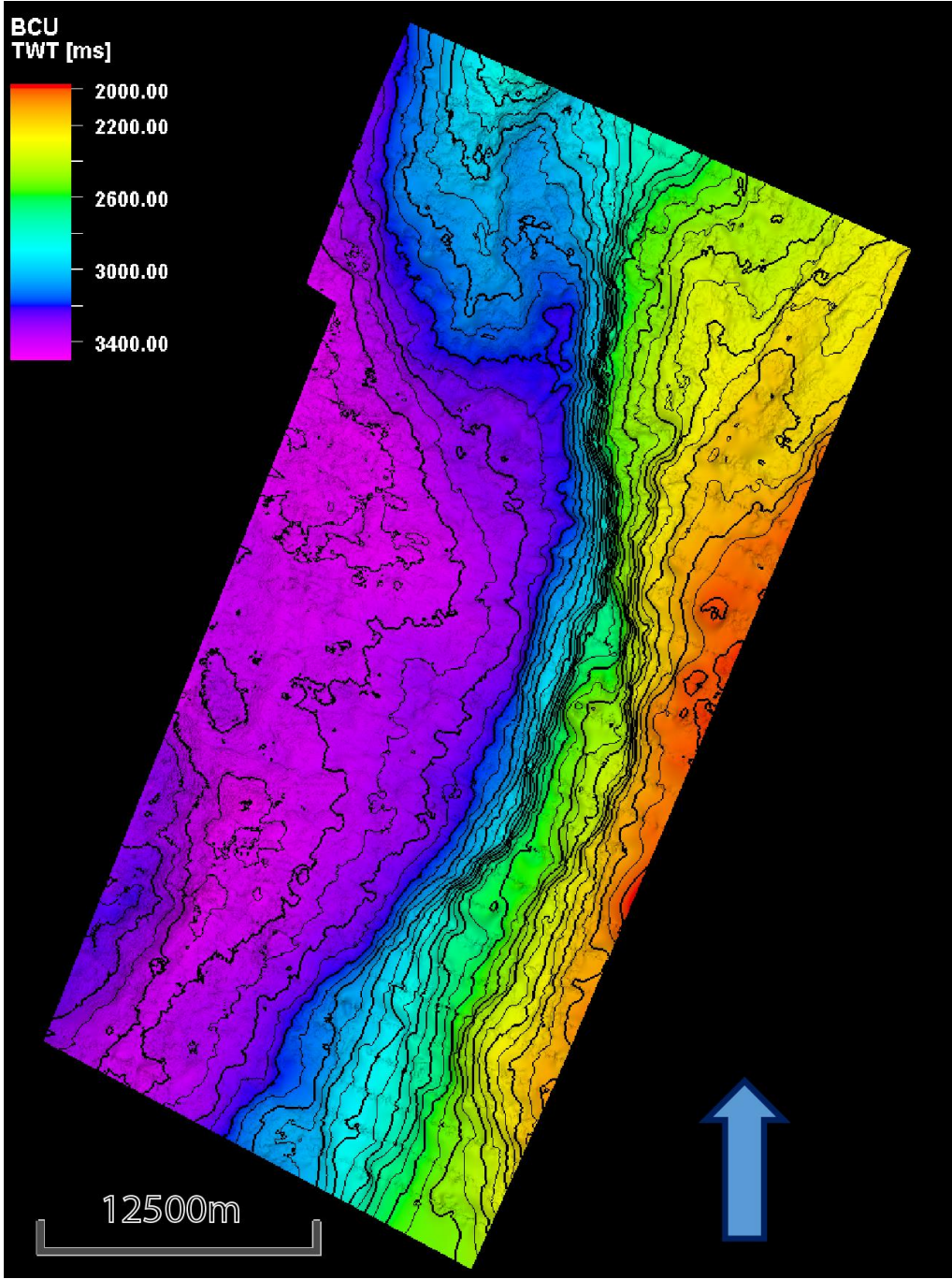


Figure 5.5: Illustration of the generated BCU TWTT structure map. The contour lines have an increment of 50 ms decreasing from a value of 3450 ms, where every second contour line is bold.

Description

Figure 5.5 shows a general increase in elevation time in a westerly direction. The increase is more abrupt in the central part than in the north and the south, where larger areas of an elevation time of 2800-3200 ms are observed. A north-trending depression of 3000-3200 ms is observed in the northern part of the map. The southwestern edge of the map shows a shallower area (3200-3400 ms) towards the west.

Interpretation

The overall westerly deepening trend observed in the BCU TWTT structure map is seen in previous structure maps (Fig. 5.2-5.4). This suggests that the main controls on the BCU surface physiography are the same as in the Top Hugin, Top Heather and Internal Draupne surfaces. The westerly deepening trend from ≈ 2200 ms to ≈ 3200 ms coincides with the location of the underlying VSEF. This large increase in elevation time cannot be observed in the other Upper Jurassic surfaces, as the stratigraphy on the VSEF footwall shows absence of Upper Jurassic strata. Upper Jurassic strata in the footwall to the VSEF. The north-trending depression shows similar relief (≈ 200 ms) in Figure 5.5 as in the Internal Draupne structure map (Fig. 5.4), which suggests that the deposition rate of Upper Draupne strata has not been larger in the depression, than in the rest of the hanging-wall of the VSEF. The shallowing area in the southwest shows a similar relief (150-200 ms) as in the Internal Draupne surface, which suggests that its controlling factors have limited syn-depositional influence. In the previous structure maps (Fig. 5.2-5.4), a monocline structure was interpreted in relation to the VSCF. This feature is only visible above the northern segment of the VSCF in the BCU structure map. This suggests that underlying Upper Draupne deposits has covered the effect of the underlying monocline on the topography in the central to southern area.

5.1.5 Internal Åsgard TWTT structure map

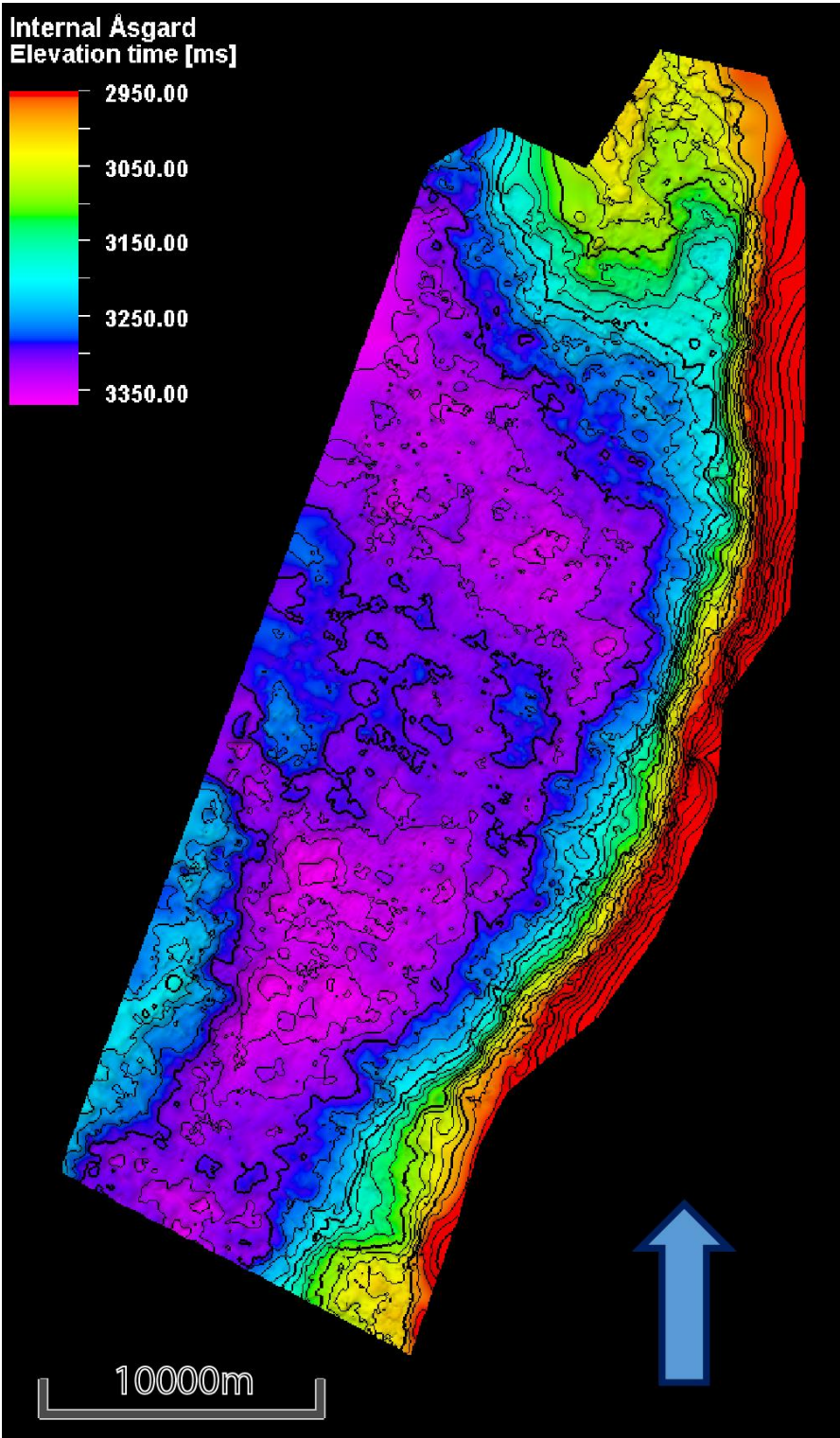


Figure 5.6: Illustration of the generated Internal Åsgard TWTT structure map. The contour lines have an increment of 25 ms decreasing from a value of 3375 ms, where every fourth contour line is bold.

Description

The internal Åsgard surface is shallower in the east and the north, with a deepening trend in a westerly direction (Fig. 5.6). In the southern and central part, the elevation time change is abrupt, from 2950 ms to 3300 ms over a short distance. The northern part includes a larger area with elevation time in the range between 3050 ms and 3250 ms, and a north-trending depression (3100-3200 ms) along the VSEF. In the southwestern part of the structure map, a shallower area (3200-3300 ms) is observed.

Interpretation

The westerly transition in the Internal Åsgard TWTT surface map (Fig. 5.6) from relatively shallow to relatively deep follows the strike of the VSEF. This suggests that the Internal Åsgard topography and the VSEF are related within the entire study area. The north-south trending depression shows a relief of ≈ 100 ms, which is less than in the BCU TWTT structure map (≈ 200 ms) (Fig. 5.5). This means that the depression has been filled with Lower Åsgard deposits. The shallower area creating the previously mentioned NW-SE syncline (5.1.3), shows a relief of ≈ 150 ms. This is less than in the BCU TWTT structure map (≈ 200 ms), which suggests that is a synclinal depocentre as the center of the syncline has been filled by more Lower Åsgard deposits than the northwestern limb. The uplifting event is likely to have initiated pre-depositional, and ceased syn-depositional.

5.1.6 Top Åsgard TWTT structure map

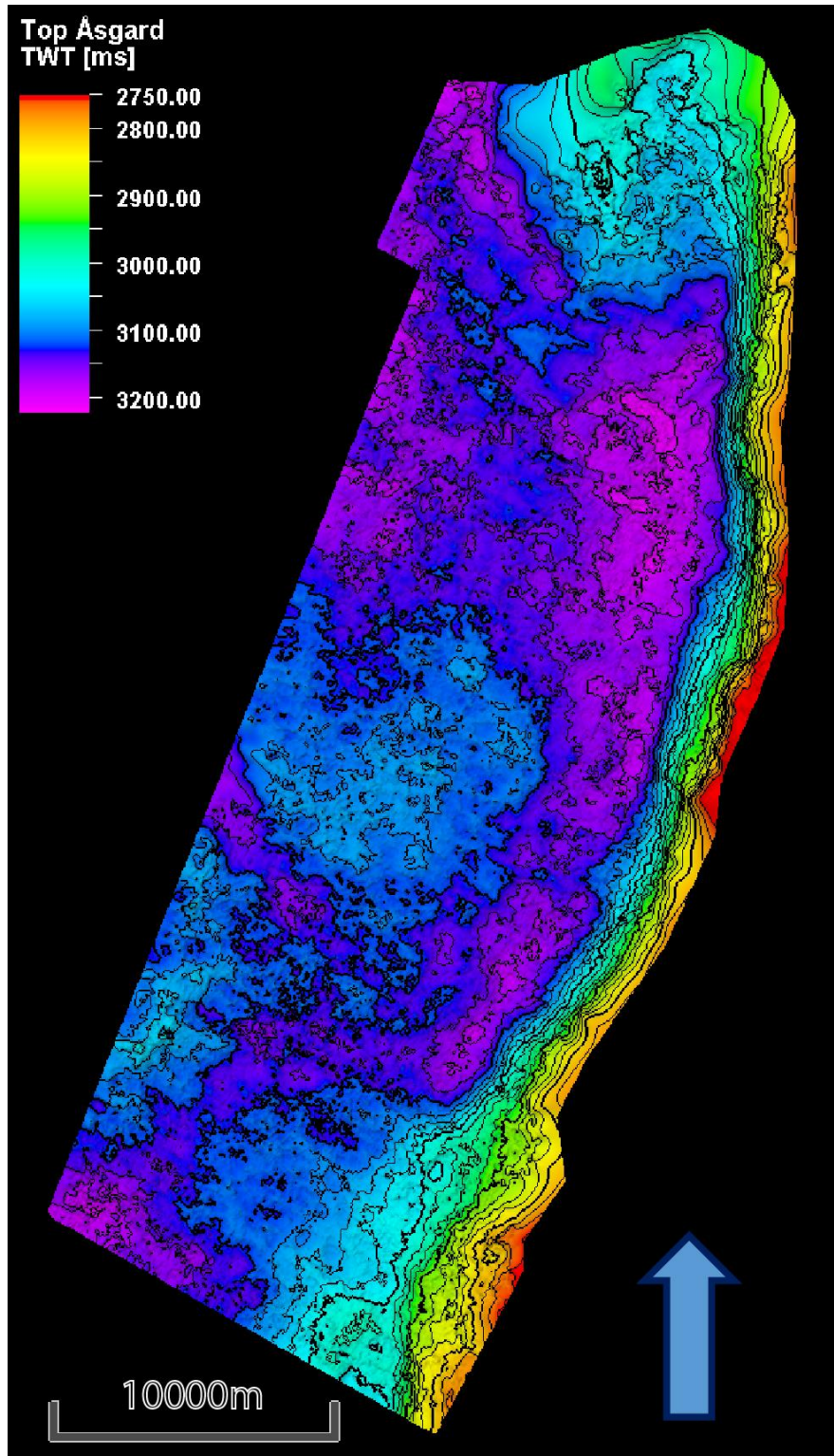


Figure 5.7: Illustration of the generated Top Åsgard TWTT structure map. The contour lines have an increment of 25 ms decreasing from a value of 3200 ms, where every fourth contour line is bold.

Description

The Top Åsgard surface (Fig. 5.7) shows a deepening trend from the southeast to the northwest. Three separate areas of shallower depth (3050 -3100 ms) are observed in the generally deep part of the map.

Interpretation

As seen in the Internal Åsgard structure map (Fig. 5.6), the abrupt westward deepening trend in the east coincide with the strike of the VSEF. The previously mentioned depression in the hanging-wall to the VSEF (subchapter 5.1.1-5.1.5) is not as visible in the Top Åsgard TWTT structure map, which suggests that deposition of Upper Åsgard strata has made the depression shallower. The three shallower areas in the map could be a result of different causes. The northernmost area coincide with a slightly shallower area in the Internal Åsgard structure map (Fig. 5.6), though the relief is larger in the Top Åsgard structure map (75-100 ms vs \approx 50 ms). This area extends further west, which suggests that it is a result of uplift or accumulated deposits sourced from the west. The central shallower area is related to the same uplifted area observed in Figure 5.4-5.6. The syncline shows a smaller relief in Figure 5.7 (50-75 ms) than in Figure 5.6 (\approx 150 ms), which suggests that the central part of the syncline has been filled by Upper Åsgard deposits, and the uplifting event has ceased during deposition of the Lower Åsgard formation. The southernmost elevated area cannot be observed in previous structure maps, which suggests that its controlling factors became active during deposition of the Upper Åsgard formation. The deepening trend across the strike of the VSEF has in general a gradient of <100 ms/km, but the gradient in the southern part related to this area, is not more than 100 ms/5 km. This gradual deepening area has a width of about 8 km, and a length of about 5 km. In terms of the geometry of the area, it suggests to be a result of a slide in the hanging wall to the VSEF, resulting in a low-relief fan.

5.1.7 Top Rødby TWTT structure map

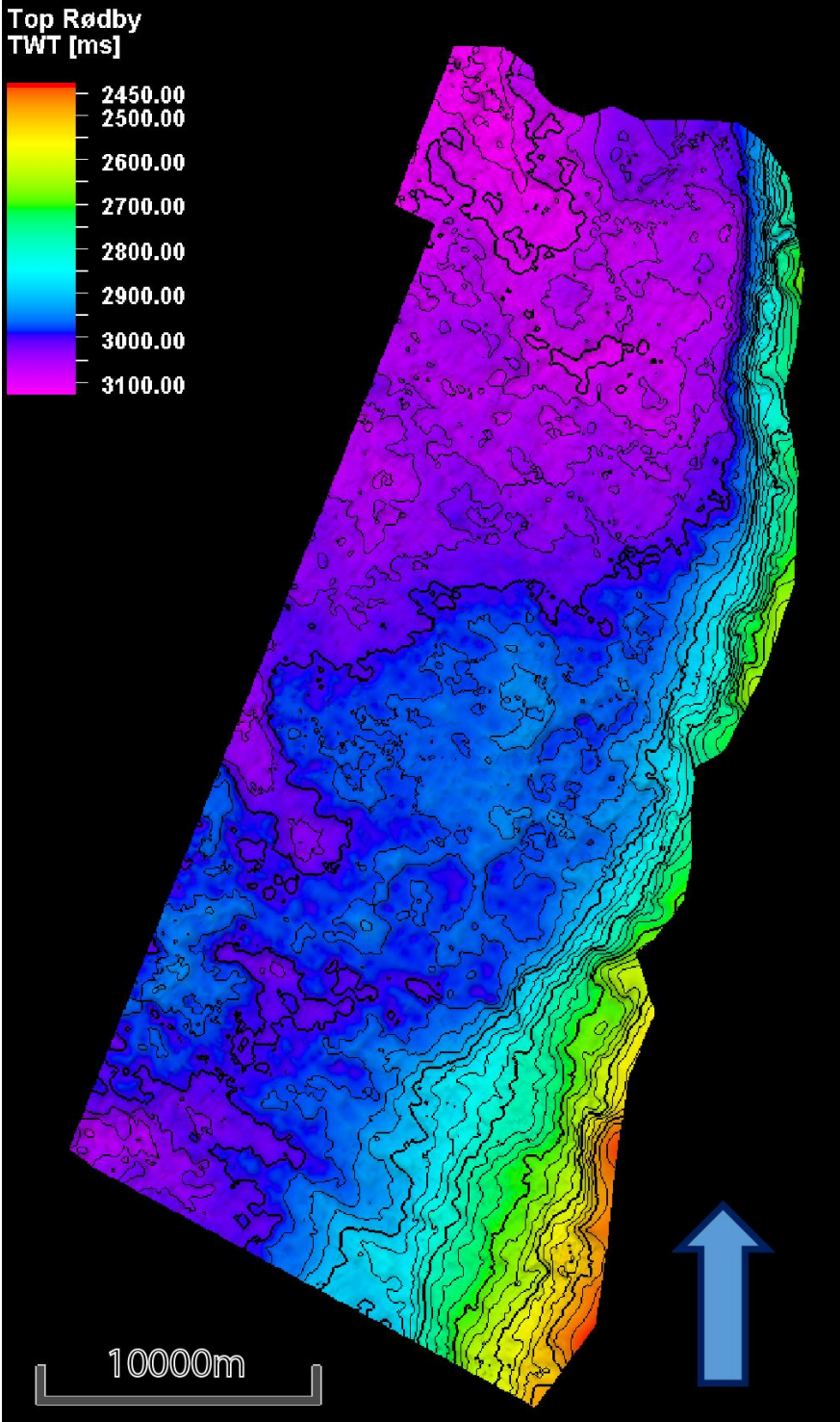


Figure 5.8: Illustration of the generated Top Rødby TWTT structure map. The contour lines have an increment of 25 ms decreasing from a value of 3150 ms, where every fourth contour line is bold.

Description

The Top Rødby TWTT structure map (Fig. 5.8) shows a deepening trend towards the west. The trend is more gradual in the southern part, with a large area of an elevation time of 2950-3000 ms.

Interpretation

Compared to Figure 5.7 of the Top Åsgard TWTT structure map, the deepening trend of the Top Rødby surface (Fig. 5.8) across the strike of the VSEF is less abrupt, especially in the central to southern part. The gradient is in general 100-200 ms/5 km in the southern and central part, while it is 100-200 ms/km in the northern part. This suggests that deposits of the Rødby+Sola interval has filled in parts of the Jurassic rift terrain created by the underlying VSEF in the central and southern area. The elevated area (2950-3000 ms) in the southwestern edge of the map (Fig. 5.8), coincides with elevated areas in stratigraphically deeper surfaces (Fig. 5.4-5.7). This suggests that this area in the Top Rødby TWTT structure map is a consequence of a previous period of uplift. The previously mentioned depression (5.1.1-5.1.6) in the northern part of the hanging-wall to the VSEF cannot be seen in the Top Rødby TWTT structure map (Fig. 5.8), which indicates that the depression has been fully filled in by Rødby+Sola deposits.

5.1.8 Top Svarte TWTT structure map

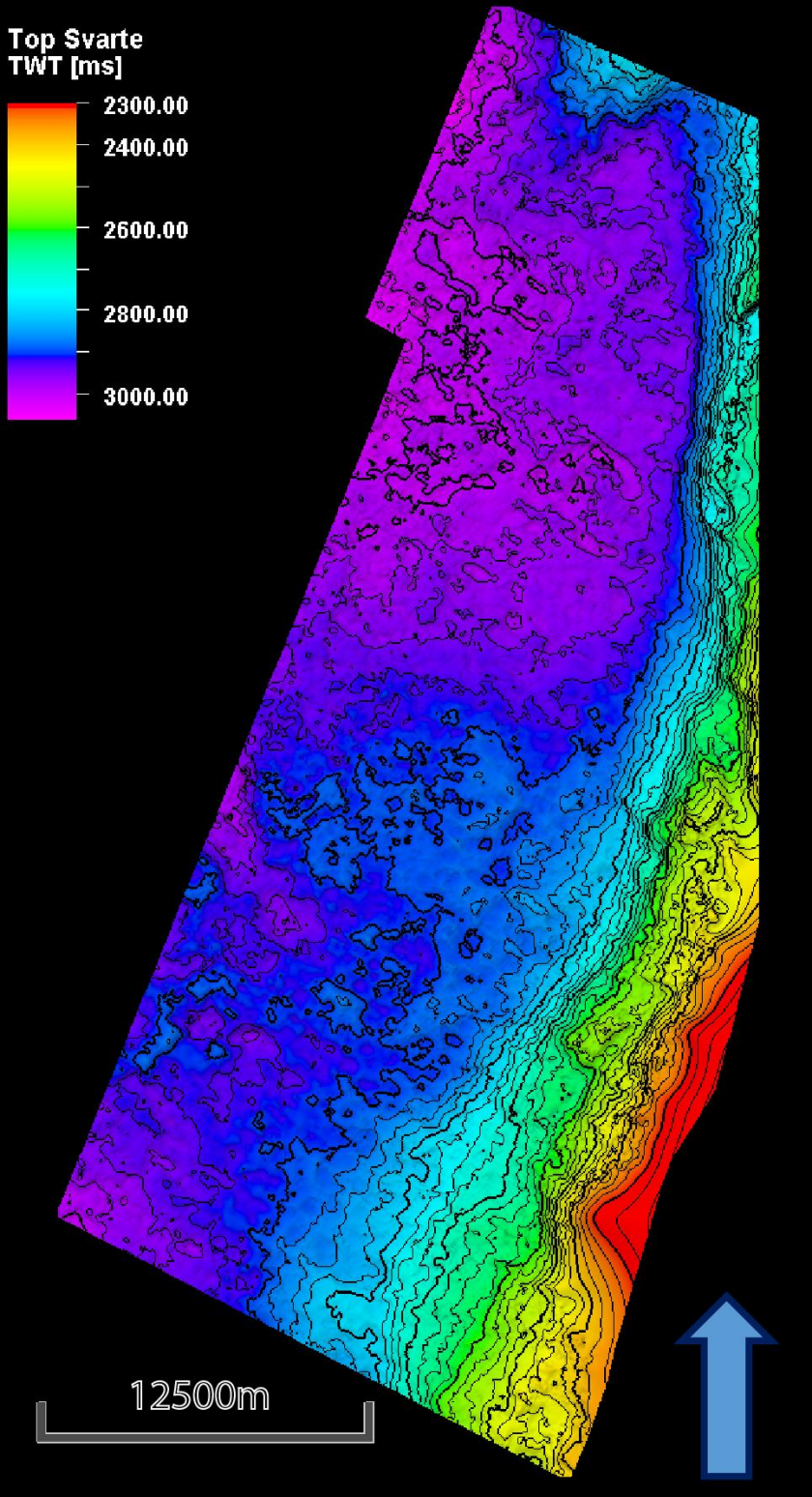


Figure 5.9: Illustration of the generated Top Svarte time structure map. The contour lines have an increment of 25 ms decreasing from a value of 3000 ms, where every fourth contour line is bold.

Description

The Top Svarte TWTT structure map (Fig. 5.9) shows a deepening trend towards the west. The trend is more gradual in the southern part, with a large area of an elevation time of 2875-2925 ms.

Interpretation

The lateral trends within the Top Svarte TWTT structure map (Fig. 5.9) shows many of the same features as the Top Rødby structure map (Fig. 5.8). The westerly deepening gradient in the northern (100-200 ms/km), and the central to southern parts is similar (100-200 ms/5 km). The elevated area in the southwest, which was observed in underlying structure maps (Fig. 5.4-5.8), is not as prominent in the Top Svarte TWTT structure map (Fig. 5.9), suggesting that deposits of the Svarte formation filled in parts of the uplifted area.

5.1.9 Top Blodøks TWTT structure map

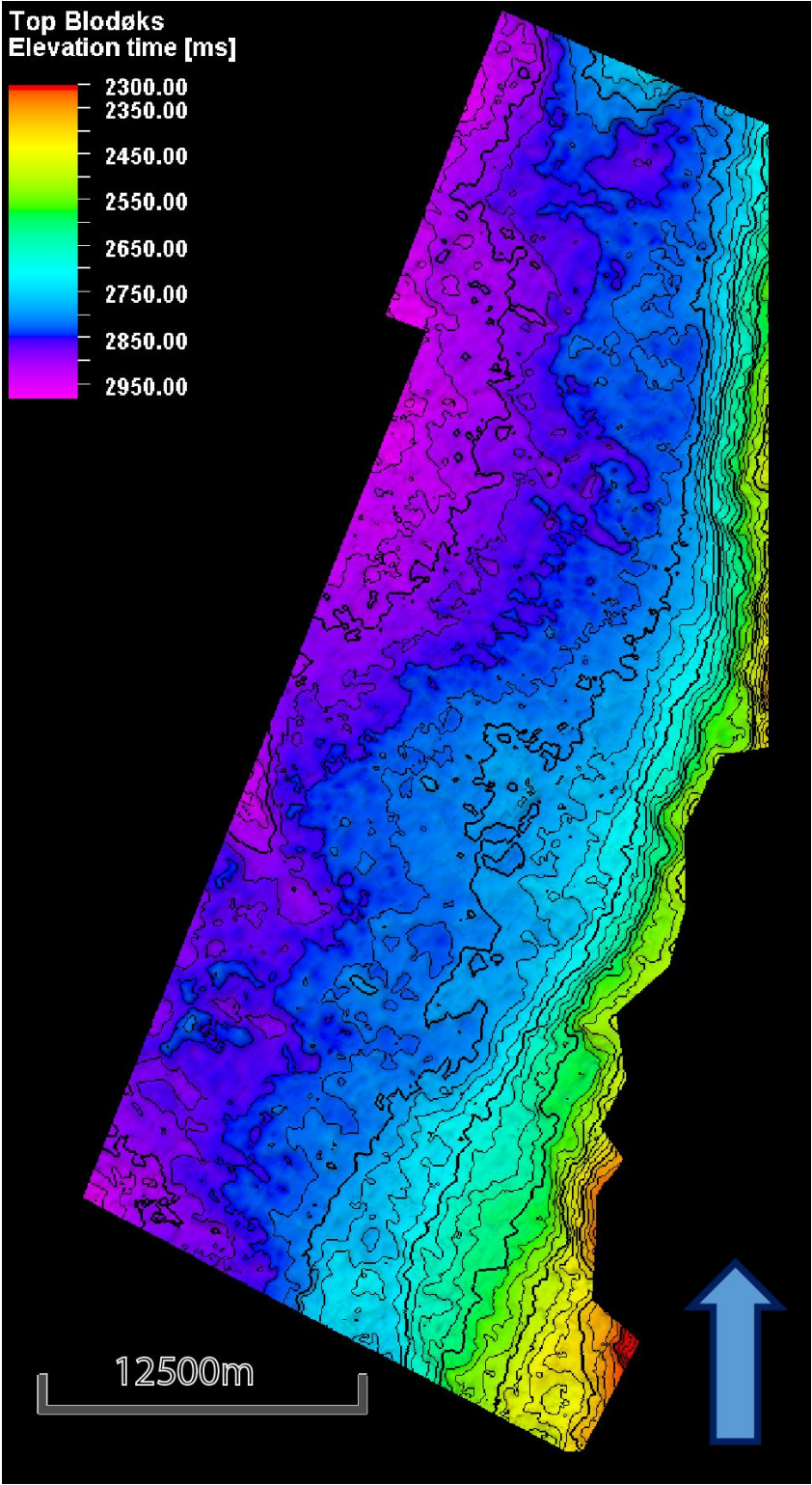


Figure 5.10: Illustration of the generated Top Blodøks time structure map. The contour lines have an increment of 25 ms decreasing from a value of 2950 ms, where every fourth contour line is bold.

Description

The Top Blodøks TWTT structure map (Fig. 5.10) shows a gradual deepening trend towards the west (100-200 ms/5 km) through the entire surface.

Interpretation

Figure 5.10 shows a change in the gradient of the deepening trend, compared to underlying surfaces. The gradient in southern area of the Top Blodøks TWTT structure map (Fig. 5.10) is similar to in the Top Svarte TWTT structure map (Fig. 5.9) (100-200 ms/5 km). In the northern part, the gradient is gentler in the Top Blodøks map (50-100 ms/km), than in the Top Svarte map (100-200 ms/km). This suggest that Blodøks deposits have leveled parts of the downfaulted areas in the northern part of the map. The elevated area in the southwest, seen in Figure 5.4-5.8, cannot be observed on this surface. This suggests that the factor controlling this feature is not affecting the Top Blodøks surface, and the area has been filled in by deposits of the Blodøks formation.

5.1.10 Internal Draupne RMS-amplitude map

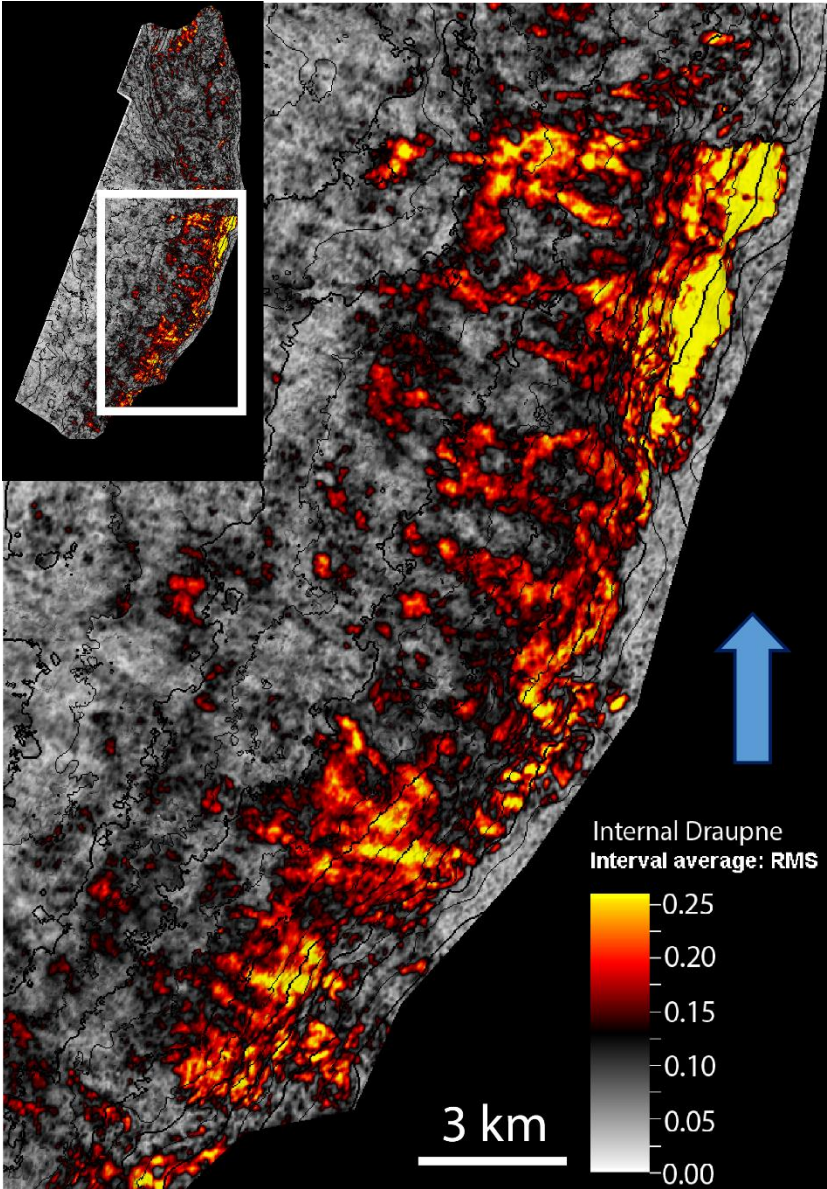


Figure 5.11: RMS-amplitude map of the interpreted Internal Draupne surface, with focus on the area of interest.

Description

In the generated RMS-amplitude map (Fig. 5.11) of the Internal Draupne TWTT structure map (Fig. 5.4) areas with high RMS-value are observed. The areas are trending basinwards on the VSEF fault scarp. The southernmost features show a NW-trend, with a gradually more westerly trend northwards. These features show a narrowing trend towards the west, are relatively straight, and show general decrease in RMS-value towards the west and towards the south. The southernmost features shows less lateral extent (3-5 km) than the northernmost (6-10 km).

Interpretation

The basinward-trending features shows differences in terms of architecture, RMS- value and orientation. The RMS contrast could be a seismic tuning effect, but no laterally converging reflectors are observed in this area on the relevant stratigraphic level. Sedimentary systems in a steep fault scarp, like slides and slumps could deposit coarse-grained lithologies, which would generate a large RMS contrast against clay-rich strata. With a locus in a steep fault scarp and the fact that the Draupne Formation is clay-rich the observed features could presumably be a lithological contrast. The lack of sinuosity could be a consequence of the fact that these slides are located in the high-gradient fault scarp of the VSEF, as streams are topographically controlled and shows in general an increased sinuosity with decreased slope-gradient (Mueller, 1968). This suggests based on the RMS value that the northernmost interpreted slides consist of coarser grained stratigraphy than the southernmost slides. The southernmost features show a NW-trend, while the same features in the north show a westerly trend. The fact that the change in orientation coincide with the strike of the VSEF suggests that the VSEF is one of the controlling factors on the distribution of the interpreted slides. Based on the change in trend, in addition to the observed variation in lateral extent, RMS-value, and degree of narrowing, the features are sub-divided into six separate features (Fig. 5.12). The two southernmost (blue and yellow) are characterized by relatively limited lateral extent, limited basinward narrowing, and limited basinward decrease in RMS-value from proximal to distal part. These features are around 5 km wide in the proximal part, and shows a basinward extent of around 5 km. The two central features (red and white) are

characterized by larger lateral extent (7 km) than the southern features, and gradually basinwards narrowing and decrease in RMS-value. These features are 6 and 3 km wide in the proximal part, and 4 and 2 km wide in the distal part, respectively. The two northernmost (purple and green) are characterized by the largest basinward extent (8-10 km), shows the strongest narrowing trend, and shows the largest RMS-value. The northernmost features have a RMS-value of >0.25 in the entire proximal end, are 5 and 3 km wide, and narrows towards a width of 1-2 km in the distal end.

5.1.11 Top Upper Draupne sst RMS-amplitude map

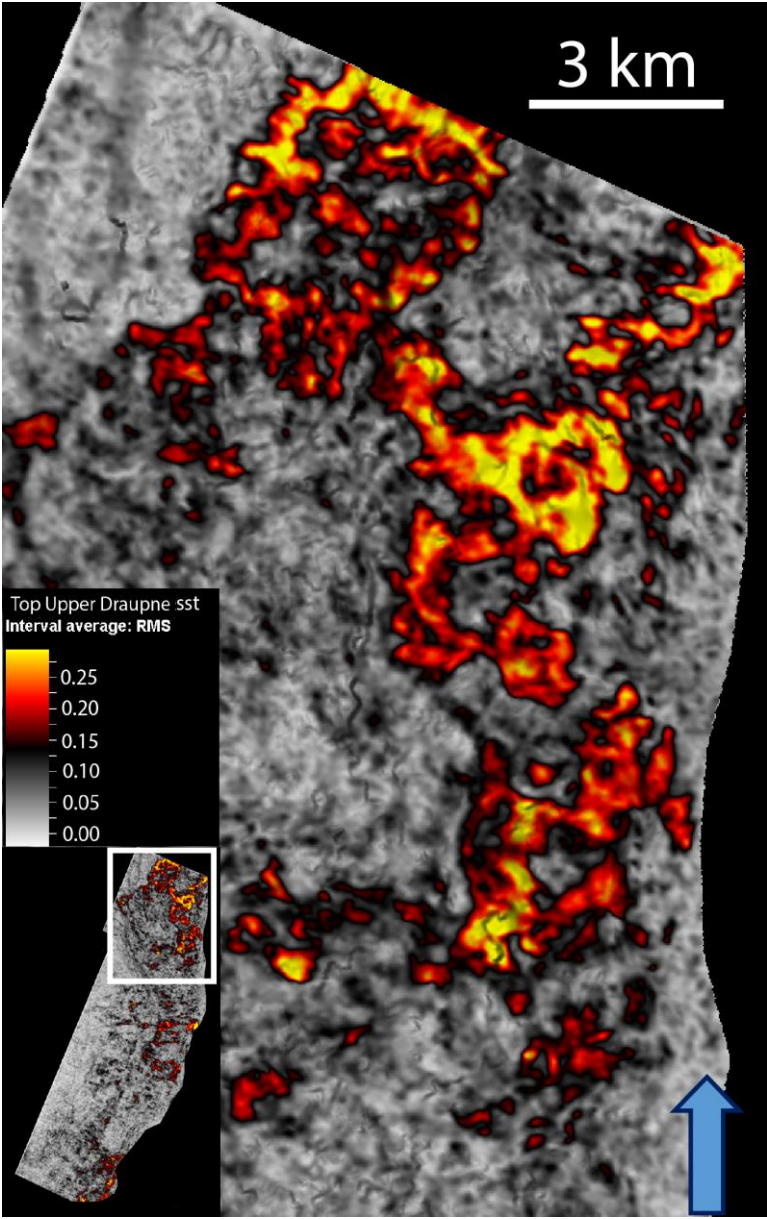


Figure 5.13: RMS-amplitude map of the interpreted Top Upper Draupne sandstone surface, with focus on the area of interest.

Description

Within the Upper Draupne formation, an interpreted horizon defining the Top Upper Draupne sandstone shows areas of increased RMS-value (Fig. 5.13). The area of increased RMS-value are concentrated in the northern part of the study area, and shows values ranging from >0.25-0.15. The observed features are trending southwards from the Heimdal terrace in the north, and shows a sinuous pattern.

Interpretation

The southward trending features show a sinuous pattern, and are trending N-S. This represents a different architecture than the interpreted slides in Figure 5.11. The slides of high RMS-value in 5.1.10 is relatively straight, unlike the features in 5.1.11, which are sinuous. This suggests that the features are a result of different depositional environments. These sinuous features show shallow depth in a cross-section, suggesting that these are channels, and not canyons. An interpretation of the Top Upper Draupne sst RMS-amplitude map (Fig. 5.14) shows a confluence between two separate channels. West of the confluence point, a channel is interpreted with a southwestward trend on the VSCF fault scarp. The main fairway are 3-5 km wide proximal to the confluence point, and narrows distally (1-3 km wide), where the main fairway is interpreted to split into three separate fairways. The bends are 3-4 km wide, and are located downdip in the interpreted N-S trending depression (Fig. 5.3). The interpreted sinuous channel suggests that this was active in a low-gradient system (Mueller, 1968). Because it is located within the N-S trending depression and favors a low-gradient system, it is likely that a large portion of the depression was infilled by older Draupne deposits before this system became active.

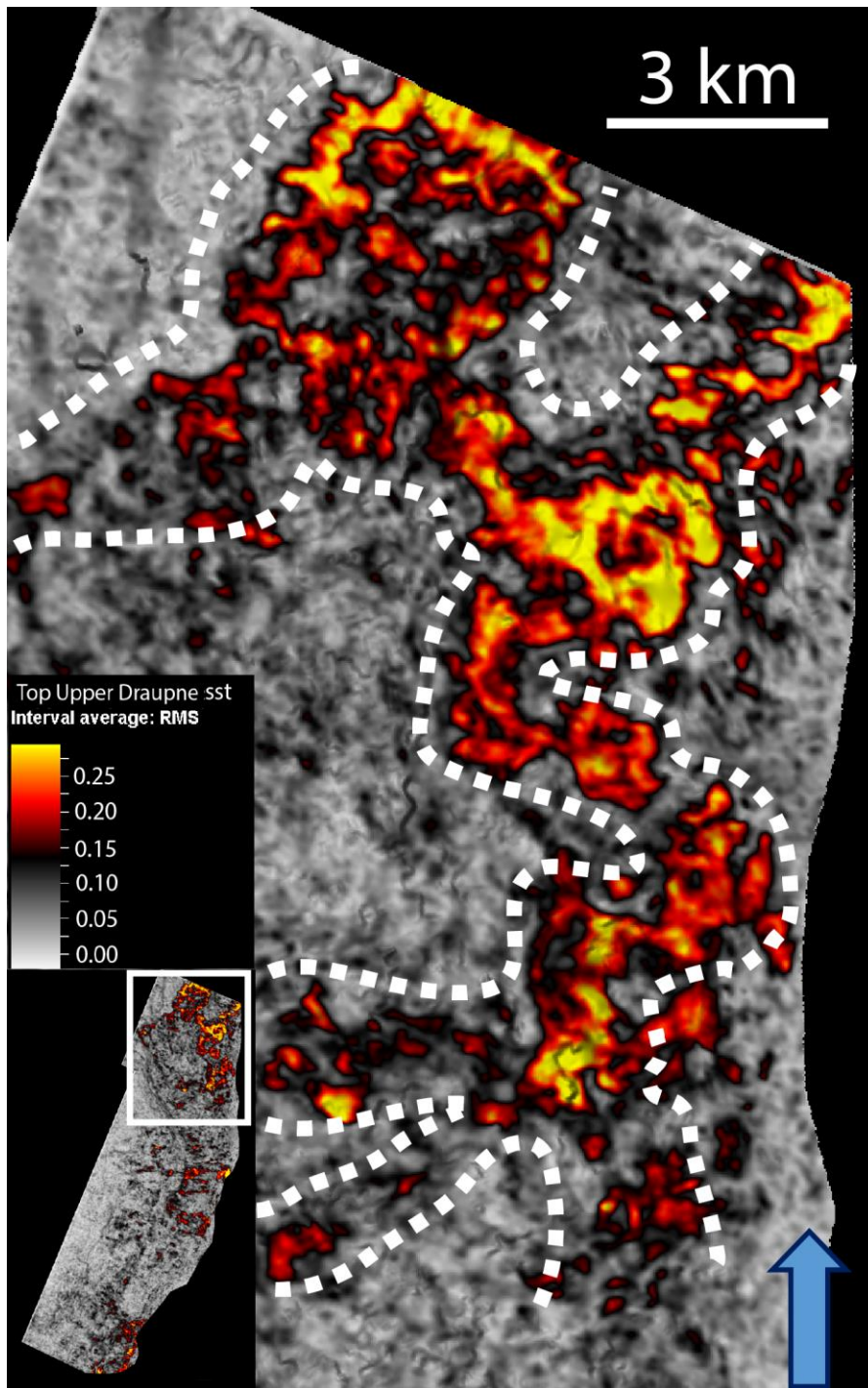


Figure 5.14: RMS-amplitude map of the interpreted Top Upper Draupne sandstone surface, with focus on the area of interest. The stippled lines indicate the path of the interpreted fairways.

5.2 Time interval maps

Chapter 5.2 will present eight TWTT thickness maps, generated by combining time structure maps from chapter 5.1. Stratigraphic and seismic architecture of every stratigraphic interval will be presented. The eight time interval maps, reflecting separate formations, are the Heather, Lower Draupne, Upper Draupne, Lower Åsgard, Upper Åsgard, Rødby+Sola, Svarte and Blodøks concluding the interval subdivision (Fig. 5.15).

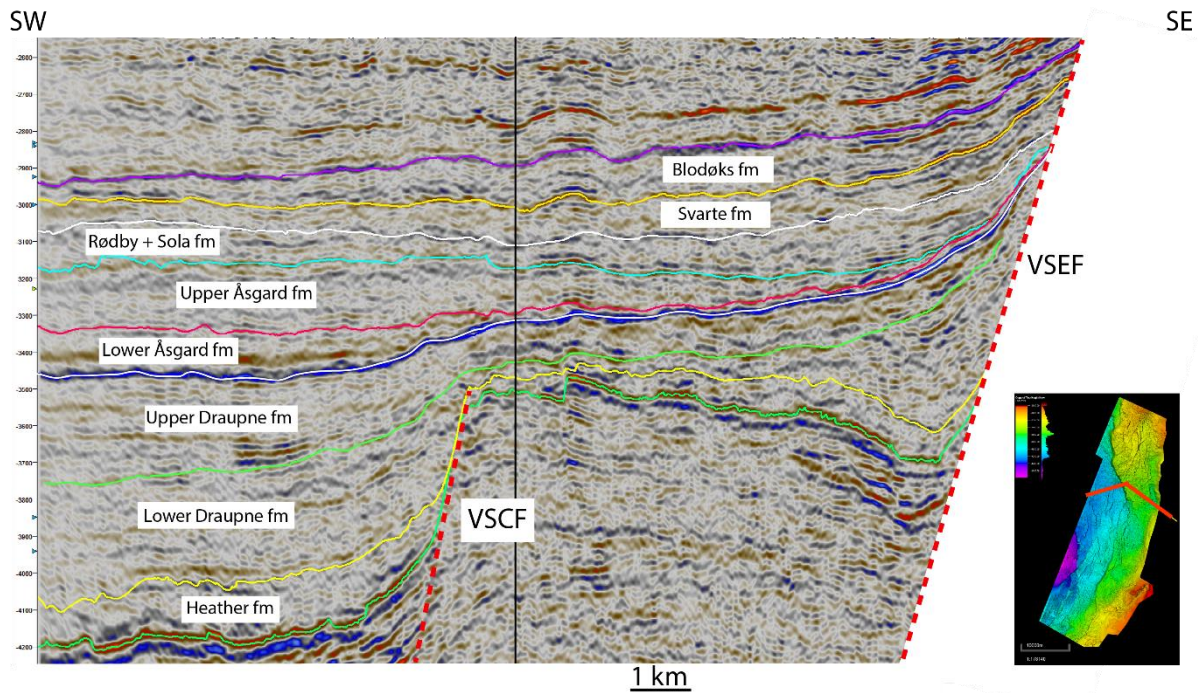


Figure 5.15: The figure illustrates a composite line cross-section reflecting the different formations studied in chapter 5.2 and the interpreted surfaces from chapter 5.1. The solid lines reflect the surfaces, and the formations are the interval in between the solid lines. In the central part of the cross-section a vertical line is visible, reflecting the bend in the composite line. This bend is illustrated in the Top Hugin reference map in the bottom right corner. Two stippled, inclined lines illustrate the VSCF and VSEF.

Figure 5.2 in chapter 5.1 shows the Top Hugin surface. This surface gives the best expression on the nature of the VSCF. The northern part of the VSCF shows a displacement of 400-600 ms, the southern part 300-400 ms, and the central part 200-300 ms, across a downstepping set of faults (Fig. 5.1, 5.2, 5.16). The northern part of the VSCF shows a NNW-SSE strike, while the southern part shows a NNE-SSW strike. These observations lead into the subdivision of the VSCF into three separate segments based on variation in displacement versus length across the strike of the fault, and strike direction. In order to estimate the impact the VSCF has on the syn- and post-rift infill, the strike of the main faults in the VSCF zone is scaled into

dimensions reflecting the displacement, and put on every TWTT thickness maps in chapter 5.2.

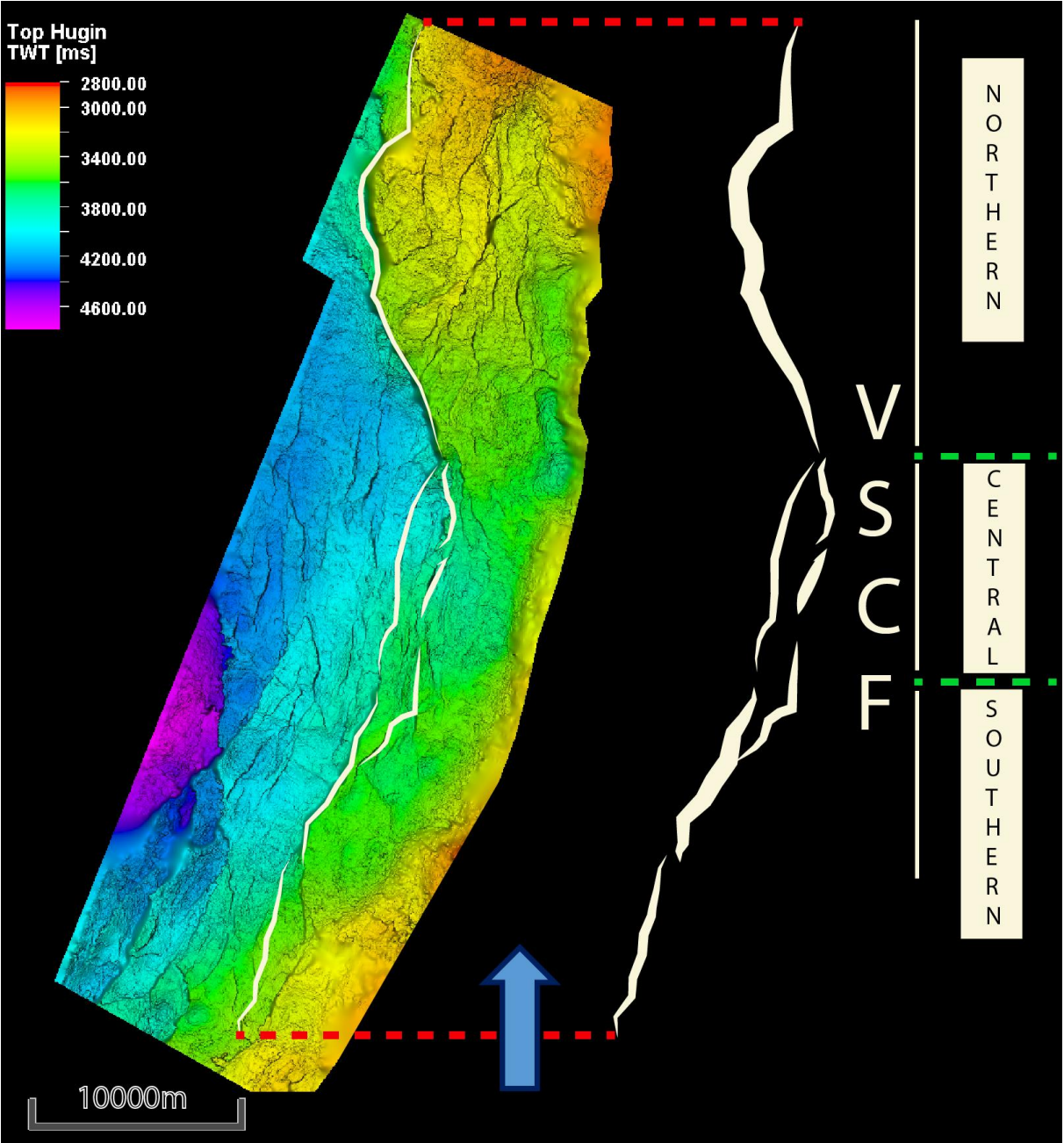


Figure 5.16: The figure illustrates a time structure map of the Top Hugin surface. The white lines in the TWTT thickness map illustrates the main faults in the VSCF zone. The red stippled lines indicates the upscaling of the fault strike, into the dimensions used in figures in subchapter 5.2.1 - 5.2.10. Thicker lines indicates larger displacement. The column on the right illustrates the subdivision of the VSCF, with every segment separated by the green stippled lines.

5.2.1 Heather TWTT thickness map

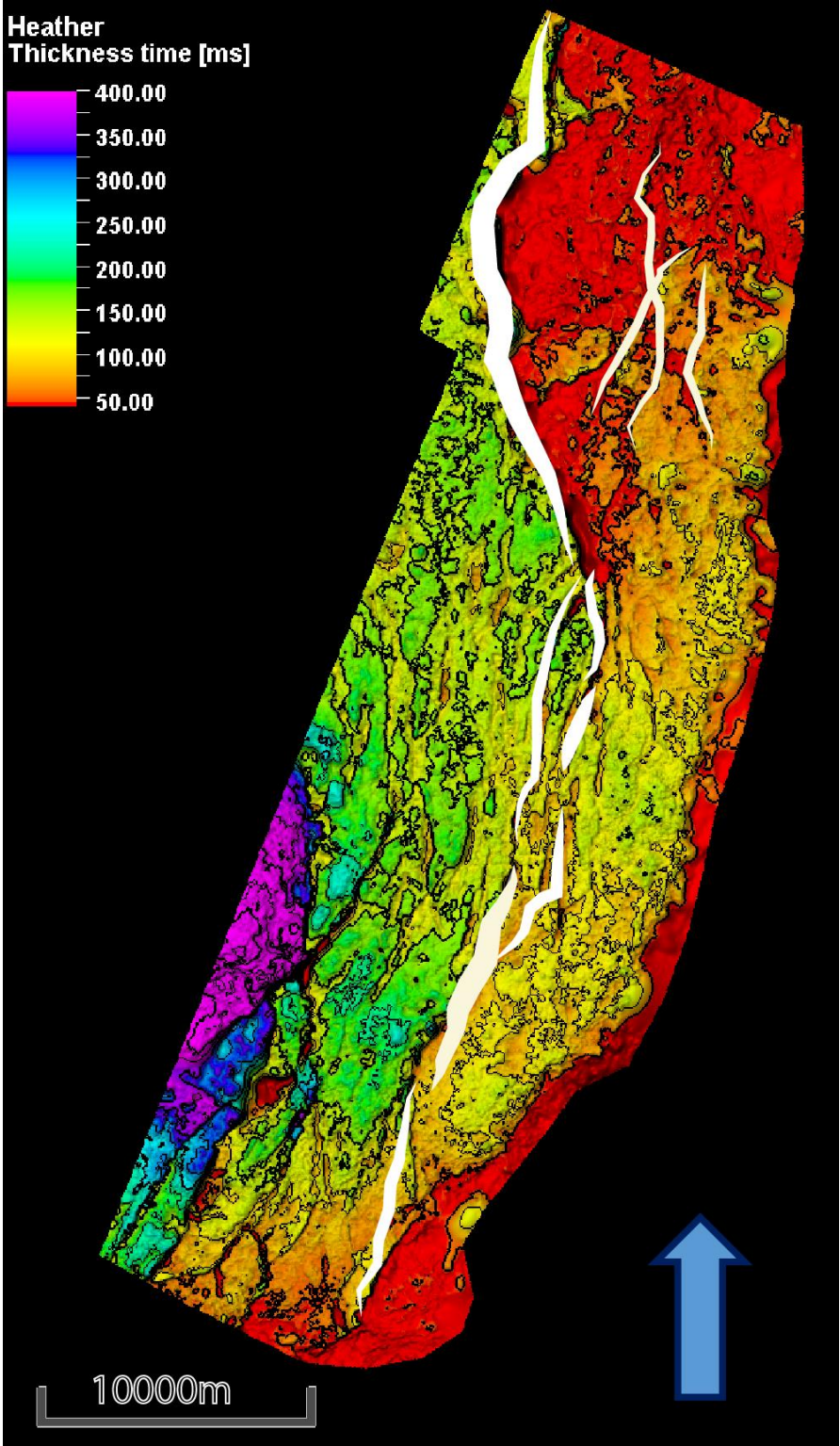


Figure 5.17: The figure illustrates a TWTT thickness map of the Heather formation. The contour lines have an increment of 50 ms where every second contour is bold. The white lines illustrate the strike of the underlying VSCF in addition to three faults in the footwall to the VSCF (Fig. 5.16). The thickness variation of the white lines illustrates variation in displacement.

Description

The Heather TWTT thickness map (Fig. 5.17) shows that deposits of the Heather formation are in general close to absent in the northern part of the footwall to the VSCF (<50 ms). Close to the northern part of the VSEF an area with a thickness of 50-150 ms is observed. An abrupt increase in thickness is observed across the northern segment of the VSCF (<50 ms to 100-150 ms). In the footwall of the central and southern segment of the VSCF, the time interval map shows a thickness time between 50 and 150 ms, with the upper end of the range in the central segment. The hanging wall thickness close to the fault plane of the VSCF, shows a thickness time between 100 and 200 ms, where the upper end of the range is located along the southern and northern segment. An abrupt increase in thickness (from <250 ms to >350 ms) is observed in the southwestern part of the TWTT thickness map (Fig. 5.17).

Interpretation

Figure 5.17 shows that the thickness decrease of the preserved Heather formation from the hanging-wall to the footwall of the VSCF is larger with increased displacement. This suggests that the main source of Heather deposits is from the west. The 50-150 ms thick area close to the northern part of the VSEF is thinning westward towards the VSCF. This suggest that the preserved deposits in this area are sourced from the structural high in the east. Every abrupt thickness change in the Heather TWTT thickness map (Fig. 5.17) coincide with underlying faults (Fig. 5.1, 5.16), suggesting that the distribution of preserved Heather deposits is in general strongly fault-influenced.

Stratigraphic and seismic architecture

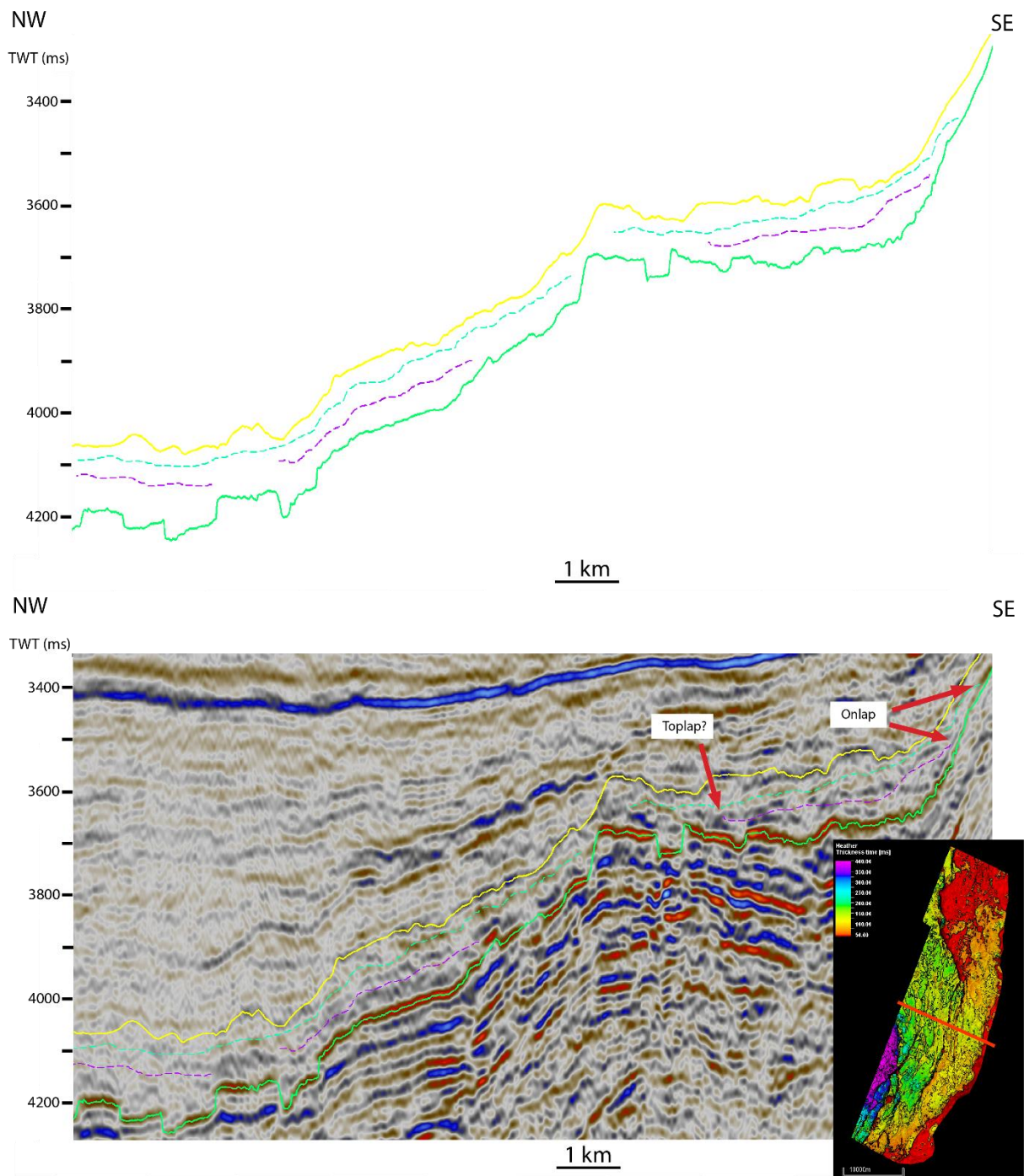


Figure 5.18: Cross-section of inline 18075 illustrating the Heather formation. Internal reflectors of positive amplitude are interpreted with dashed lines, showing their terminations. Onlaps and toplaps are visible. The map in the lower right corner shows the position of the cross-section with the Heather time interval map as reference.

Figure 5.18 shows a cross-section of inline 18075 with focus on the Heather interval illustrated between the yellow and green solid horizons. The horizons defines the Top Heather (yellow) and Top Hugin (green) surfaces, acting as the upper and lower bounding surfaces, respectively. Top Heather is a medium-amplitude trough, while the Top Hugin is a high-amplitude peak. Two dashed lines in different colors are reflecting internal terminating reflectors within the Heather interval. The reflectors onlaps the Top Hugin surface and internal toplaps in the Top Heather surface is observed. The internal reflectors of the Heather interval are sub-parallel to chaotic, with a medium value of amplitude.

5.2.2 Lower Draupne TWTT thickness map

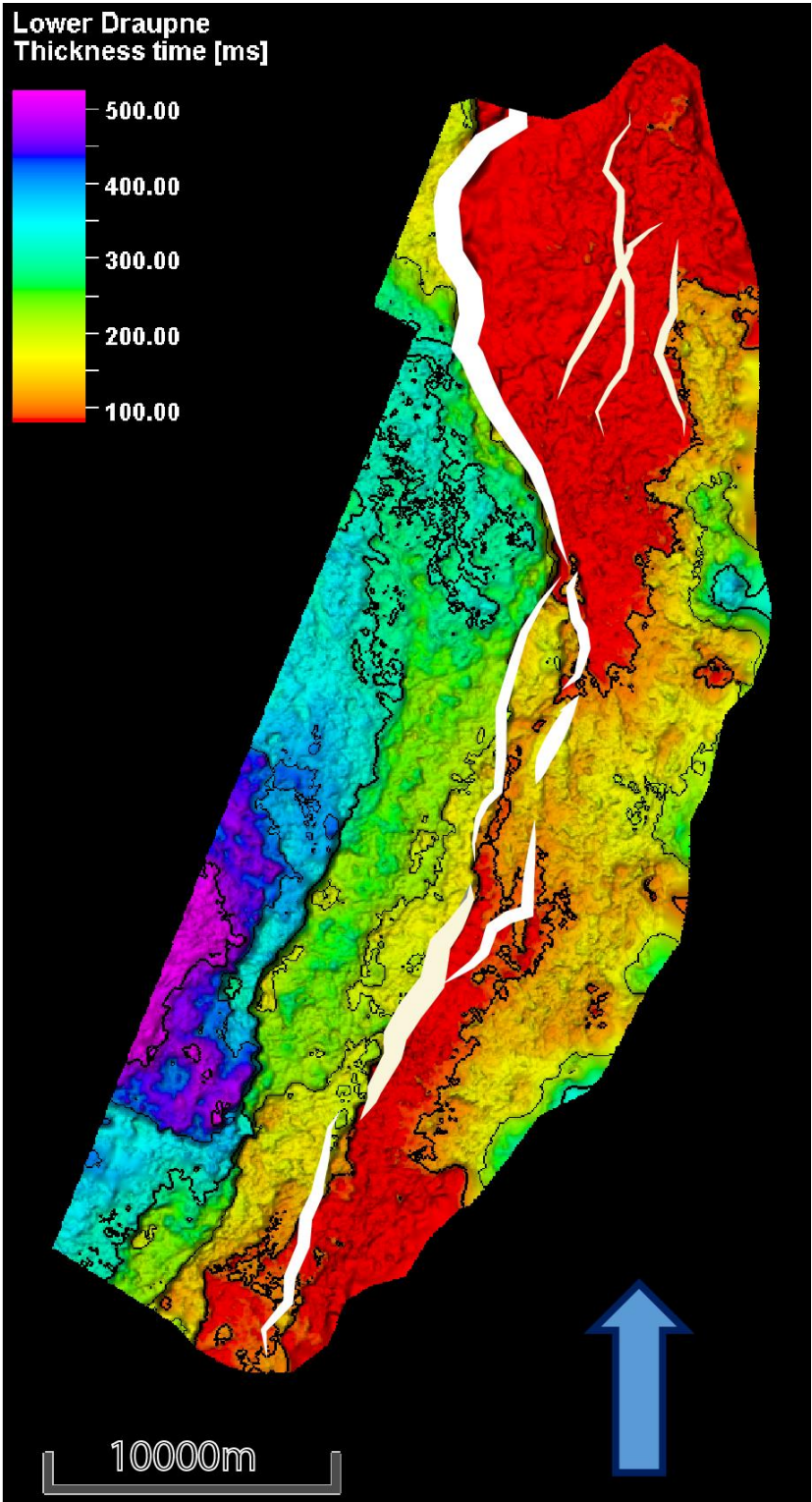


Figure 5.19: Figure 5.19 illustrates a TWTT thickness map of the Lower Draupne formation. The contour lines has an increment of 100 ms where every second contour is bold. The white lines illustrates the strike of the underlying VSCF in addition to three faults in the footwall to the VSCF (Fig. 5.16). The thickness variation of the white lines illustrate variation in displacement.

Description

The Lower Draupne TWTT thickness map (Fig. 5.19) shows a general increase in thickness towards the west. Large areas with a thickness of <100 ms are observed in the northern part of the map in addition to a less dominant area of similar thickness in the south. Along the eastern edge of the map, preserved Lower Draupne deposits with a thickness ranging from 100 ms to more than 300 ms is observed. The interval thickens from 150 ms to 350 ms TWTT thickness from east to west over a distance of 10 km in the central part of the study area. In general the Lower Draupne deposits thickens towards the west in the hanging-wall to the VSCF, and thins towards the west in the footwall to the VSCF.

Interpretation

Figure 5.19 shows the same trend as the Heather TWTT thickness map (Fig. 5.17) with increased formation thickening across high-displacement parts of the underlying VSCF. The variation in thickening trend across the strike of the central part of the VSCF compared to the southern and northern part, suggests that the nature of the VSCF takes part in controlling the distribution of preserved Lower Draupne stratigraphy. The westerly thickening trend of the formation in the hanging-wall to the VSCF suggests a different source than the preserved deposits in the footwall, which thins towards the west. The trend in thickness variation suggest that the main source of hanging-wall deposits is from the west, and the main source of the footwall deposits is from the east. A different source, suggests that the deposits may originate from different depositional environments.

Stratigraphic and seismic architecture

Figure 5.20 shows a cross-section of inline 17979 with focus on the Lower Draupne interval illustrated between the blue and yellow solid horizons. The horizons defines the Internal Draupne (blue) and Top Heather (yellow) surfaces, acting as the upper and lower bounding surfaces, respectively. Internal Draupne is a medium to high-amplitude peak, while the Top Heather is a medium-amplitude trough. Several dashed lines in different colors are reflecting internal terminating reflectors within the Lower Draupne interval. The overall internal architecture shows a wide range of terminations. The interval onlaps the Top Heather surface and shows internal toplap and onlap. The internal reflectors of the Lower Draupne interval are parallel to sub-parallel, with a medium to high value of amplitude.

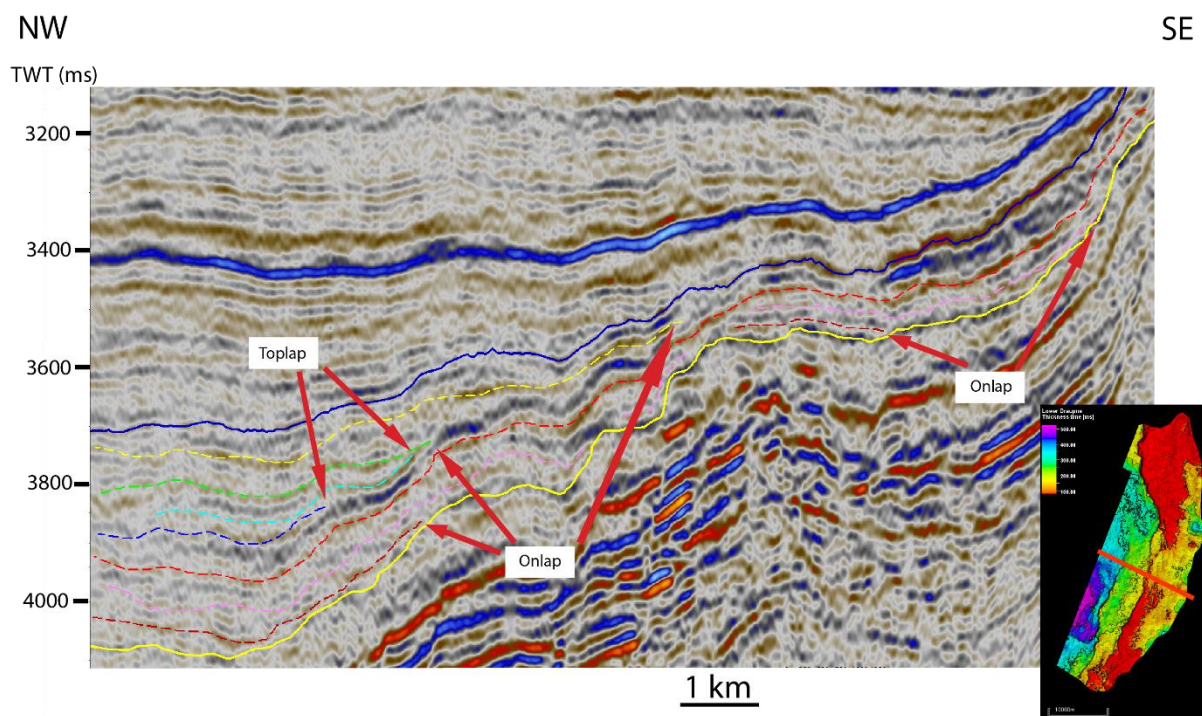
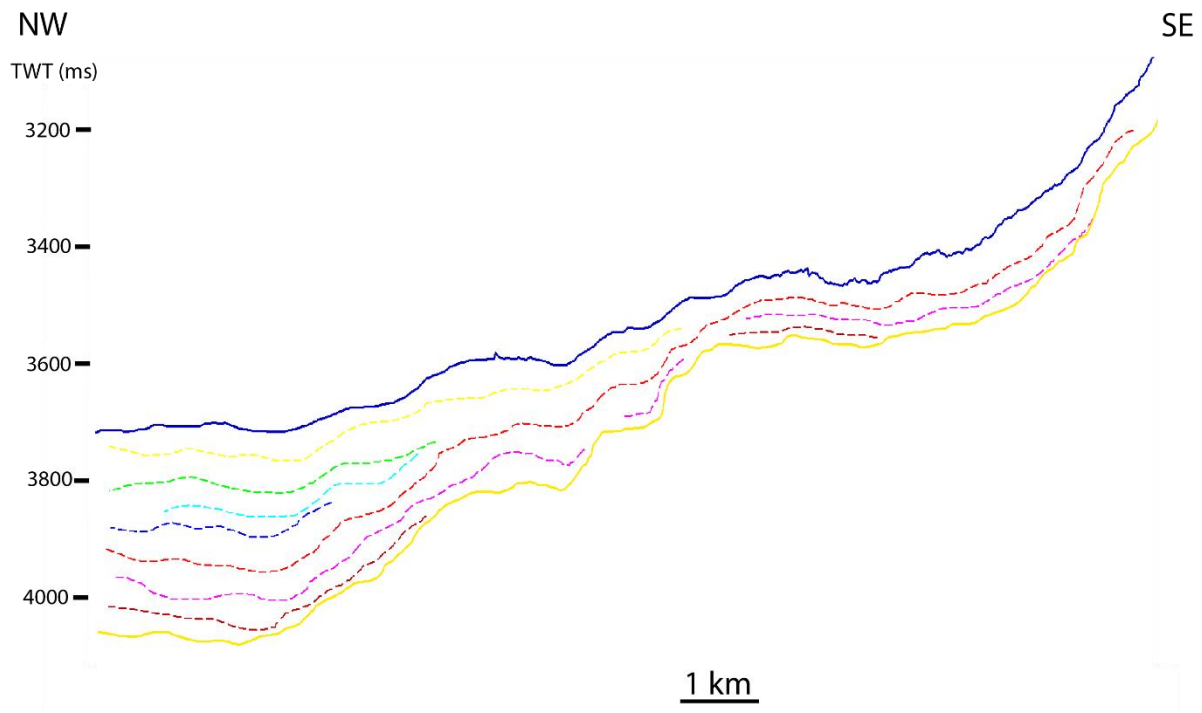


Figure 5.20: Cross-section of inline 17979 illustrating the Lower Draupne formation. Internal reflectors of positive amplitude are interpreted with dashed lines, showing their terminations. Onlaps and toplaps are visible. The map in the lower right corner shows the position of the cross-section with the Lower Draupne time interval map as reference.

5.2.3 Upper Jurassic Wedge TWTT thickness map

Description

The Upper Jurassic Wedge TWTT thickness map includes mainly the proximal terrace area on the VSEF hanging wall, excluding the deeper parts of the study area. The thickness map is equivalent to the Lower Draupne TWTT thickness map (Fig. 5.19). A relatively thick (100 to >250 ms) area along the eastern edge of the map is observed. The northernmost area shows a thickness increase southwards along the strike of the VSEF. The southern and northern part of the wedge shows a basinward thinning trend from >250 ms to <100 ms, while the central part shows a more gradual basinward thinning trend.

Interpretation

A southward deepening trend of the N-S trending depression along the strike of the VSEF was observed in Fig. 5.3. This observation coincide with the southward thickening trend of the Upper Jurassic wedge (Fig. 5.21), suggesting that the Upper Jurassic wedge has filled a large portion of the topography. Several faults were observed in the northern part of the proximal terrace area in the Top Hugin TWTT structure map (Fig 5.2). The northernmost part of the wedge has similar orientation as the strike of one of these faults (Fig. 5.21), suggesting that the underlying structural configuration is controlling the architecture of the wedge. The lack of preserved

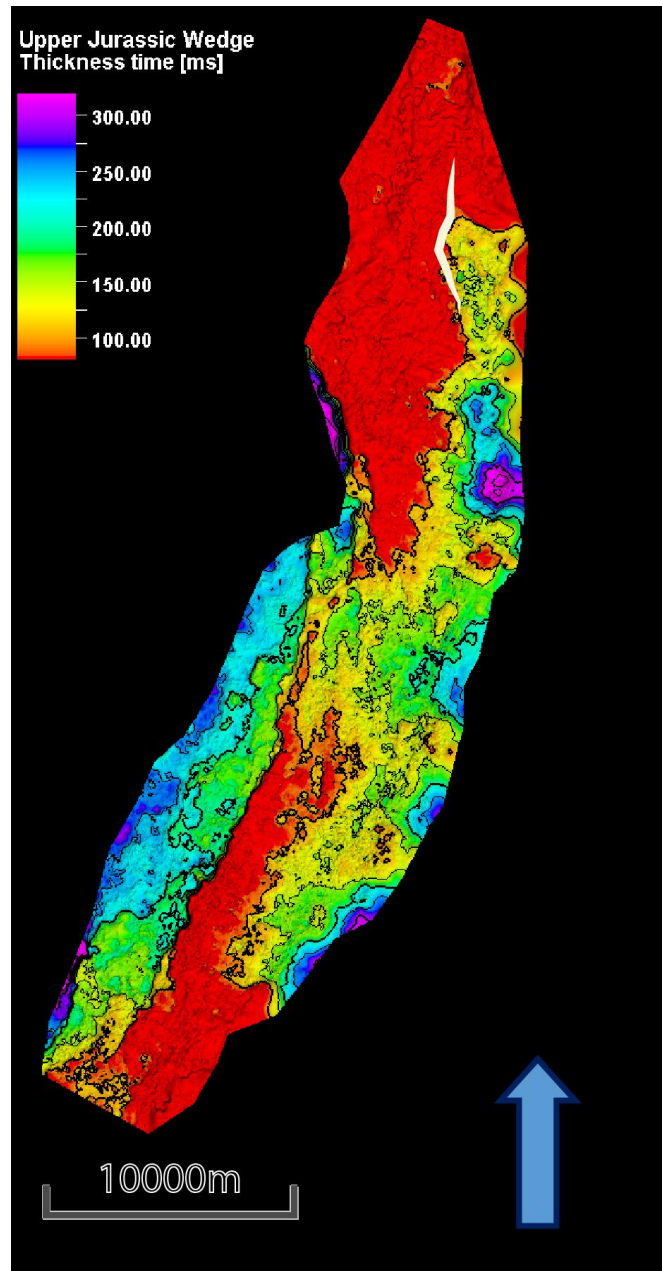


Figure 5.21: Figure 5.21 illustrates a TWTT thickness map of the Upper Jurassic Wedge. The contour lines has an increment of 50 ms where every second contour is bold. The white line indicates an underlying fault.

stratigraphy (>100 ms) of the Lower Draupne interval, west of this underlying fault, suggests that the structural configuration in this area has prevented a further westward deposition. The configuration has rather encouraged a southward deposition, resulting with the depression being filled.

5.2.4 Upper Draupne TWTT thickness map

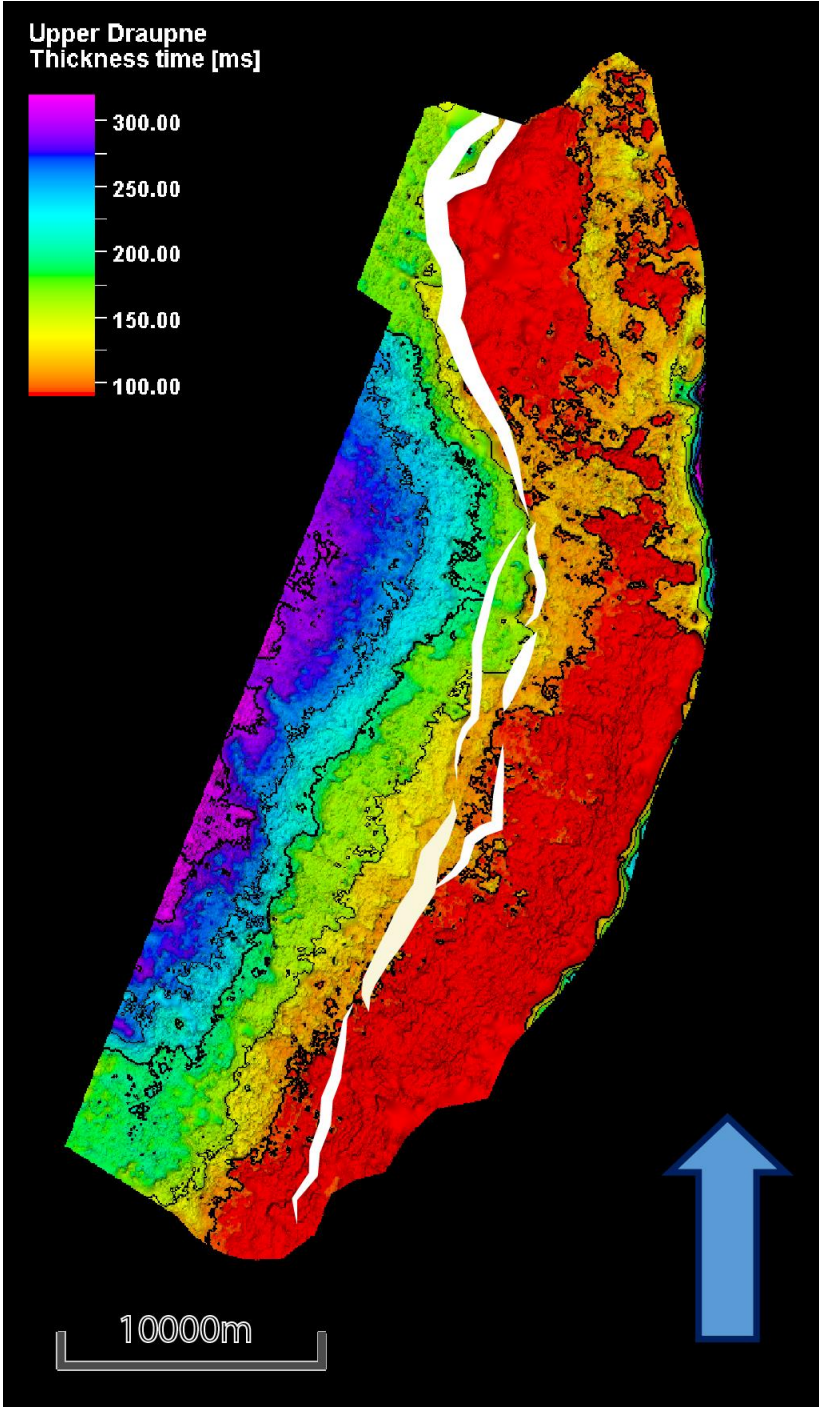


Figure 5.22: The figure illustrates a TWTT thickness map of the Upper Draupne formation. The contour lines has an increment of 50 ms, increasing from a value of 100 ms, where every second contour is bold. The white lines illustrates the strike of the underlying VSCF in addition to three faults in the footwall to the VSCF (Fig. 5.16). The thickness variation of the white lines illustrate variation in displacement.

Description

The Upper Draupne TWTT thickness map shows a thickness time ranging from <100 ms in the east to >300 ms in the west. The westward increase in thickness time is in general gradual throughout the entire time interval map. A north-south trending elongated area with a thickness of 100-150 ms is observed in the northeast.

Interpretation

Figure 5.22 shows that the thickness time in the area coinciding the VSCF footwall is in general <100 ms. A westward transition from the footwall to hanging wall of the VSCF shows a gradual increase in thickness time towards the western edge of the map. The north-south trending 100-150 ms area extends laterally towards the area of increased thickness time on the VSCF hanging wall, leaving an isolated area of <100 ms in the north.

Stratigraphic and seismic architecture

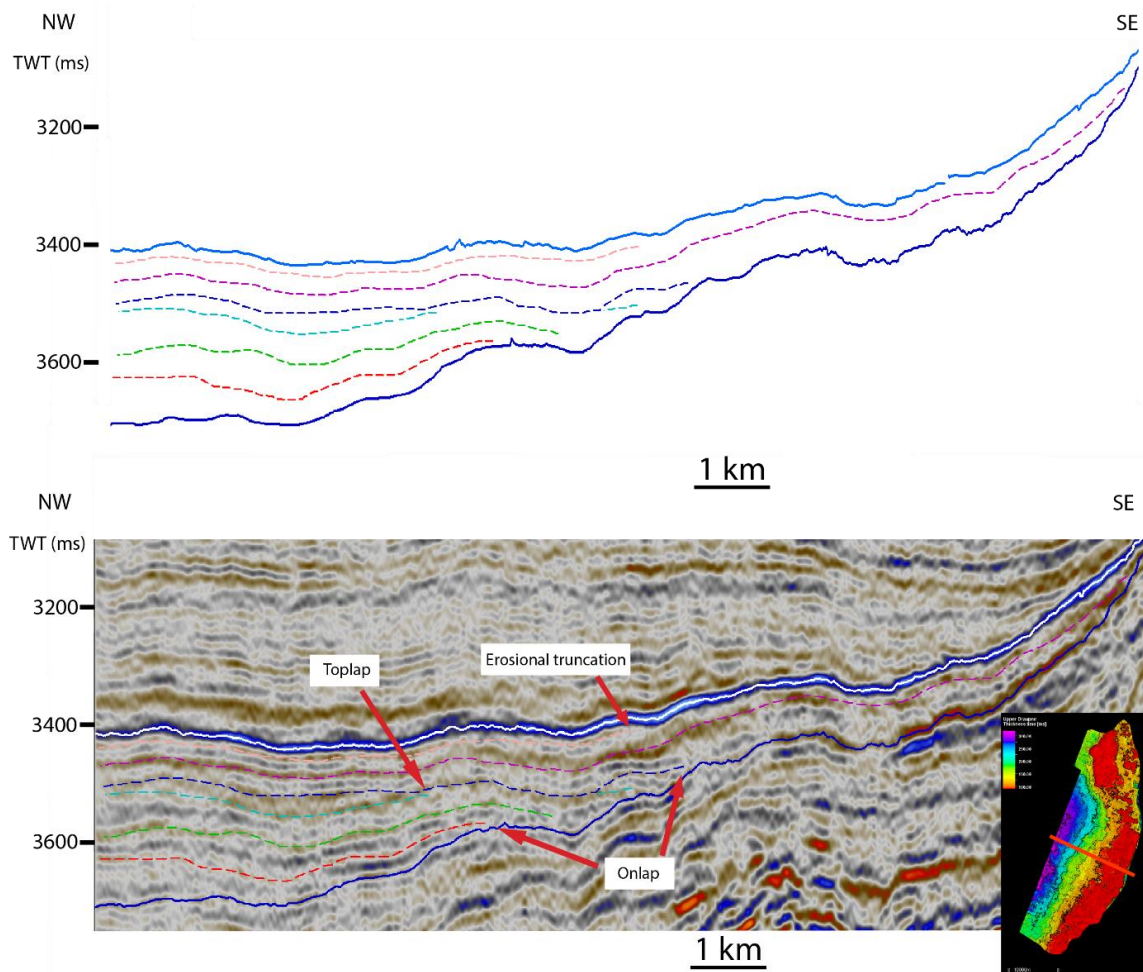


Figure 5.23: Cross-section of inline 17979 illustrating the Upper Draupne formation. Internal reflectors of positive amplitude are interpreted with dashed lines, showing their terminations. Onlaps, toplaps and erosional truncations are visible. The map in the lower right corner shows the position of the cross-section with the Upper Draupne time interval map as reference.

Figure 5.23 shows a cross-section of inline 17979 with focus on the Upper Draupne interval illustrated between the white and blue solid horizons. The horizons defines the BCU (white) and Internal Draupne (blue) surfaces, acting as the upper and lower bounding surfaces, respectively. The BCU is a high-amplitude trough, while the Internal Draupne is a medium to high-amplitude peak. Several dashed lines in different colors are reflecting internal terminating reflectors within the Upper Draupne interval. Onlapping terminations on the Internal Draupne surface are interpreted in addition to erosional truncations on the BCU surface. Internal toplap is interpreted. The internal reflectors of the Upper Draupne interval are parallel to sub-parallel, with a low to high value of amplitude, in general decreasing with increased travel time.

5.2.5 Lower Åsgard TWTT thickness map

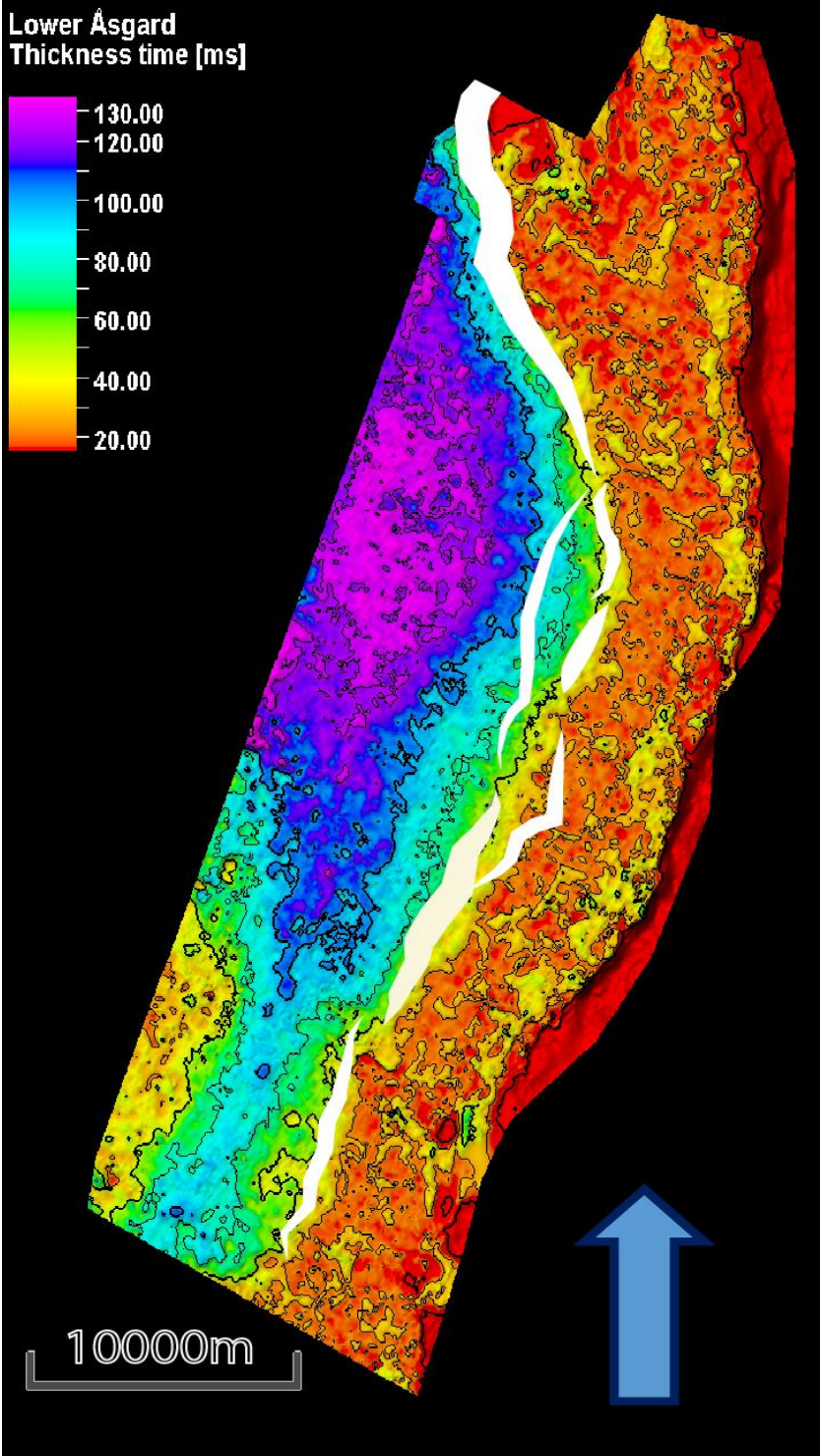


Figure 5.24: The figure illustrates a TWTT thickness map of the Lower Åsgard formation. The contour lines have an increment of 25 ms where every second contour is bold. The white lines illustrate the strike of the underlying VSCF (Fig. 5.16). The thickness variation of the white lines illustrate variation in displacement.

Description

The TWTT thickness map of the Lower Åsgard formation (Fig. 5.24) shows a general thickening trend towards the west, where the westward thickness increase is largest across the strike of the underlying VSCF. In the southwestern edge of the map a thinner area (<50 ms) is observed. A north-trending thickening area (25-50 ms) is observed in the northeastern edge of the study area.

Interpretation

The abrupt thickness increase across the strike of the underlying VSCF suggests that the underlying structural configuration is a controlling factor. In subchapter 5.1.5, infill of Lower Åsgard deposits in a north-trending depression in the northeastern part of the study area was suggested. This was based on a relief decrease in the depression from the BCU TWTT structure map (Fig. 5.5) to the Internal Åsgard TWTT structure map (Fig. 5.6). A north-trending thickening area (25-50 ms) coinciding with this depression is observed in Fig. 5.24, supporting this theory. The thin area in the southwestern edge (<50 ms) is coinciding with the elevated area described in subchapter 5.1.5 (Fig. 5.7). The decrease in preserved deposits on this high suggests a link to the uplift of this area. The observation of similar elevated topography in stratigraphically lower surfaces (Fig. 5.5, 5.6) suggests that the Lower Åsgard formation was deposited during or after the uplifting event.

Stratigraphic and seismic architecture

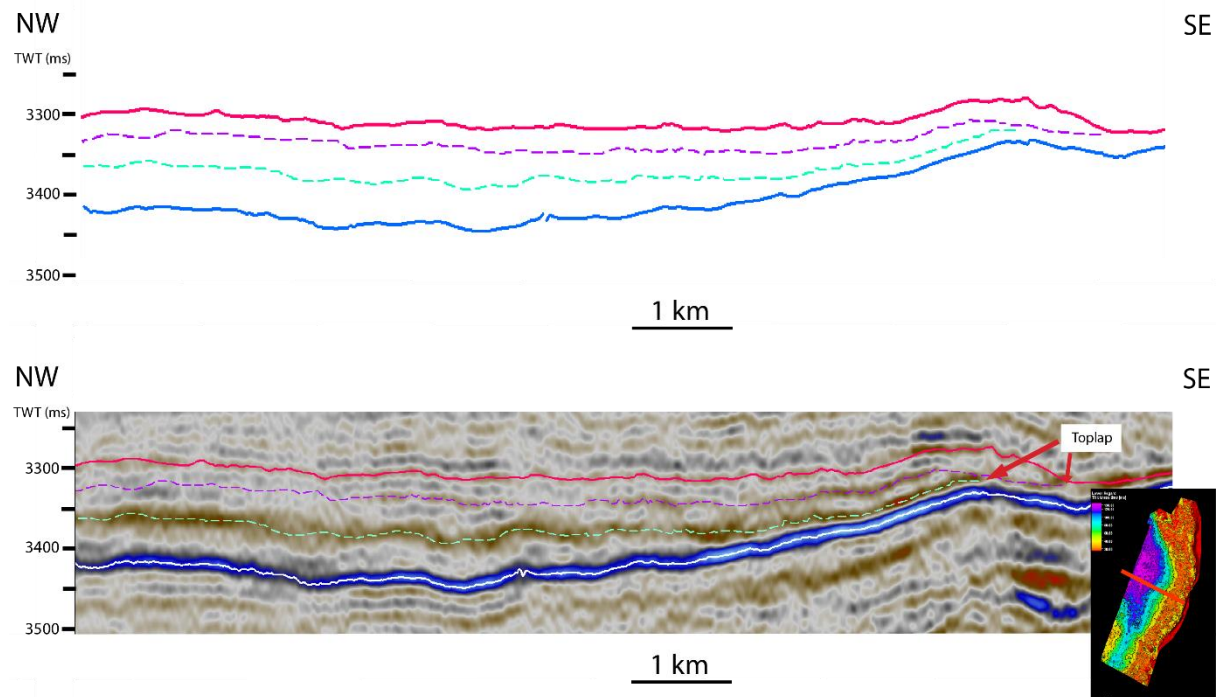


Figure 5.25: Cross-section of inline 18043 illustrating the Lower Åsgard formation. Internal reflectors of positive amplitude are interpreted with dashed lines, showing their terminations. Toplaps are the only visible reflector termination. The map in the lower right corner shows the position of the cross-section with the Lower Åsgard time interval map as reference.

Figure 5.25 shows a cross-section of inline 18043 with focus on the Lower Åsgard interval illustrated between the red and blue solid horizons. The horizons defines the Internal Åsgard (red) and BCU (blue) surfaces, acting as the upper and lower bounding surfaces, respectively. Internal Åsgard is a medium-amplitude peak, whereas the BCU is a high-amplitude trough. Two dashed lines in different colors are reflecting internal terminating reflectors within the Lower Åsgard interval. The reflectors shows, in addition to the Internal Åsgard surface, southeastern onlap terminations on the BCU surface. The internal reflectors of the Lower Åsgard interval are parallel in the entire cross-section, with a widening of the lowermost peak towards the northwest. The peaks in the interval shows in general medium amplitude values.

5.2.6 Upper Åsgard TWTT thickness map

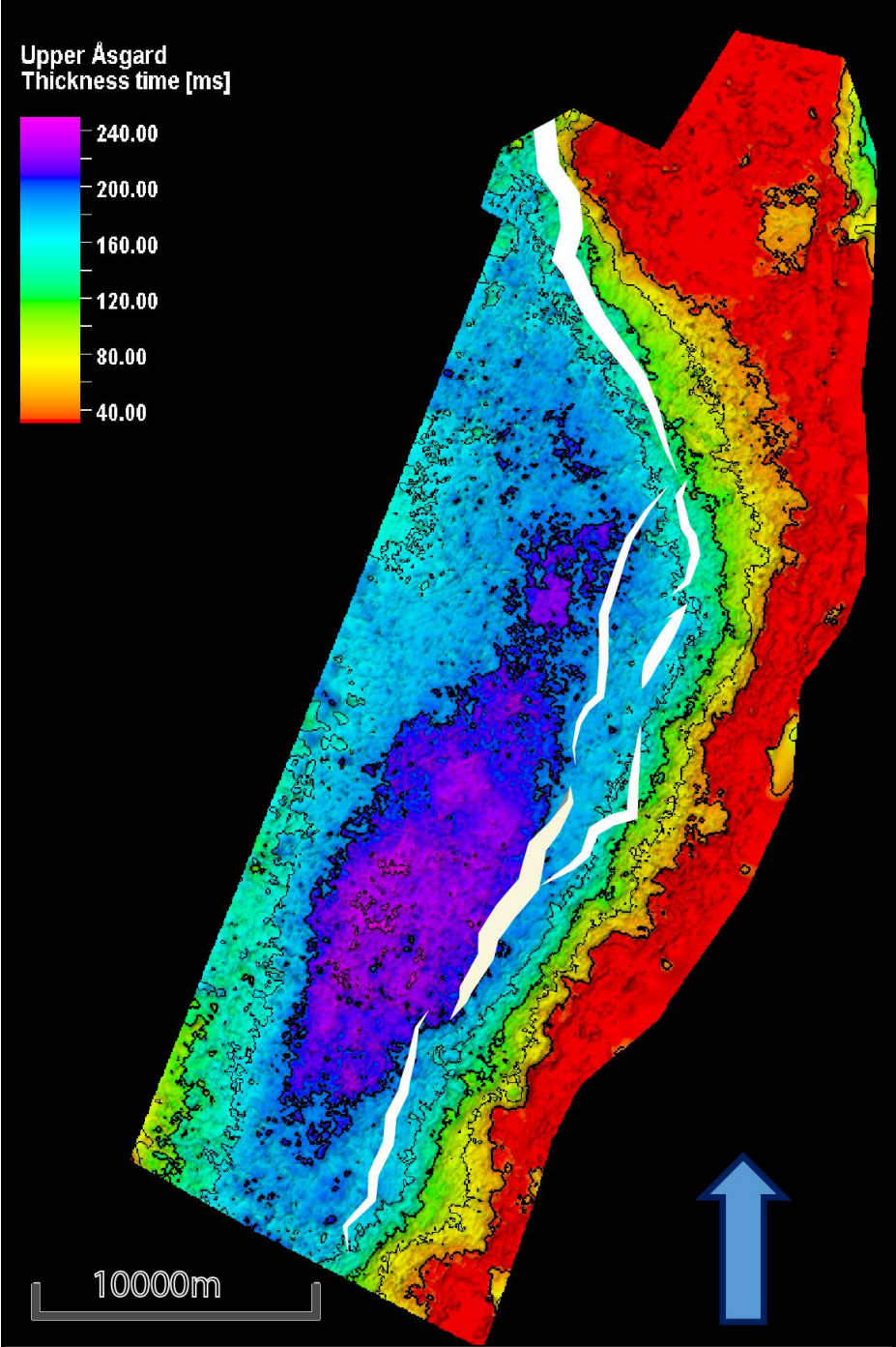


Figure 5.26: This figure illustrates a TWTT thickness map of the Upper Åsgard formation. The contour lines has an increment of 40 ms, increasing from a value of 40 ms, where every second contour is bold. The white lines illustrates the strike of the underlying VSCF (Fig. 5.16). The thickness variation of the white lines illustrate variation in displacement.

Description

The Upper Åsgard TWTT thickness map (Fig. 5.26) shows a main depocentre in the hanging-wall to the underlying VSCF. The eastern and northern part of the interval has limited thickness (<40 ms), and the westerly increase in thickness coincide with the strike of the VSCF.

Interpretation

The thickening trend towards the west is remained in the Upper Åsgard TWTT thickness map (Fig. 5.26), and the pattern between the thickening trend and the strike of the underlying VSCF suggests that the distribution of preserved Upper Åsgard deposits is controlled by the underlying structural configuration. The Lower Åsgard TWTT thickness map (Fig. 5.25) shows a general lack of preserved deposits (<50 ms thickness) on the footwall to the underlying VSCF, whereas Upper Åsgard deposits of a 40-120 ms thickness are preserved in the footwall to the VSCF. This suggests that the underlying structural configuration has less influence in controlling the distribution of Upper Åsgard deposits compared to Lower Åsgard deposits. The main depocentre is located in the central part of the study area, translating southwards from the main depocentre in the Lower Åsgard interval (Fig. 5.25). The thinning area in the southwestern edge of the map (Fig. 5.26) suggests that the underlying structural configuration in the area has maintained an impact on the distribution of preserved Upper Åsgard deposits.

Stratigraphic and seismic architecture

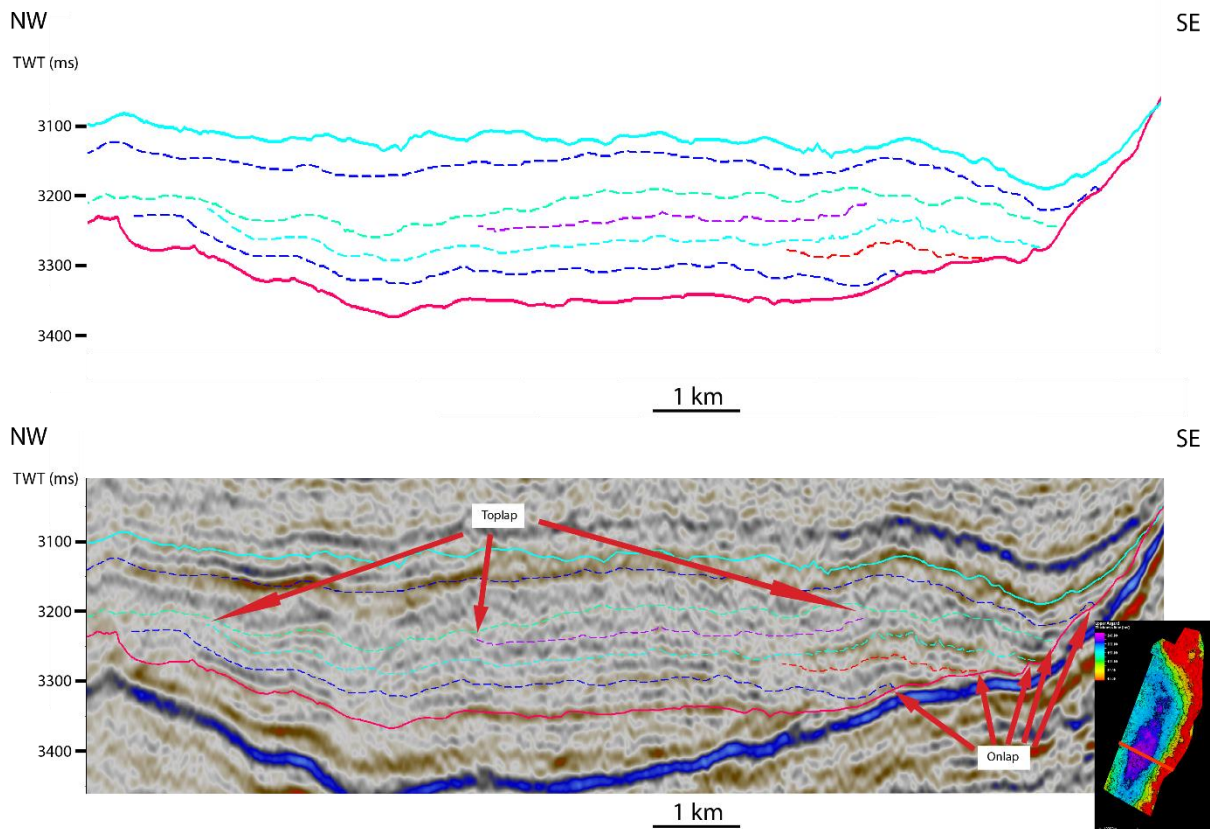


Figure 5.27: Cross-section of inline 17232 illustrating the Upper Åsgard formation. Internal reflectors of positive amplitude are interpreted with dashed lines, showing their terminations. Onlaps and toplaps are visible. The map in the lower right corner shows the position of the cross-section with the Upper Åsgard time interval map as reference.

Figure 5.27 shows a cross-section of inline 17232 in the dataset, with the Upper Åsgard interval illustrated between the cyan and red solid horizons. The horizons defines the Internal Åsgard surface (red) and Top Åsgard surface (cyan), acting as the lower and upper bounding surface of the Upper Åsgard interval, respectively. Both the Internal Åsgard and the Top Åsgard surfaces are peaks of medium amplitude. Towards the southeast, several terminating reflectors illustrated as dashed lines, are observed within the Upper Åsgard interval. These reflectors are together with the upper bounding surface onlapping the lower bounding surface. Internal toplaps are interpreted. The overall seismic architecture of the Upper Åsgard interval shows reflectors of medium to low amplitude with limited lateral variation, and increasing continuity with travel time.

5.2.7 Rødby + Sola TWTT thickness map

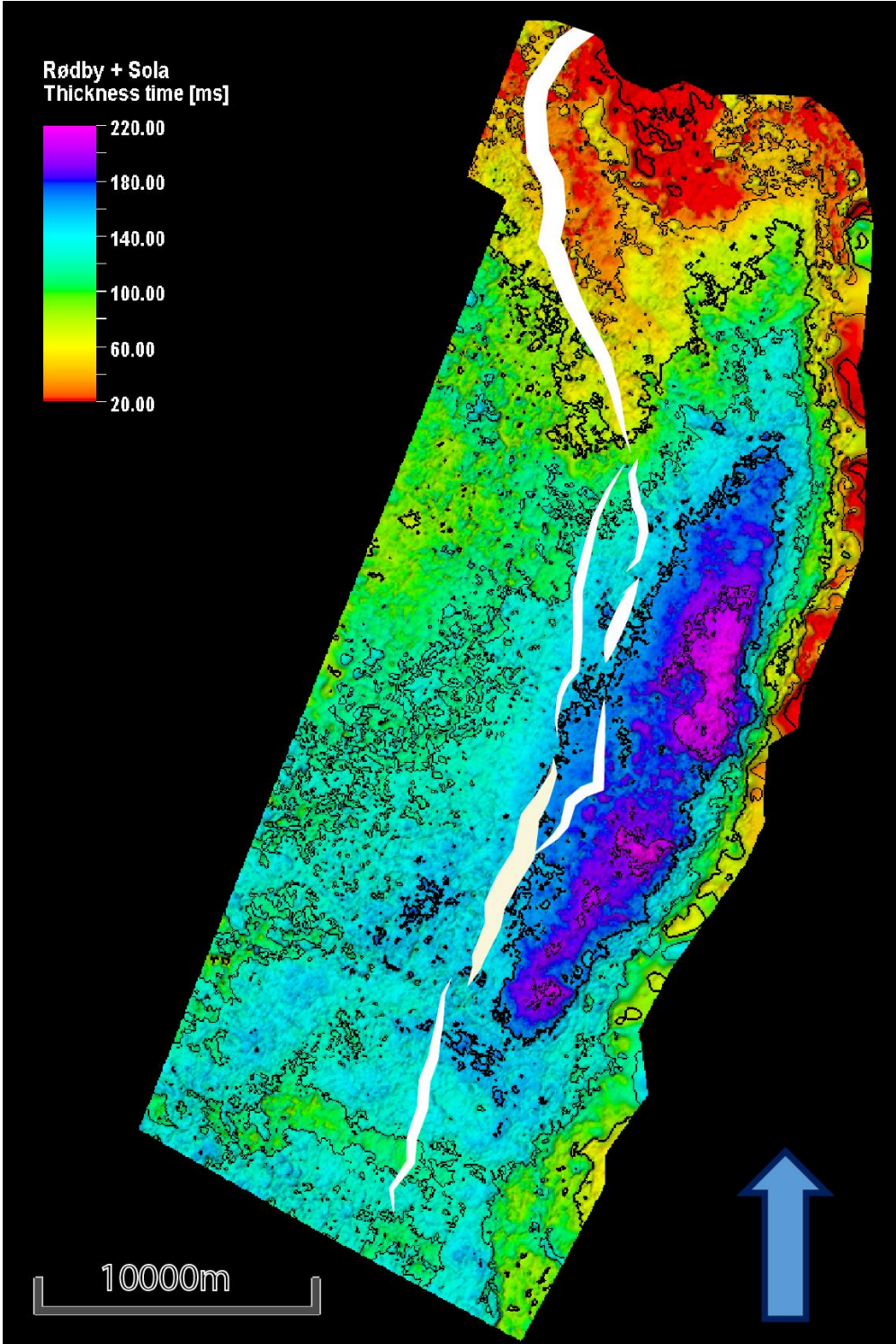


Figure 5.28: The figure illustrates a TWTT thickness map of the Rødby and Sola formations combined. The contour lines has an increment of 40 ms where every second contour is bold. The white lines illustrates the strike of the underlying VSCF (Fig. 5.16). The thickness variation of the white lines illustrate variation in displacement.

Description

The Rødby+Sola TWTT thickness map shows a main depocentre (>160 ms thickness) in the central part of the footwall to the underlying VSCF, with a northward trend. The interval is in the footwall to the northern segment of the VSCF in general thin (<80 ms thickness).

Interpretation

The depocentre of the Rødby+Sola TWTT thickness map in the footwall to the VSCF has a similar trend as the strike of the underlying VSCF and VSEF. This suggests that the underlying structural configuration controls the distribution of preserved Rødby+Sola deposits. The location of the depocentre differs from in the Lower- and Upper Åsgard TWTT thickness maps (Fig. 5.24, 5.26), where the depocentres are located in the hanging-wall to the VSCF. They show a general thickening of the intervals towards the west, while the Rødby+Sola TWTT thickness map (Fig. 5.28) shows a general thinning towards the west. The thickening trends suggests a sediment source in the Rødby+Sola interval in the east, and a main source in the Åsgard intervals located in the west. Subchapter 5.1.7 (Fig. 5.8) suggests that a depression in the northeastern part of the study area was fully filled in by Rødby+Sola deposits. In the footwall to the underlying VSCF, Figure 5.28 shows a northern trend of Rødby+Sola deposits more than 80 ms thick. This area coincides with the underlying depression observed in Figure 5.2-5.7, and supports the theory that it was fully filled in by Rødby+Sola deposits.

Stratigraphic and seismic architecture

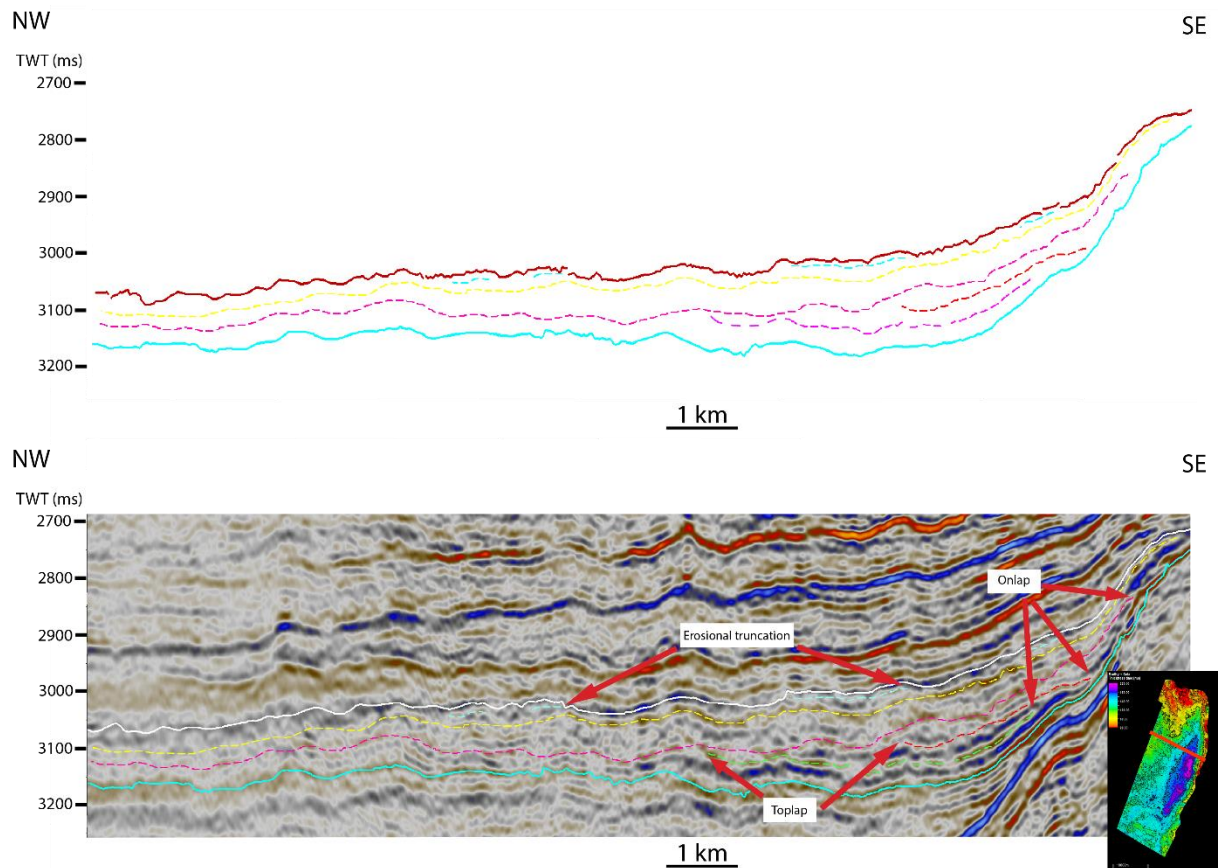


Figure 5.29: Cross-section of inline 18432 illustrating the Rødby+Sola interval. Internal reflectors of positive amplitude are interpreted with dashed lines, showing their terminations. Onlaps, toplaps and erosional truncations are visible. The map in the lower right corner shows the position of the cross-section with the Rødby+Sola time interval map as reference.

Figure 5.29 shows a cross-section of inline 18432, with focus on the Rødby+Sola interval illustrated between the white and cyan solid horizons. The horizons defines the Top Rødby (white) and the Top Åsgard (cyan) surfaces, acting as the upper and lower bounding surfaces, respectively. Top Rødby is a medium to high-amplitude trough with signs of decreasing seismic energy towards the northwest. The Top Åsgard horizon is a reflector of medium amplitude, with the same decreasing trend in energy. Dashed lines of various coloring are reflecting internal terminating reflectors within the Rødby+Sola interval. The reflectors onlap the underlying bounding surface in a northeasterly direction, and shows internal toplap. The uppermost dashed reflector (cyan) shows erosional truncations related to the upper bounding surface. Both of the bounding surfaces onlap the blue BCU horizon. The amplitude of the reflectors is in general increasing towards the southeast, while the continuity is similar throughout the entire cross-section

5.2.8 Svarte TWTT thickness map

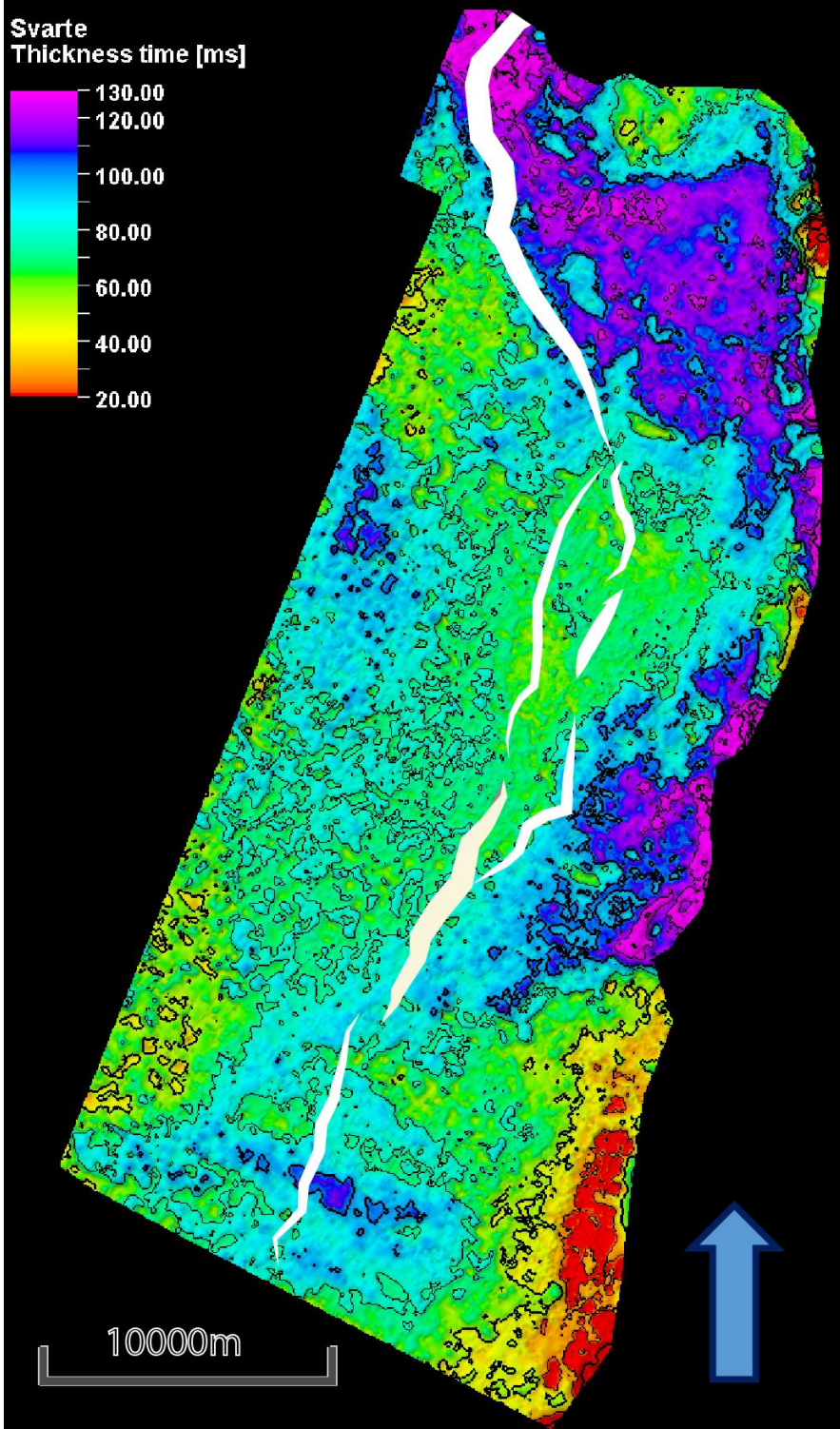


Figure 5.30: The figure illustrates a TWTT thickness map of the Svarte formation. The contour lines have an increment of 25 ms where every second contour is bold. The white lines illustrate the strike of the underlying VSCF (Fig. 5.16). The thickness variation of the white lines illustrates variation in displacement.

Description

The Svarte TWTT thickness map shows two separate depocentres of >125 ms thickness, both located in the footwall to the underlying VSCF. No distinct thickness trend can be observed in Figure 5.30.

Interpretation

The Svarte TWTT thickness map (Fig. 5.30) shows an in general thin interval with limited lateral thickness variations, which may prevent the formation from having one distinct depocentre as seen in stratigraphically lower intervals (Fig. 5.18, 5.20, 5.22, 5.24, 5.26, 5.28). A significant change in gross depositional environment in upward stratigraphic succession could have influenced the distribution pattern. The thickest areas (>125 ms thickness) are located in the footwall to the underlying VSCF, suggesting that the underlying structural configuration has an influence on the distribution of the preserved Svarte deposits. The lack of a concentrated depocentre suggests that the underlying structural configuration has less influence on the distribution of the preserved Svarte deposits, than in stratigraphically lower intervals.

Stratigraphic and seismic architecture

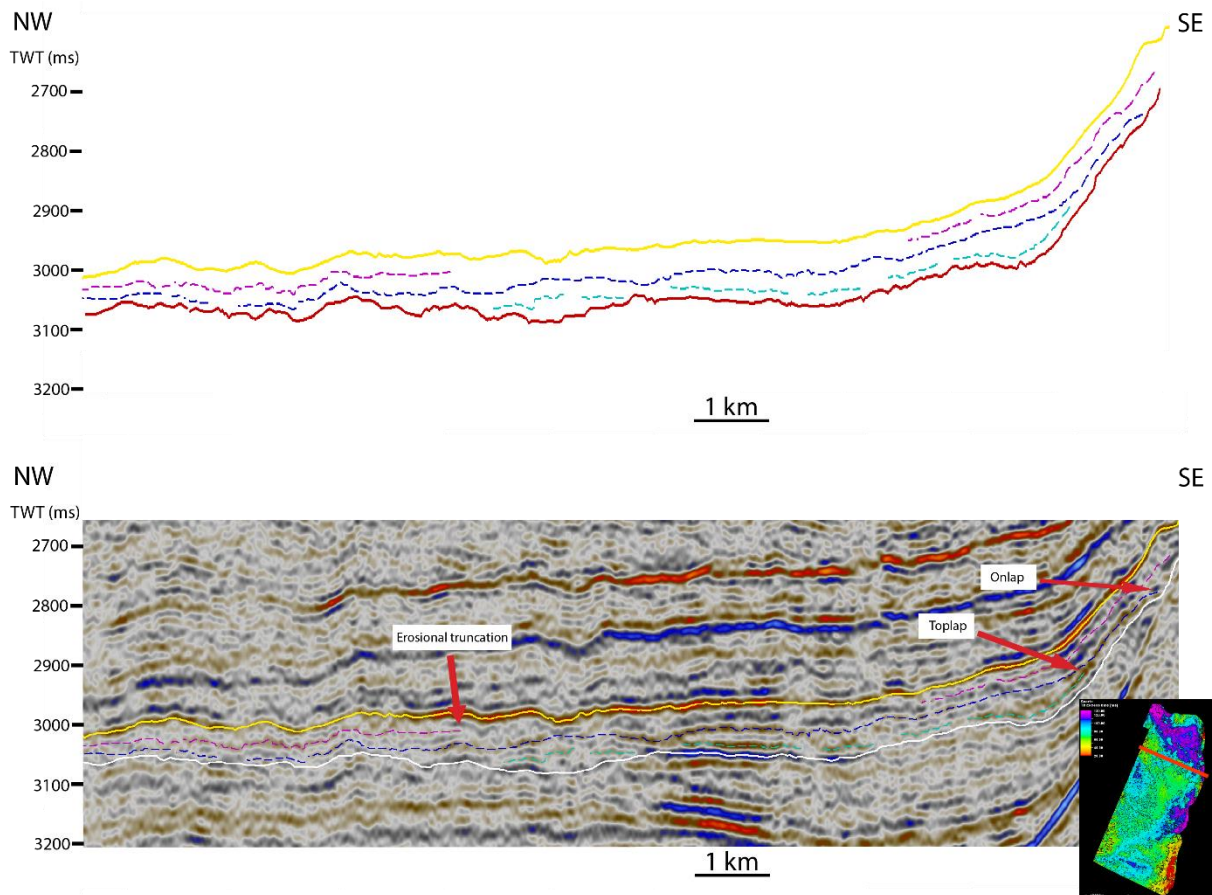


Figure 5.31: Cross-section of inline 18715 illustrating the Svarte formation. Internal reflectors of positive amplitude are interpreted with dashed lines, showing their terminations. Onlaps, toplaps and erosional truncations are visible. The map in the lower right corner shows the position of the cross-section with the Svarte time interval map as reference.

Figure 5.31 shows a cross-section of inline 18715 with focus on the Svarte fm interval illustrated between the yellow and white solid horizons. The horizons defines the Top Svarte (yellow) and the Top Rødby (white) surfaces, acting as the upper and lower bounding surfaces, respectively. Top Svarte is a high amplitude peak, whereas the Top Rødby is a medium-high amplitude trough. Several dashed lines in different colors are reflecting internal terminating reflectors within the Svarte fm interval. The reflectors shows erosional truncation related to the Top Svarte surface and signs of onlap on the Top Rødby surface. Internal southwestern toplap is interpreted within the interval. The internal reflectors of the Svarte fm interval are subparallel in the southeastern part, with lack of continuity towards the northwest. The peaks in the interval shows everything from high to low amplitude, while the troughs reflects moderate to low amplitude.

5.2.9 Blodøks TWTT thickness map

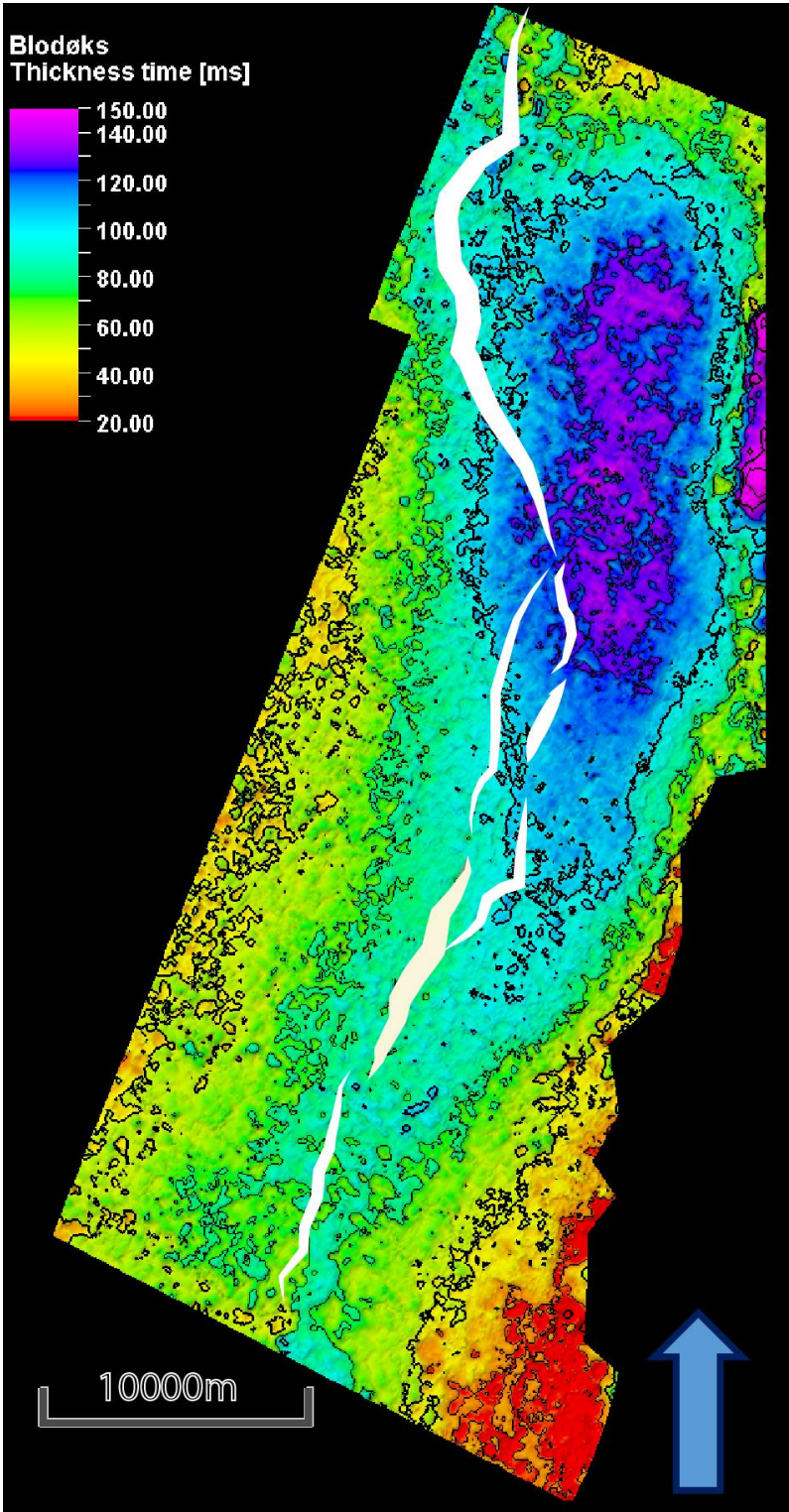


Figure 5.32: The figure illustrates a TWTT thickness map of the Blodøks formation. The contour lines has an increment of 25 ms where every second contour is bold. The white lines illustrates the strike of the underlying VSCF (Fig. 5.16). The thickness variation of the white lines illustrate variation in displacement.

Description

The Blodøks TWTT thickness map shows a main depocentre in the northern part of the map with a thickness of 125-150 ms. The map shows a gradual thinning trend towards the southwest.

Interpretation

The location of the depocentre in the Blodøks TWTT thickness map (Fig. 5.32) shows a northward depocentre translation compared to the Rødby+Sola thickness map (Fig. 5.28). The depocentre is trending north-south across the strike of the underlying VSCF. This suggests that the underlying structural configuration has limited to no influence on the distribution of the preserved Blodøks deposits.

Stratigraphic and seismic architecture

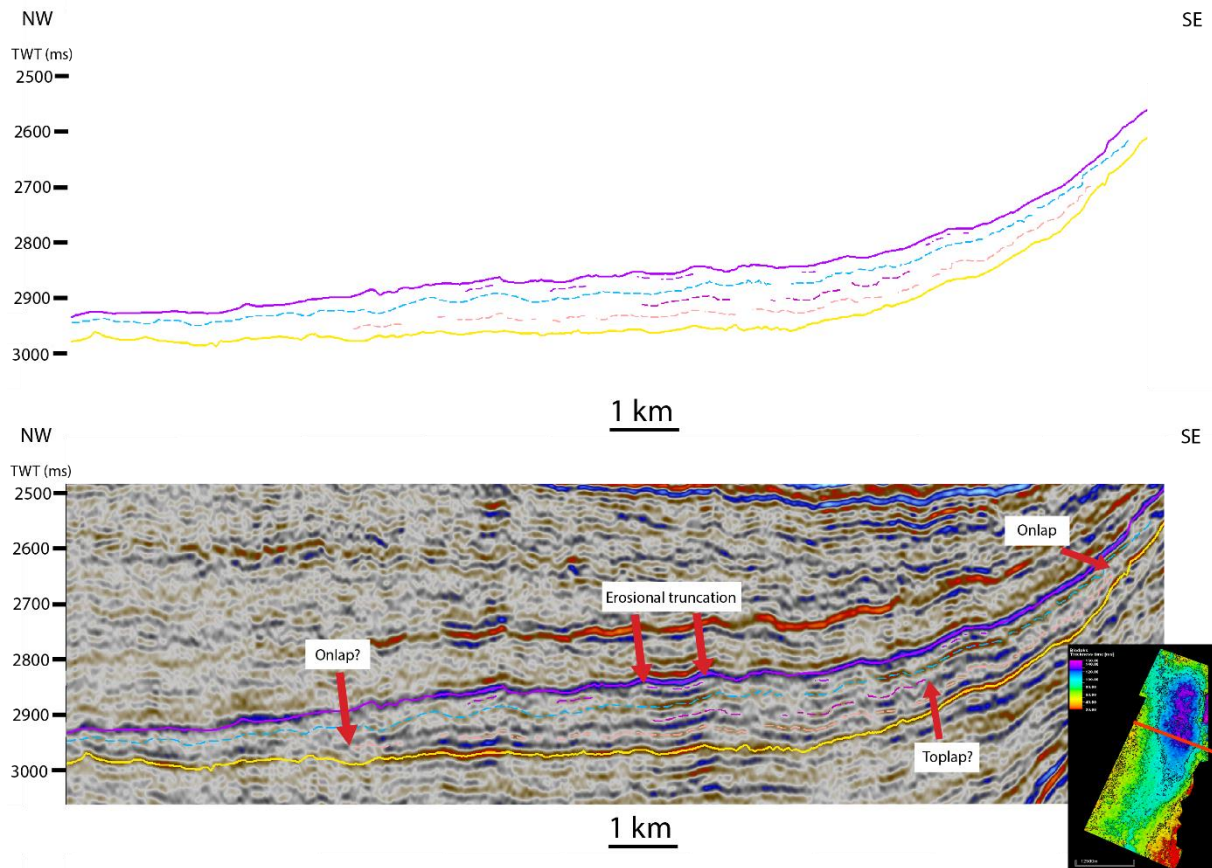


Figure 5.33: Cross-section of inline 19682 illustrating the Blodøks formation. Internal reflectors of positive amplitude are interpreted with dashed lines, showing their terminations. Onlaps, toplaps and erosional truncations are visible. The map in the lower right corner shows the position of the cross-section with the Blodøks time interval map as reference.

Figure 5.33 shows a cross-section of inline 19682 with focus on the Blodøks interval illustrated between the purple and yellow solid horizons. The horizons defines the Top Blodøks (purple) and the Top Svarte (yellow) surfaces, acting as the upper and lower bounding surfaces, respectively. Top Blodøks is a high to medium-amplitude trough, whereas the Top Svarte is a high-amplitude peak. Several dashed lines in different colors are reflecting internal terminating reflectors within the Blodøks interval. The reflectors onlap the Top Svarte surface in both a northwestern and southeastern direction, but the northwestern onlap might be a result of laterally thinning and fade below seismic resolution. Internal toplap is interpreted, but could also be a result of thinning and fade below seismic resolution. Erosional truncations related to the Top Blodøks surface is interpreted. The reflectors of the Blodøks interval are low to medium continuous, with an area of clearly lower continuity in the central part (lack of seismic energy/noise). The reflectors are peaks and troughs of moderately low amplitude.

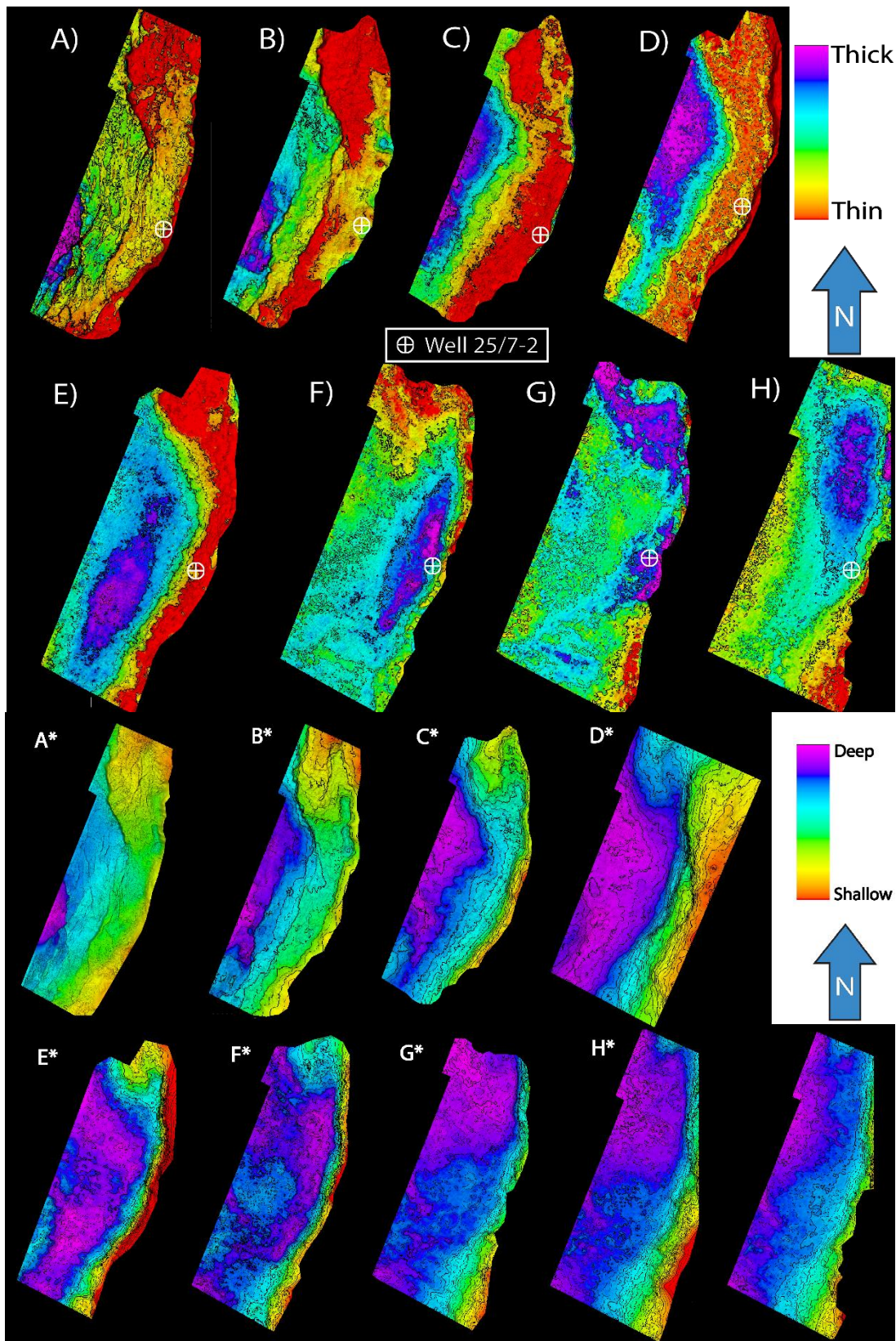


Figure 5.34: The figure shows every TWTT thickness maps (A-H) and TWTT structure maps (A*-H*) from chapter 5. They are sorted in an upward stratigraphic succession, with the deepest, A/A* Heather interval/Top Hugin to the top, H/H* Blodøks interval/Top Svarte. The color legend is not absolute and illustrates only relative thickness/depth variations in every map. The maps are not to scale, and the location of well 25/7-2 is used as reference point.

5.3 Wheeler diagrams

This chapter presents the workflow of generating the Wheeler diagrams, and the resulting three Wheeler diagrams, made from selected cross-sections in the study area. These are generated from TWTT thickness maps, their internal architecture, and the time span between top and base of every interval. Diagram 1 and 2 covers the northern part of the study area, while Diagram 3 covers the southern part.

5.3.1 Diagram 1

Figure 5.36 illustrates the cross-section selected for the generation of Diagram 1. It covers the VSCF hanging wall in the northwestern end, and a structural high between the VSCF hanging wall and the northern part of the N-S trending depression in the southeast.

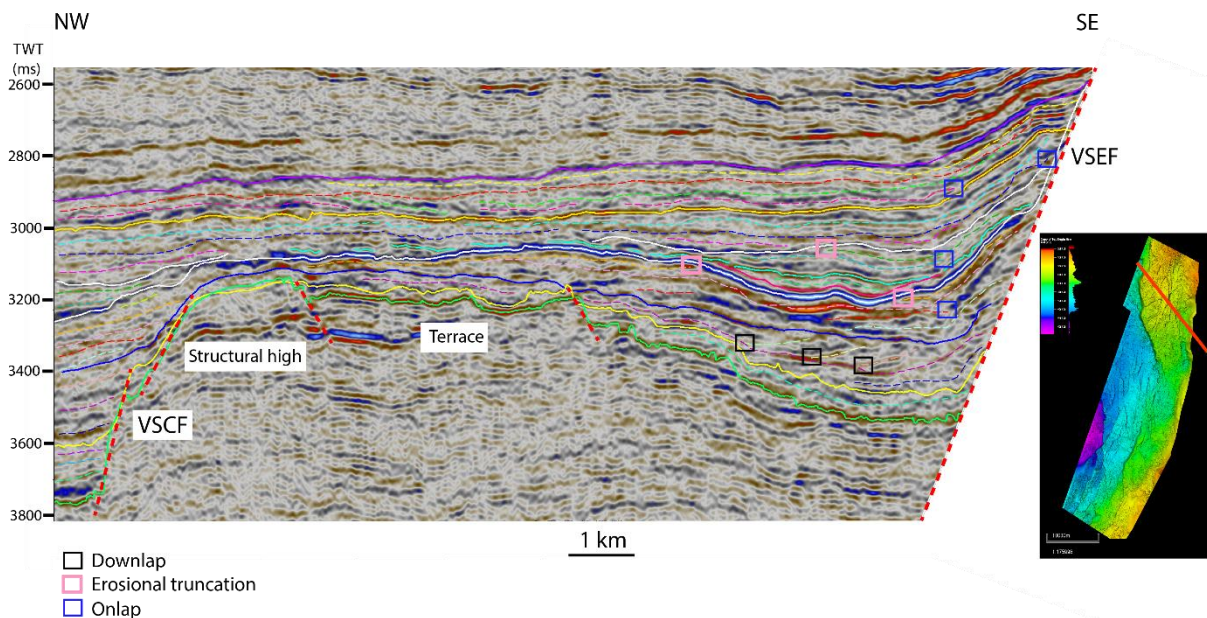


Figure 5.35: Cross-section used for generation of Diagram 1 in this study. Solid lines reflect the surfaces described in chapter 5.1. Stippled lines reflect internal reflectors. The red, stippled lines illustrate faults. Top Hugin time structure map is used as reference, highlighting the cross-section with the red line.

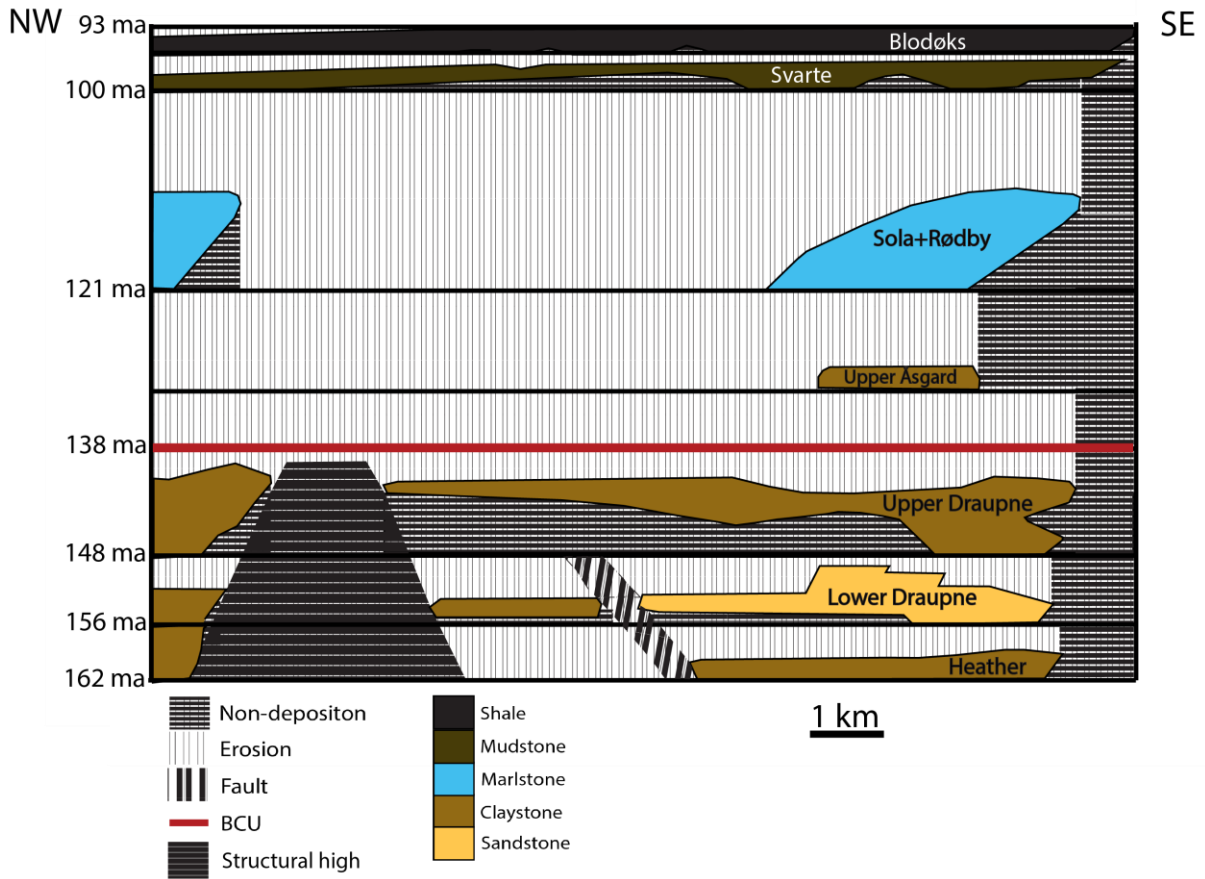


Figure 5.36: Diagram 1. Black, horizontal lines illustrates timelines corresponding to the age of the formation tops used in this study. The colored areas reflects the lateral extension of every formation related to time. Every interval onlap the vertically underlying interval, for instance in the northwestern end Svarte fm onlap the Rødby+Sola fm interval, while the Svarte fm onlap the Upper Draupne fm in the central part. The lithologies are highly generalized, where the clay-rich Lower Draupne in the VSEF hanging wall are referred to as a sandstone because of its interbedded sandstones (NPD,2018).

Description

Figure 5.36 illustrates the Wheeler diagram generated from Figure 5.35. The terminating relationship between the individual intervals are laterally visualized in the figure. Diagram 1 shows laterally missing, with the Lower Åsgard interval entirely missing, and the Upper Åsgard represented with a thin unit of limited lateral presence. In the central part of the cross-section, a structural high of opposite dipping normal faults is observed (Fig. 5.35). This structural configuration suggests that this is a horst, and the presence of this elevated high prevents preservation of deposits. Whether the absence of deposits on the structural high is a result of erosion or non-deposition is hard to estimate, based on interpretation of this diagram alone. The lack of deposits is visible both in Figure 5.35 and Figure 5.36, where Figure 5.36 shows that deposits of the Svarte interval onlap pre-Cretaceous strata.

Because of the absence of Lower Cretaceous strata on the structural high, it is hard to use the Wheeler diagram alone to determine whether this is a consequence of erosion or if this structural high was subject to non-deposition in the Early Cretaceous. Two southeastward dipping normal faults are observed in Fig. 5.35 between the structural high to the northwest and the VSEF hanging wall depression to the southeast. These are bounding a shallow SE-dipping terrace area, which is the southernmost end of the Heimdal Terrace (Fig. 3.1). On this downfaulted terrace Diagram 1 (Fig. 5.36) shows that significant amount of Lower- and Upper Draupne deposits are preserved. The Upper Draupne deposits are overlain by deposits of the Svarte interval, which means that deposits of the Lower Cretaceous (Lower-, Upper Åsgard and Rødby+Sola) are absent. Deposits of the Heather interval are preserved in the hanging wall of the southeasternmost terrace-bounding fault, which differs from the footwall where Heather deposits are missing. This indicates that the fault has been a controlling factor on the preservation of Heather deposits in the northern part of the study area. A set of dipping reflectors are observed in the southeastern hanging wall wedge within the Lower Draupne interval (Fig. 5.36). These are interpreted as downlaps on a stratigraphically older Lower Draupne reflector. This interpretation suggests that the controlling factor providing the interpreted downlaps was not active in the early stage of the Lower Draupne interval. The Upper Draupne reflectors terminates in general on the Internal Draupne surface towards the northwest, which is interpreted as an onlapping surface. This observation and interpretation shows that the preserved Upper Draupne deposits are in general younger towards the northwest (Fig. 5.36). The BCU surface cuts Upper Draupne reflectors, interpreted as erosional truncations, indicating that Upper Draupne deposits was subject to erosion. Preserved Lower Cretaceous strata (Upper Åsgard, Rødby+Sola) is observed in the VSEF hanging wall depression (Fig. 5.35). This suggests that the underlying depression was not leveled before later in the Cretaceous, while the Åsgard and Rødby+Sola deposits was not preserved on the erosion-prone structural high. The Top Rødby surface cuts reflectors of the Rødby+Sola interval, suggesting that this interval was subject to erosion. The interval shows a general southeastward onlapping trend. Reflectors in the early stage of the Svarte interval are terminating towards the underlying structural high, suggesting that older Svarte strata deposited on the structural high was subject to erosion. The Top Blodøks

surface, cuts the youngest reflector within the Blodøks interval, suggesting that the Top Blodøks surface was acting as an erosional surface.

5.3.2 Diagram 2

Figure 5.37 illustrates the cross-section selected for the generation of Diagram 2. It covers the hanging- and the footwall of the northern VSCF, including the southern part of the VSEF hanging-wall depression.

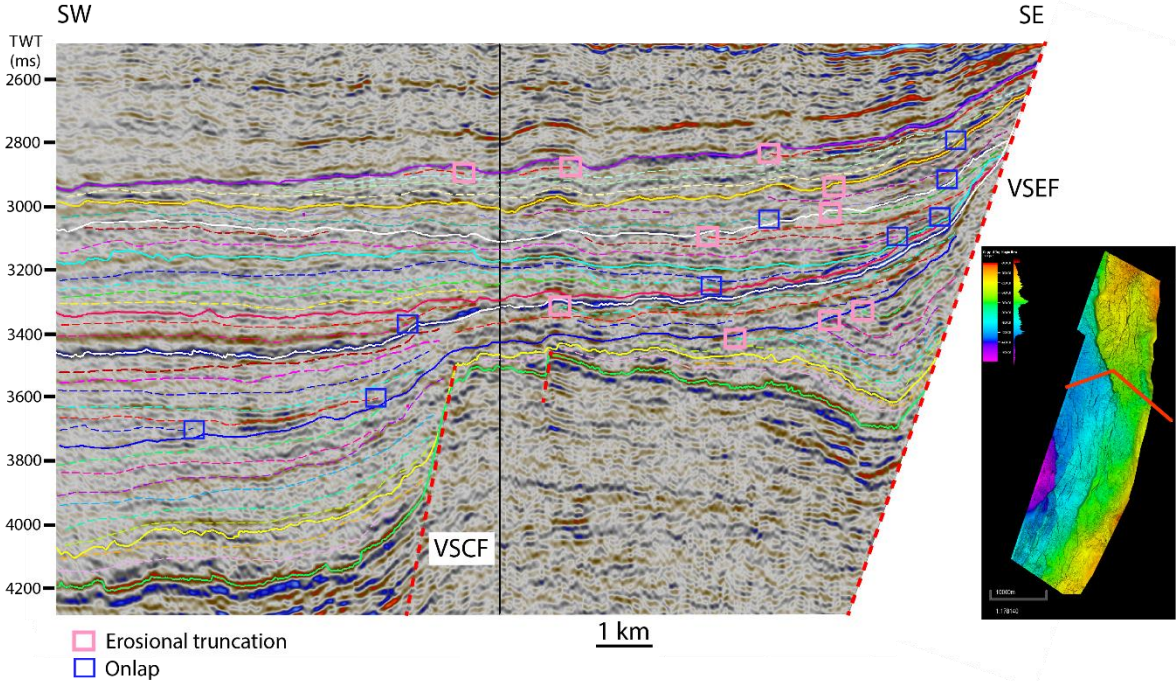


Figure 5.37: Cross-section used for generation of Diagram 2 in this study. Solid lines reflects the surfaces described in chapter 5.1. Stippled lines reflects internal reflectors. The red, stippled lines illustrates the VSCF and VSEF. Top Hugin time structure map is used as reference, highlighting the cross-section with the red line, where the black vertical line reflects the bend in the cross-section.

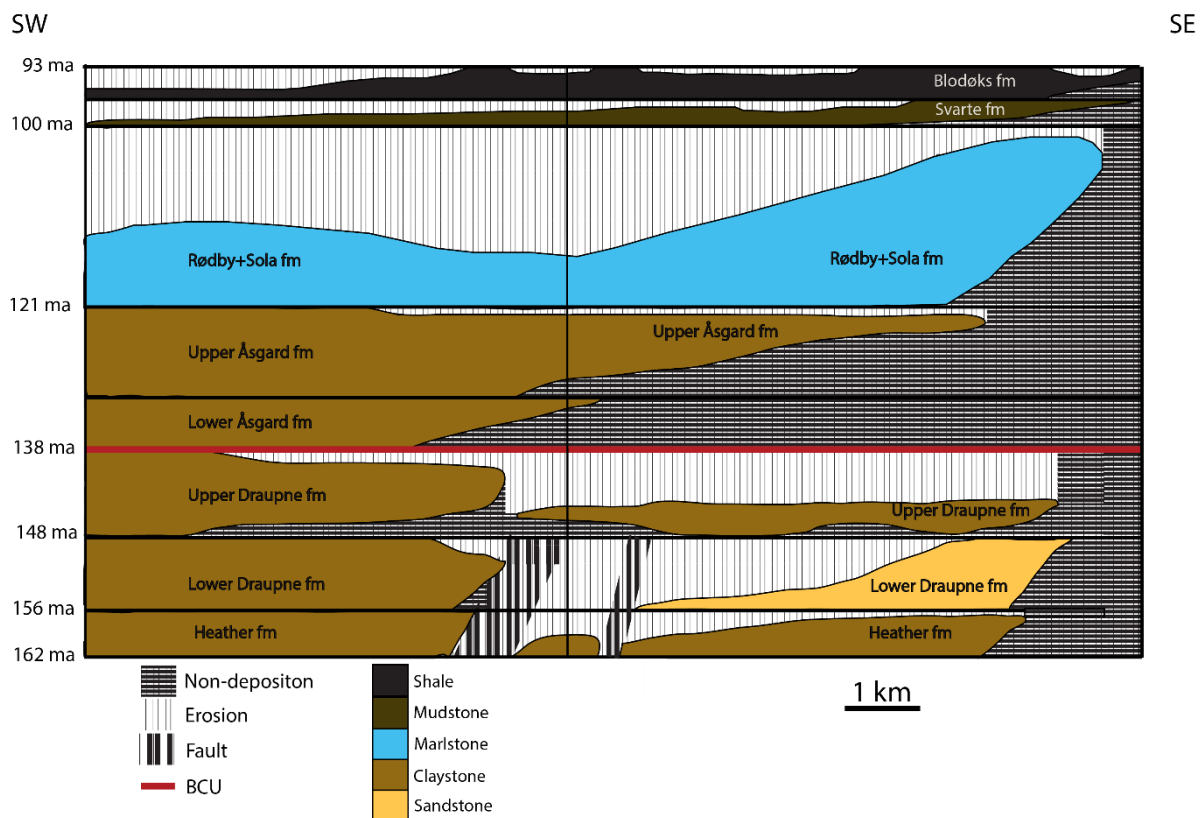


Figure 5.38: Diagram 2. Black, horizontal lines illustrates timelines corresponding to the age of the formation tops used in this study. The colored areas reflects the lateral extension of every formation related to time. The lithologies are highly generalized, where the clay-rich Lower Draupne in the VSEF hanging wall are referred to as a sandstone because of its interbedded sandstones (NPD,2018).

Description

Figure 5.38 illustrates the Wheeler diagram generated from Figure 5.38. The terminating relationship between the individual intervals are laterally visualized in the figure. Two southwestward dipping faults are observed (Fig. 5.37). Offset of the Top Heather and the Internal Draupne surfaces are observed across the faults. Only a minor amount of Heather deposits is preserved in the terrace zone between the faults, suggesting erosion of Heather and Lower Draupne deposits in this area. The VSEF hanging wall depression is mainly filled with Lower Draupne deposits (Fig. 5.37). The internal reflectors of the Lower Draupne in this area are synclinal where the southwestern limb is cut by the Internal Draupne surface. This observation suggests erosion of the Lower Draupne deposits, an observation that is also seen in the VSCF hanging wall. An abrupt southeasterly thinning of the Upper Draupne interval is observed in the immediate VSCF footwall (Fig. 5.37). No

offset of the Upper Draupne is observed, but the abrupt thinning suggests that it is controlled by the underlying structural configuration. This interpretation suggests that the Upper Draupne deposits are in general younger in the VSCF hanging wall, than in the footwall. Wheeler diagram 2 (Fig. 5.38) shows that the youngest stratigraphy preserved in the hanging wall is eroded on the footwall. The preserved Upper Draupne deposits onlap the Internal Draupne surface towards the southeast, suggesting that the interval is filled from the southwest. The Lower- and Upper Åsgard deposits shows a similar southeastward onlap on underlying bounding surfaces, which results in gradually younger preserved deposits towards the southeast. Deposits of the Upper Åsgard interval are present towards the VSEF, where the interval onlap Upper Draupne strata directly, exposing a large time gap of absent strata (Fig. 5.38). Deposits of the Rødby+Sola interval shows the same southeastern onlap on underlying strata. Interpreted erosional truncation between the Top Rødby surface and Rødby+Sola reflectors leaves a large erosional time gap of the younger Rødby+Sola deposits. Southeastward onlap on underlying strata is observed in both the Svarte interval and the Blodøks interval. The youngest reflectors in both intervals are cut by the overlying surface, interpreted as erosional truncations. This interpretation suggests that the Top Svarte and the Top Blodøks surface act as erosional surfaces, and have eroded gradually older strata towards the southwest (Fig. 5.38).

5.3.3 Diagram 3

Figure 5.39 illustrates the cross-section selected for the generation of Diagram 3. It covers the hanging- and the footwall of the southern VSCF, in addition to downfaulted areas towards the southwest.

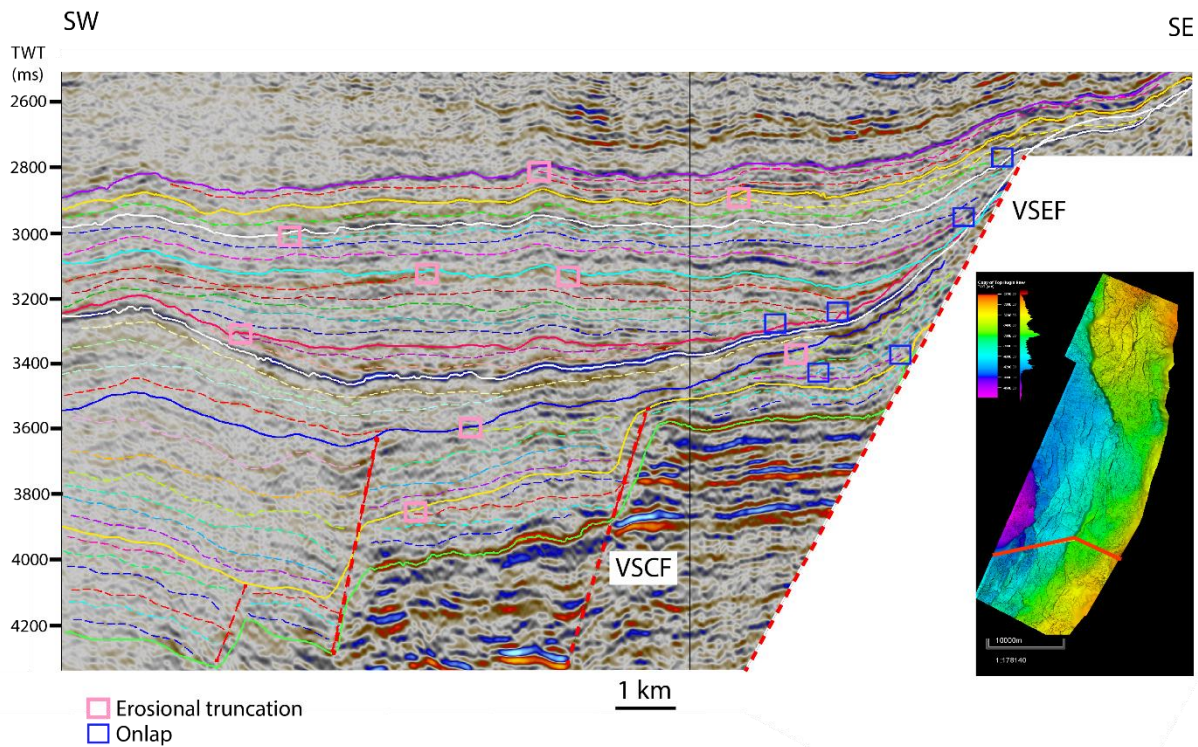


Figure 5.39: Cross-section used for generation of Diagram 3 in this study. Solid lines reflects the surfaces described in chapter 5.1. Stippled lines reflects internal reflectors. The red nearly vertical lines reflects faults. The red, stippled lines illustrates faults. Top Hugin time structure map is used as reference, highlighting the cross-section with the red line, where the black vertical line reflects the bend in the cross-section.

W

E

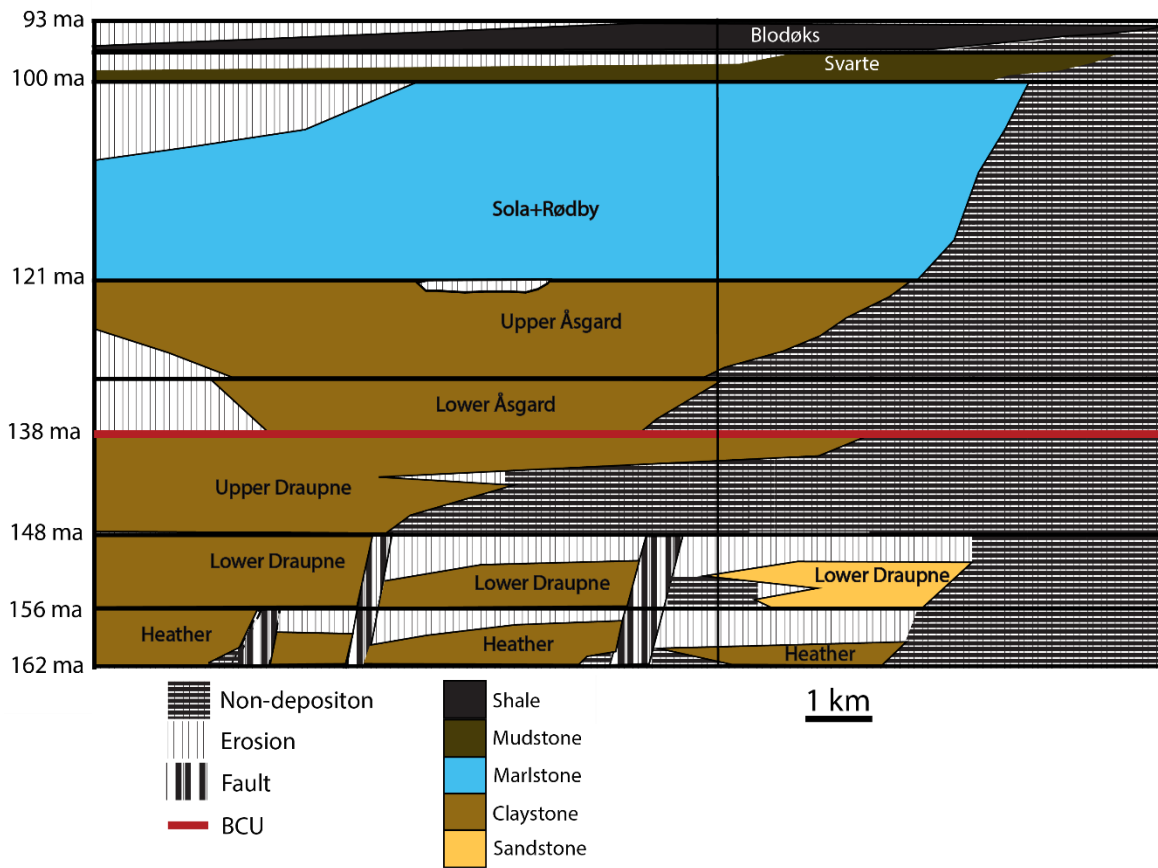


Figure 5.40: Diagram 3. Black, horizontal lines illustrates timelines corresponding to the age of the formation tops used in this study. The colored areas reflects the lateral extension of every formation related to time. The lithologies are highly generalized, where the clay-rich Lower Draupne in the VSEF hanging wall are referred to as a sandstone because of its interbedded sandstones (NPD,2018).

Description

Figure 5.40 illustrates the Wheeler diagram generated from Figure 5.39. The terminating relationship between the individual intervals are laterally visualized in the figure. Three faults are observed southwest of the VSEF in the cross-section (Fig. 5.39). The southwestern fault exhibits offset on the Top Hugin surface, while the two central faults in the cross-section exhibits offset in both the Top Hugin surface and the Top Heather surface. This observation is illustrated in Diagram 3 (Fig. 5.40) as the southwestern fault is only influencing deposits of the Heather interval, while the two central faults has influence on the stratigraphically younger Lower Draupne deposits. A stratigraphically thicker column of preserved Heather and Lower Draupne deposits are observed in the southwestern hanging walls than in the VSEF and VSCF hanging walls. This suggests that

the reflectors of the Heather interval and the Lower Draupne are erosional truncated by the Top Heather- and Internal Draupne surfaces, respectively. This erosional time gap of the youngest Heather- and Lower Draupne deposits is visualized in Diagram 3 (Fig. 5.40). The Lower Draupne package on the VSEF hanging wall, shows a stratigraphically older reflector with further lateral extension than the overlying reflector. This observation suggests a retrogradational relationship between the reflectors. The same relationship is observed in the Upper Draupne interval in a southeasterly direction. The interpreted retrograding reflectors in the Lower Draupne interval are overlain by a reflector of further lateral extension suggesting the retrogradational pattern being followed by a period of progradation (Fig. 5.40). The preserved deposits of the Lower Åsgard interval are concentrated in the depression in central part of the cross-section (Fig. 5.39). The internal reflectors of the Lower Åsgard interval shows a terminating relationship with The BCU- and Internal Åsgard surfaces in a southeasterly and southwesterly direction. Onlapping Lower Cretaceous strata towards the southeast was observed in Diagram 1 and 2, but onlap and toplap towards the southwest was not observed. These terminations are related to the uplift of the stratigraphy, which has been described in 5.1 and 5.2, and is visualized in Fig. 5.40. The youngest preserved reflector of the Upper Åsgard interval is cut by the overlying Top Åsgard surface, suggesting that it was acting as an erosional surface. This cut-off is visualized as an erosional feature along strike of the underlying VSCF (Fig. 5.40). The preserved strata of the Rødby+Sola-, the Svarte-, and the Blodøks interval show onlap on underlying surfaces towards the southeast, and show cut-off of the youngest reflectors towards the southwest. This suggests that the bounding surfaces, Top Rødby, Top Svarte and Top Blodøks were eroding underlying strata. The southwestward erosional time gaps of these intervals are visualized in Fig. 5.40.

6. Discussion

The discussion chapter focuses on the controls on the depositional distribution from the syn-rift to the post-rift stage. This is done by comparing the generated structure- and thickness maps from chapter 5, and discuss the observed trends in an upward stratigraphic succession. Interpretation of generated Wheeler diagrams are used to support the suggested trends from the generated structure- and thickness maps. Conceptual models of deep-marine sedimentary systems and examples from the western flank of the South Viking Graben are used to determine the distribution of Upper Jurassic reservoir rocks in the study area.

6.1 Shift in location of depocentres through time

Figure 5.34 shows every thickness- and structure map generated in this study. The structure maps in the same figure show a general westward deepening trend. This is what we would expect from an area located on the eastern downthrown flank of a rift-basin. The main depocentre in the lowermost interval in this study (Heather Formation) is located in the VSWF hanging wall (Fig. 5.34A). Figure 5.39 covering the southwestern part of the study area, shows that the southwesternmost fault (linked to the VSWF) in the cross-section exhibit displacement of the Top Hugin structure map, but no displacement of the Top Heather structure map is observed. However, the adjacent fault in Figure 5.39 exhibits displacement of the Top Heather structure map. This suggests that the fault growth of the southwestern fault ceased before the cessation of the adjacent fault to the northeast. A consequence of this is that less strata of the Heather interval is preserved on the footwall of the southwestern fault than in the hanging wall. Interpretation of the internal architecture of the Heather interval in Figure 5.39 suggest that the partial absence of Heather deposits on the footwall of the southwestern fault is a result of erosion, visualized in Figure 5.40. The erosional impact on Heather interval deposits on the footwall of the southwesternmost fault (5.40) suggests that later fault growth cessation of faults towards the northeast limits the main depocentre of the Heather interval to the hanging wall of the VSWF and adjacent faults. Based on the subdivision of basin-fill architecture by (Prosser, 1993) (Chapter 2.6) the deposits of the Heather Formation show a geometry that is comparable to the idealized geometry of a rift-initiation basin-fill (Fig. 2.7). Predictions on syn-rift depocentre development from a numerical fault

growth model by Cowie et al. (2000) suggest that the earliest formed syn-rift depocentres should be of limited lateral extent. This theory supports the observed lateral limitations of the Heather Formation depocentre.

A distinct difference between the deeper parts of the Top Hugin surface (Fig. 5.34A*) and the Top Heather surface (Fig. 5.34B*) is that the abrupt deepening of the Top Heather surface is localized further north. This suggests that the VSWF has interacted and linked with adjacent faults within the Heather time interval. Deposits of the Heather interval in the VSCF hanging wall show a prominent thickness variation across the strike of faults (Fig. 5.34A observed in the Top Hugin structure map (Fig. 5.34A*). These thickness variations are not observed in the Lower Draupne thickness map (5.34B). This suggests that the small sub-basins created in the minor fault's hanging walls, in the initiation stage of the rift-event, were filled by deposits of the Heather Formation.

The Heather and Lower Draupne TWTT thickness maps show a distinct thickness of preserved deposits on the proximal terrace area, bounded by VSEF and VSCF. The rift initiation and rift climax stages are characterized with hanging wall subsidence (Prosser, 1993; Gawthorpe & Leeder, 2000). This tectonic effect is presumably the controlling factor on why the Heather and Lower Draupne Formations show a general westward thinning on the proximal terrace. The introduction to chapter 5.2 shows a subdivision of the VSCF into three segments based on displacement versus length, and strike direction. Fault segment boundaries are in many cases characterized by an increased density of small-displacement faults (Jackson & Leeder, 1994; Mack & Seager, 1995; Gawthorpe & Leeder, 2000). The northern and southern segment show a prominently larger displacement versus length than the central segment. This observation and the fact that the northern and the southern segment have different strikes indicates that the southern and northern segment of the VSCF were two different faults, which interacted and became linked in by the central segment. Based on work by Gawthorpe & Leeder (2000) this theory suggests that the fault growth ceased before the through-going fault zone stage (Fig. 2.5). (Fig. 2.5B) by Gawthorpe & Leeder (2000) shows the interaction and linkage stage, where segment A and B are separated by a relay ramp. This illustration can be compared to the VSCF, where the southern and northern segments refers to segment A and B in the figure,

while the central segment of the VSCF refers to the relay ramp. In chapter 5.2.2 the main source of the Lower Draupne interval deposits on the VSCF footwall was interpreted to be located in the east. It was also suggested that the nature of the VSCF was a controlling factor on the distribution of these deposits, as the westerly thinning trend on the terrace was more prominent on the footwall of the high-displacement northern and southern segments of the VSCF. This is supported by the fact that the displacement rate is a proxy for the rate of hanging wall subsidence (Gupta et al. 1998, Cowie et al. 2000). The interpretations from chapter 5.2.2 and the comparison between the nature of the VSCF and the conceptual model of a normal fault array evolution (Fig. 2.5), suggests that the central segment was acting as a route for sediment dispersal of Lower Draupne deposits from the footwall to the hanging wall of the VSCF.

As observed in cross-sections and Wheeler diagrams in chapter 5.3 (Fig. 5.35-5.40) the VSCF and minor faults to the west do not exhibit displacement of the Internal Draupne surface, and the overlying Upper Draupne deposits. This suggests that the fault growth of the VSCF and other visualized faults in chapter 5.3 ceased prior to the onset of the Upper Draupne time interval. Related to the basin fill subdivision by Prosser (1993), a fault growth cessation during the late Lower Draupne time interval or at the onset of the Upper Draupne time interval, suggests that Upper Draupne strata is deposited during the immediate post-rift stage. This is a controversial statement, as the entire Draupne Formation generally is considered as rift climax. Construction of additional Wheeler diagrams in the study area would reveal a more accurate analysis, which could show fault displacement in the interpreted Upper Draupne strata. This would interpret the formation as rift climax. In terms of shift in location of depocentre, the Upper Draupne Formation (Fig. 5.34C) shows a northward depocentre migration from the Lower Draupne Formation (Fig. 5.34B). This suggests that the VSWF hanging wall topography was filled during the Lower Draupne time interval, and that a main depocentre growth is observed. Growth of the depocentre is supported by Cowie et al. (2000) suggesting that with continued extension, early formed depocentres may coalesce with adjacent ones to form enlarged depocentres.

The transition from the Upper Draupne interval (Fig. 5.34C) to the Lower Cretaceous Lower Åsgard interval (Fig. 5.34D) is concomitant with a northeastward migration of the depocentre. As described in chapter 5.2.5 the Lower Åsgard TWTT thickness map (Fig. 5.34D) shows a thinning of the interval in the southwestern edge of the map. The Internal Åsgard TWTT structure map (Fig. 5.34E*) shows a shallowing of the surface in the same area. This suggests that the thinning of the Lower Åsgard interval is a result of uplift in the area. Thomas & Coward (1996) suggest that thin-skinned inversion may have become active in the fault-bounded terrace zones in the eastern South Viking Graben, during Late Volgian-Late Ryazanian. This would possibly generate hanging wall folds with bathymetric expression. Figure 5.39 shows that this hanging wall fold has bathymetric expression for the overlying stratigraphy, which gradually gets less prominent in an upward stratigraphic succession. The suggested theory by Thomas & Coward (1996) fits the observations and interpretations from the Internal Åsgard TWTT structure map, and Lower Åsgard TWTT thickness map and the timing of the event estimated by Thomas & Coward (1996). The fold observed in the southwestern part of Figure 5.39, is presumably a result of this thin-skinned inversion of the VSWF in the study area. The bathymetric expression can also be observed in the Lower Cretaceous TWTT structure maps, where the shallower southwestern area is less prominent from the Internal Åsgard TWTT structure map (Fig. 5.34E*) to the Top Svarte TWTT structure map (Fig. 5.34H*). Observed erosional truncations towards the high in Figure 5.39, suggests that the high was subject to erosion during the time the Åsgard intervals were deposited. This erosional period is visualized in Wheeler diagram 3 (Fig. 5.40).

Figure 5.34 shows that the main depocentre in the Upper Åsgard interval (Fig. 5.34E) has migrated southwards from the Lower Åsgard interval (Fig. 5.34D). The Top Åsgard TWTT structure map (Fig. 5.34F*) shows a shallowing of the surface, which coincides with the location of the Upper Åsgard depocentre. This suggests that the shallowing of the Top Åsgard surface is a result of a significant amount of preserved deposits in this area, rather than a result of uplift. In Figure 5.34F* a north-south trending depression is observed in

between the shallowing area to the west, and the VSEF slope-apron to the east. This indicates that the Upper Åsgard interval was fed from a source in the west.

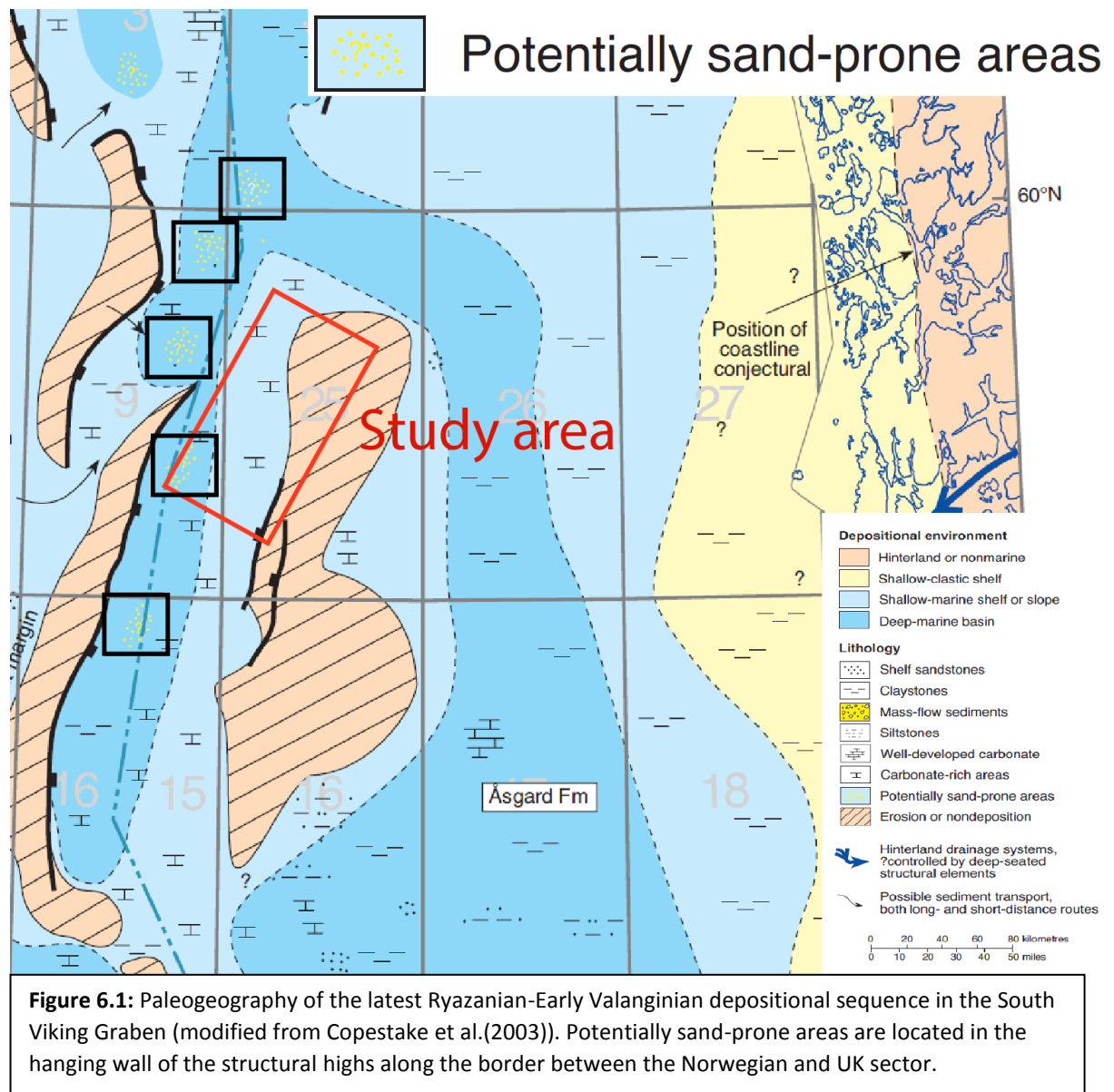


Figure 6.1 shows a paleogeographic map of the South Viking Graben in the latest Ryazanian-Early Valanginian, a period where Åsgard formation deposition was ongoing. The Upper Åsgard TWTT thickness map (Fig. 5.34E) shows a presumably westerly-sourced thickening of the interval. Suggested erosion of structural highs on the western flank of the South Viking Graben, and the highlighted potentially sand-prone areas close to the study area (Fig. 6.1) could be the answer to why the Upper Åsgard TWTT thickness map (Fig. 5.34E) shows a thickening of the interval. Figure 5.39 shows interpreted erosional

truncations, visualized in Figure 5.40, between the Upper Åsgard interval and the overlying Rødby+Sola interval. This is only observed in the main depocentre of the Upper Åsgard interval, suggesting that the Top Åsgard surface was acting as an erosional surface on the shallowing area observed in the central parts of the study area (Fig. 5.34F*).

Wheeler diagram 2 (Fig. 5.38), which covers the northern part of the Rødby+Sola depocentre, shows a large time gap of erosion and non-deposition on the footwall of the underlying VSCF, where Upper Åsgard deposits onlap Upper Draupne deposits towards the southeast. Wheeler diagram 3, covering the southern part of the study area, shows preserved Upper Draupne deposits on the footwall of the underlying VSCF, but similar depositional history. This suggests that the fault-related topography in the VSCF hanging was not filled in before the late Upper Åsgard time interval.

The along VSEF-strike trending depression observed in the Top Åsgard TWTT structure map (Fig. 5.34F*) can not be observed Top Rødby TWTT structure map (Fig. 5.34G*). The location of the depression coincides with the location of the main depocentre of the Rødby+Sola interval (Fig. 5.34F), suggesting that the topography was filled in by Rødby+Sola deposits. The location of the Rødby+Sola depocentre shows an eastward migration from the location of the Upper Åsgard depocentre. The Rødby+Sola depocentre are elongated along strike of the VSEF, covering the deepest part of the Top Åsgard structure map (Fig. 5.34F*). This is the stratigraphically deepest interval depocentre that is located on the VSCF footwall, which supports the interpretation that the fault-related topography in the VSCF hanging wall was filled in by the time the Rødby+Sola interval was deposited.

The Svarte TWTT thickness map (Fig. 5.34G) shows a map with limited lateral thickness variation, and exhibit no concentrated depocentre as the underlying intervals do. The similar bathymetric architecture in the Top Rødby TWTT structure map (5.34G*), and the Top Svarte TWTT structure map (Fig. 5.34H*) reflects the limited lateral thickness variation of the Svarte interval. The Wheeler diagrams (Fig. 5.36, 5.38, 5.40) show that the Top

Svarte surface acts as an erosional surface on the Svarte deposits. The erosion is less prominent towards the west in every diagram. This gradual erosional trend could explain why the Svarte TWTT thickness map (Fig. 5.34G) shows a gradually thickening trend towards the northwest, in a pattern that is similar to the strike of the underlying VSCF. If this is the case, the structural configuration created by VSCF activity was still affecting the distribution of preserved deposits at the stratigraphic level of the Svarte Formation.

The uppermost interval in this study, the Blodøks Formation shows a northward migration of the depocentre in its TWTT thickness map (Fig. 5.34H) from the Rødby+Sola TWTT thickness map (Fig. 5.34F). A similar erosional trend on the Blodøks Formation as on the Svarte Formation is shown in the Wheeler diagrams (Fig. 5.36, 5.38, 5.40), which explains why the depocentre is located in the northeast. The depocentre is continuous and shows a north-south trend across the underlying VSCF. This indicates that the underlying structural configuration has limited to no influence on the preserved Blodøks deposits, as the only interval in this study.

6.2 Reservoir characteristics

Figure 5.11 and 5.13 show RMS-amplitude maps of two surfaces, the Internal Draupne (Fig. 5.11) and an interpreted Top Upper Draupne sandstone surface (Fig. 5.13). In chapters 5.1.10 and 5.1.11 the RMS effects are interpreted to be lithological contrasts, within the clay-rich Draupne formation. The RMS effects observed in the Internal Draupne RMS amplitude map were characterized as relatively straight, and showed a decrease in RMS-value towards the west and towards the south. A sub-division of the RMS effects was done based on variation in lateral extent, RMS-value, and degree of narrowing, visualized in Figure 5.12.

The Top Upper Draupne sst RMS amplitude map shows RMS effects in a sinuous south-trending pattern. This sinuous architecture of the RMS effects, coincides with a thickening area of the Upper Draupne Formation visualized in the Upper Draupne TWTT thickness map (Fig. 5.22). The thickening of the area where the RMS effects is located suggests that the RMS effects are channels or canyons. However, no prominent depression related to the interpreted Top Upper Draupne sandstone surface is observed in cross-section, suggesting that the RMS effects presumably are channels.

The majority of interpreted channels are located in the depression observed on the Upper Jurassic TWTT structure maps (Fig. 5.1-5.4), which by the time of deposition of the Upper Draupne sandstone was partially filled in with Upper Jurassic strata. The updip end of the depression is bounded in the west by an eastward dipping fault, creating a graben structure (Fig. 5.36). In this area the Lower Draupne deposits, reflecting a progradational stacking pattern, are to a larger extent preserved than the Lower Draupne deposits in the downdip end of the depression (Fig. 5.35-5.36). The progradational stacking pattern, suggests input of clastic material down the VSEF fault scarp, which theoretically could be a reservoir. However, no RMS response is observed related to the progradational interval.

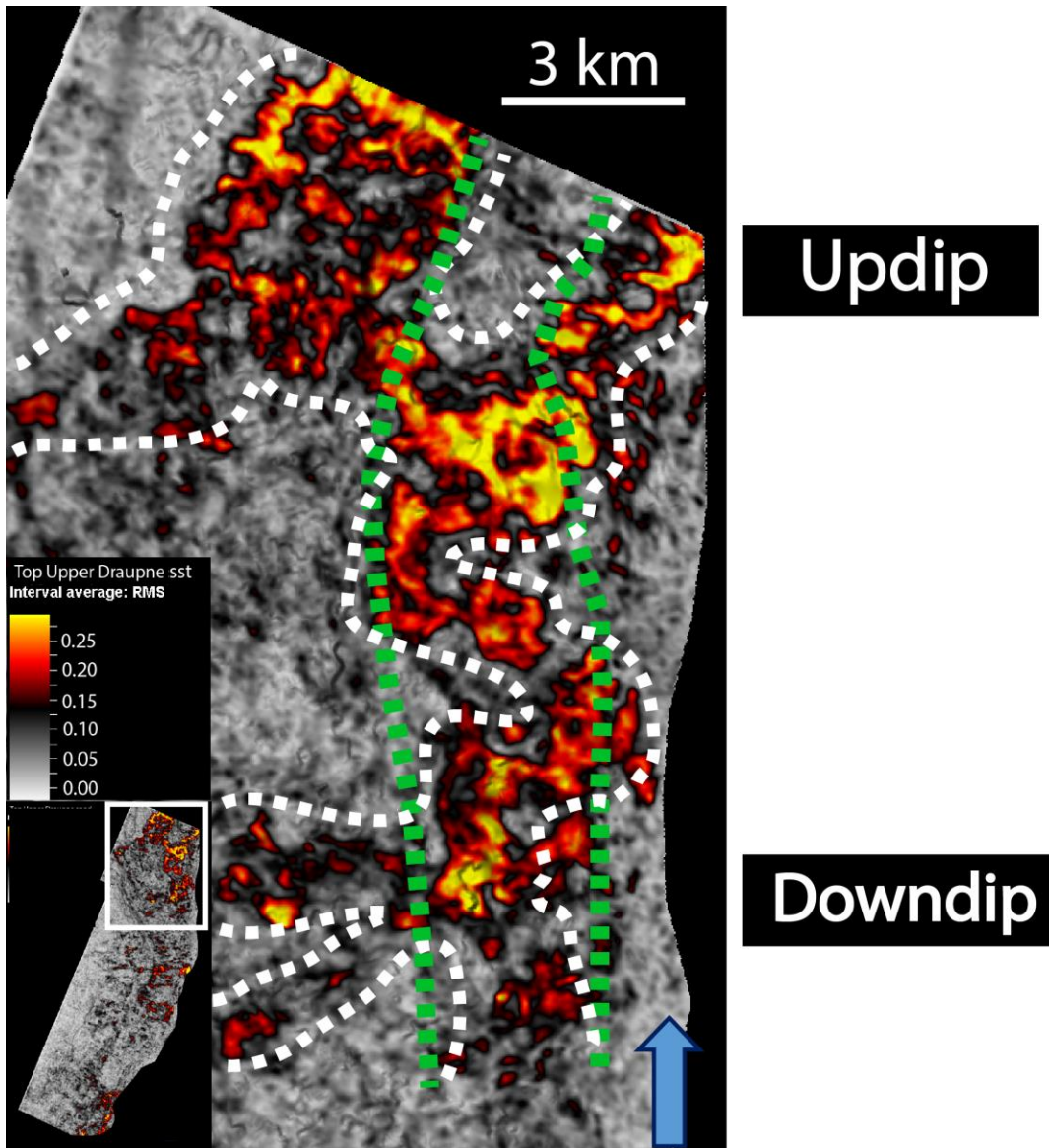


Figure 6.2: RMS-amplitude map of the Upper Draupne channels. Green stippled lines indicate the underlying depression. The depression has its downdip end in the south, and its updip end in the north.

The updip end of the VSEF hanging wall depression (Fig. 6.2) shows a general strong RMS contrast in the central part of the downfaulted area, suggesting that the extent of the channel is topographically controlled. Towards the northern edge of the study area, the depression is shallowing and its bounding faults show larger displacement. In the results a downslope confluence of the channels was mentioned (Chapter 5.1.11). Northwards from this point, the channel-path is not coinciding with the axial part of the depression, but is instead localized in two separate structural highs. The seismic dataset has its northward extent terminating here, making a further northward examination of the channels

impossible. This topographically upward change from a high RMS-contrast in the axial part of the depression to a high RMS-contrast in the bounding structural highs in the updip end suggests that the RMS-contrast in the channels could be a result of presence of hydrocarbons, and not only a lithological contrast. The hydrocarbons would in this case spill into structural highs, which could explain the separation of the RMS-contrast, and the abandonment of RMS-contrast in the axial part of the depression. In this case, the updip end of the depression could act as a leakage point, where the hydrocarbons would leak northwards.

The area of large RMS contrast related to the Internal Draupne surface (Fig. 5.11) was the target of well 25/7-2. The well report characterizes the Upper Jurassic reservoir with very poor reservoir quality, rich in conglomerates (NPD, 2018). The age of the Internal Draupne surface, coincide with the age of the slope-apron fan reservoirs in the UK sector of the South Viking Graben (Early Volgian). Reservoirs rich in conglomerates and the Internal Draupne RMS contrast's lack of sinuosity suggests that the interpreted fairways was active in a high-gradient system, like the gravel-rich slope apron fans depositional system (Mueller, 1968).

Sinuosity features are often related to low-gradient depositional environments (Mueller, 1968), which suggests that the sinuous channels (Fig. 5.14) was active in a low-gradient system. The Top Upper Draupne sandstone is stratigraphically shallower and younger than the Internal Draupne surface. Every basin-floor fan reservoir in the UK sector was deposited later than the slope-apron fan reservoirs (Fraser et al. 2003). The observed sinuosity and the age relationship between the Internal Draupne and the Top Upper Draupne sandstone' surfaces, with respect to comparable age-related reservoirs in the UK sector, suggests that the sinuous channels are developed within a basin floor fan environment. Due to the lack of well control in this area, this hypothesis has a high degree of uncertainty.

7. Conclusion

The aim of this thesis was to understand how a change in tectonic regime from syn-rift to post-rift has implications on the formation of depocentres. This was conducted through interpretation of 3D seismic reflection data. The following sections provides a main conclusion of this study, in addition to providing ideas for further work.

7.1 Main conclusions

The history of shifts in depocentre location through time was established by comparing TWTT structure-, TWTT thickness maps, and Wheeler diagrams. In addition, the distribution of Upper Jurassic reservoir rocks was studied. The main conclusions are:

- The depocentre shift reveals that the tectonic control on sediment dispersal decreases through time
- The central segment of the VSCF was acting as a route for sediment dispersal of Lower Draupne deposits from the footwall to the hanging wall.
- The downthrown VSCF hanging wall topography was not filled in before the deposition of the Mid Aptian-Albian Rødby+Sola formations.
- The Upper Jurassic structural configuration was influencing the sediment distribution until the deposition of the Upper Cenomanian – Lower Turonian Blodøks formation.
- The Upper Jurassic reservoir rocks in the study area are localized in two separate areas, in different stratigraphic levels. They are deposited in two different depositional environments.

References:

- Amosu, A., & Sun, Y. (2017). WheelerLab: An interactive program for sequence stratigraphic analysis of seismic sections, outcrops and well sections and the generation of chronostratigraphic sections and dynamic chronostratigraphic sections. *SoftwareX*, 6, 19-24.
- Branter, S. R. (2003). The East Brae field, blocks 16/03a, 16/03b, UK North Sea. *Geological Society, London, Memoirs*, 20(1), 191-197.
- Brown, A. R., Brown, A. R., Brown, A. R., Géophysicien, E. U., & Brown, A. R. (1996). Interpretation of three-dimensional seismic data.
- Catuneanu, O. (2006). *Principles of sequence stratigraphy*. Elsevier.
- Catuneanu, O., Galloway, W. E., Kendall, C. G. S. C., Miall, A. D., Posamentier, H. W., Strasser, A., & Tucker, M. E. (2011). Sequence stratigraphy: methodology and nomenclature. *Newsletters on stratigraphy*, 44(3), 173-245.
- Cherry, S. T. J. (1993, January). The interaction of structure and sedimentary process controlling deposition of the Upper Jurassic Brae Formation Conglomerate, Block 16/17, North Sea. In *Geological Society, London, Petroleum Geology Conference series* (Vol. 4, No. 1, pp. 387-400). Geological Society of London.
- Copestake, P., Sims, A. P., Crittenden, S., Hamar, G. P., Ineson, J. R., Rose, P. T., & Tringham, M. E. (2003). Lower Cretaceous. *The Millennium Atlas: Petroleum Geology of the Central and Northern North Sea. Geological Society, London*, 191-211.
- Covault, J. A., Normark, W. R., Romans, B. W., & Graham, S. A. (2007). Highstand fans in the California borderland: The overlooked deep-water depositional systems. *Geology*, 35(9), 783-786.
- Coward, M. P. (1995). Structural and tectonic setting of the Permo-Triassic basins of northwest Europe. *Geological Society, London, Special Publications*, 91(1), 7-39.
- Coward, M.P., Dewey, J., Hempton, M., and Holroyd, J., 2003. Tectonic evolution, In: Evans, D., Graham, C., Armour, A., Bathurst, P. (Eds.), *The millenium atlas: petroleum geology of the central and northern North Sea*. Geological Society of London, pp. 17–33.
- Cowie, P. A., Gupta, S., & Dawers, N. H. (2000). Implications of fault array evolution for synrift depocentre development: insights from a numerical fault growth model. *Basin Research*, 12(3-4), 241-261.
- Dawers, N. H., & Underhill, J. R. (2000). The role of fault interaction and linkage in controlling synrift stratigraphic sequences: Late Jurassic, Statfjord East Area, Northern North Sea. *AAPG bulletin*, 84(1), 45-64.
- Emery, D., & Myers, K. J. (1996). Sequence stratigraphy.
- Fisher, M. J., & Mudge, D. C. (1998). Triassic. *Petroleum Geology of the North Sea: Basic Concepts and Recent Advances, Fourth Edition*, 212-244.
- Fletcher, K. J. (2003). The South Brae Field, Blocks 16/07a, 16/07b, UK North Sea. *Geological Society, London, Memoirs*, 20(1), 211-221.

- Fletcher, K. J. (2003). The Central Brae Field, Blocks 16/07a, 16/07b, UK North Sea. *Geological Society, London, Memoirs*, 20(1), 183-190.
- Fraser, S.I., Robinson, A.M., Johnson, H.D., Underhill, J.R., Kadolsky, D.G.A., Connell, R., Johannessen, P. & Ravnås, R. 2003. Upper Jurassic. In: Evans, D., Graham, C., Armour, A. & Bathurst, P. (eds) *The Millennium Atlas: Petroleum Geology of the Central and Northern North Sea*. The Geological Society, London, 157–189
- Færseth, R. B. (1996). Interaction of Permo-Triassic and Jurassic extensional fault-blocks during the development of the northern North Sea. *Journal of the Geological Society*, 153(6), 931-944.
- Gambaro, M., & Donagemma, V. (2003). The T-block fields, block 16/17, UK North Sea. *Geological Society, London, Memoirs*, 20(1), 369-382.
- Garland, C. R. (1993, January). Miller Field: reservoir stratigraphy and its impact on development. In *Geological Society, London, Petroleum Geology Conference series* (Vol. 4, No. 1, pp. 401-414). Geological Society of London.
- Garland, C. R., Haughton, P., King, R. F., & Moulds, T. P. (1999, January). Capturing reservoir heterogeneity in a sand-rich submarine fan, Miller Field. In *Geological Society, London, Petroleum Geology Conference series* (Vol. 5, No. 1, pp. 1199-1208). Geological Society of London.
- Gawthorpe, R. L., and J. M. Hurst, (1993), Transfer zones in extensional basins: their structural style and influence on drainage development and stratigraphy: *Journal of the Geological Society of London*, v. 150, p. 1137–1152.
- Gawthorpe, R. L., Sharp, I., Underhill, J. R., & Gupta, S. (1997). Linked sequence stratigraphic and structural evolution of propagating normal faults. *Geology*, 25(9), 795-798.
- Gawthorpe, R. L., & Leeder, M. R. (2000). Tectono-sedimentary evolution of active extensional basins. *Basin Research*, 12(3-4), 195-218.
- Glennie, K.W. (1990) Outline of the North Sea history and structural framework. In: *Introduction to the Petroleum Geology of the North Sea*, 2nd edn, Ed. by K.W. Glennie), pp. 25-62. Black-well Scientific Publications, Oxford.
- Gupta, S., Cowie, P. A., Dawers, N. H., & Underhill, J. R. (1998). A mechanism to explain rift-basin subsidence and stratigraphic patterns through fault-array evolution. *Geology*, 26(7), 595-598.
- Harris, J. P., & Fowler, R. M. (1987). Enhanced prospectivity of the Mid-Late Jurassic sediments of the south Viking Graben, northern North Sea. *Petroleum geology of north west Europe: London, Graham & Trotman*, 879-898.
- Hodgson, N. A., Farnsworth, J., & Fraser, A. J. (1992). Salt-related tectonics, sedimentation and hydrocarbon plays in the Central Graben, North Sea, UKCS. *Geological Society, London, Special Publications*, 67(1), 31-63.
- Hunt, D., & Tucker, M. E. (1992). Stranded parasequences and the forced regressive wedge systems tract: deposition during base-level fall. *Sedimentary Geology*, 81(1-2), 1-9.
- Isaksen, D. and Tonstad, K. (eds.) 1989: A revised Cretaceous and Tertiary lithostratigraphic nomenclature for the Norwegian North Sea. NPD-Bulletin No. 5, 59 pp.

- Isaksen, G. H., & Ledje, K. H. I. (2001). Source rock quality and hydrocarbon migration pathways within the greater Utsira High area, Viking Graben, Norwegian North Sea. *AAPG bulletin*, 85(5), 861-883.
- Jackson, C., & Larsen, E. (2008). Temporal constraints on basin inversion provided by 3D seismic and well data: a case study from the South Viking Graben, offshore Norway. *Basin Research*, 20(3), 397-417.
- Jackson, C. L., & Larsen, E. (2009). Temporal and spatial development of a gravity-driven normal fault array: Middle–Upper Jurassic, South Viking Graben, northern North Sea. *Journal of Structural Geology*, 31(4), 388-402.
- Jackson, C. A., Kane, K. E., & Larsen, E. (2010). Structural evolution of minibasins on the Utsira High, northern North Sea; implications for Jurassic sediment dispersal and reservoir distribution. *Petroleum Geoscience*, 16(2), 105-120.
- Jackson, J., & Leeder, M. (1994). Drainage systems and the development of normal faults: an example from Pleasant Valley, Nevada. *Journal of Structural Geology*, 16(8), 1041-1059.
- Knott, S. D., Burchell, M. T., Jolley, E. J., & Fraser, A. J. (1993, January). Mesozoic to Cenozoic plate reconstructions of the North Atlantic and hydrocarbon plays of the Atlantic margins. In *Geological Society, London, Petroleum Geology Conference series* (Vol. 4, No. 1, pp. 953-974). Geological Society of London.
- Knott, S. D., Beach, A., Welbon, A. I., & Brockbank, P. J. (1995). Basin inversion in the Gulf of Suez: implications for exploration and development in failed rifts. *Geological Society, London, Special Publications*, 88(1), 59-81.
- Mack, G. H., & Seager, W. R. (1995). Transfer zones in the southern Rio Grande rift. *Journal of the Geological Society*, 152(3), 551-560.
- Mitchum Jr, R. M., Vail, P. R., & Sangree, J. B. (1977). Seismic stratigraphy and global changes of sea level: Part 6. Stratigraphic interpretation of seismic reflection patterns in depositional sequences: Section 2. Application of seismic reflection configuration to stratigraphic interpretation.
- Morley, C. K., R. A. Nelson, T. L. Patton, and S. G. Munn, 1990, Transfer zones in the East African rift system and their relevance to hydrocarbon exploration in rifts: *AAPG Bulletin*, v. 74, p. 1234–1253.
- Mueller, J. E. (1968). An introduction to the hydraulic and topographic sinuosity indexes. *Annals of the Association of American Geographers*, 58(2), 371-385.
- NPD. 2018. NPD Factpages and Factmaps (Online). The Norwegian Petroleum Directorate. Available: www.npd.no (Accessed April 2018).
- Peacock, D. C. P., & Sanderson, D. J. (1994). Geometry and development of relay ramps in normal fault systems. *AAPG bulletin*, 78(2), 147-165.
- Pegrum, R. M., & Ljones, T. E. (1984). 15/9 Gamma gas field offshore Norway, new trap type for North Sea Basin with regional structural implications. *AAPG Bulletin*, 68(7), 874-902.
- Porębski, S. J., & Steel, R. J. (2006). Deltas and sea-level change. *Journal of Sedimentary Research*, 76(3), 390-403.

- Posamentier, H. W., & Allen, G. P. (1999). *Siliciclastic sequence stratigraphy: concepts and applications* (Vol. 7). Tulsa: SEPM (Society for Sedimentary Geology).
- Posamentier, H. W., & Kolla, V. (2003). Seismic geomorphology and stratigraphy of depositional elements in deep-water settings. *Journal of sedimentary research*, 73(3), 367-388.
- Posamentier, H. W., Walker, R. G., (2006). Deep-water turbidites and submarine fans. In: Posamentier, H. W., Walker, R. G. (eds.), *Facies Models Revisited*. Society for Sedimentary Geology (SEPM), Special Publication 84, 397–520.
- Prosser, S. (1993). Rift-related linked depositional systems and their seismic expression. *Geological Society, London, Special Publications*, 71(1), 35-66.
- Ravnås, R., & Steel, R. J. (1997). Contrasting styles of Late Jurassic syn-rift turbidite sedimentation: a comparative study of the Magnus and Oseberg areas, northern North Sea. *Marine and Petroleum Geology*, 14(4), 417-449.
- Ravnås, R., Nøttvedt, A., Steel, R. J., & Windelstad, J. (2000). Syn-rift sedimentary architectures in the Northern North Sea. *Geological Society, London, Special Publications*, 167(1), 133-177.
- Roberts, A. M., Yielding, G., Kuszniir, N. J., Walker, I. M., & Dorn-Lopez, D. (1995). Quantitative analysis of Triassic extension in the northern Viking Graben. *Journal of the Geological Society*, 152(1), 15-26.
- Rooksby, S.K. 2003. The Miller Field, Blocks 16/7B, 16/8B, UK North Sea. In: Gluyas, J.G. & Hitchens, H.M. (eds) United Kingdom Oil and Gas Fields, Commemorative Millennium Volume. Geological Society, London, Memoir, 20, 159–164.
- Schultz, E. H. (1982). The Chronosome and Supersome: terms proposed for low-rank chronostratigraphic units. *Bulletin of Canadian Petroleum Geology*, 30(1), 29-33.
- Sharp, I. R., Gawthorpe, R. L., Underhill, J. R., & Gupta, S. (2000). Fault-propagation folding in extensional settings: Examples of structural style and synrift sedimentary response from the Suez rift, Sinai, Egypt. *Geological Society of America Bulletin*, 112(12), 1877-1899.
- Sheriff, R. E. (1980). Seismic Sequence Analysis: The Implementation. In *Seismic Stratigraphy* (pp. 69-83). Springer, Dordrecht.
- Spence, S., & Kreutz, H. (2003). The Kingfisher field, Block 16/8a, UK North Sea. *Geological Society, London, Memoirs*, 20(1), 305-314.
- Steel, R., & Ryseth, A. (1990). The Triassic—Early Jurassic succession in the northern North Sea: megasequence stratigraphy and intra-Triassic tectonics. *Geological Society, London, Special Publications*, 55(1), 139-168.
- Stow, D. A., Bishop, C. D., & Mills, S. J. (1982). Sedimentology of the Brae Oilfield, North Sea: fan models and controls. *Journal of Petroleum Geology*, 5(2), 129-148.
- Stow, D. A. (1983). Sedimentology of the Brae Oilfield area, North Sea: a reply. *Journal of Petroleum Geology*, 6(1), 103-104.

- Thomas, D. W., & Coward, M. P. (1996). Mesozoic regional tectonics and South Viking Graben formation: evidence for localized thin-skinned detachments during rift development and inversion. *Marine and Petroleum Geology*, 13(2), 149-177.
- Turner, C. C., Cohen, J. M., Connell, E. R., & Cooper, D. M. (1987). A depositional model for the South Brae oilfield. *Petroleum geology of north west Europe*, 14, 853-864.
- Underhill, J. R., & Partington, M. A. (1994). Use of maximum flooding surfaces in determining a regional control on the Intra-Aalenian (Mod-Cimmerian) Sequence boundary: Implications for North Sea Basin development and Exxon's sea-level chart. *Recent advances in siliciclastic sequence stratigraphy*, 58, 449-484.
- Underhill, J. T., & Partington, M. A. (1993, January). Jurassic thermal doming and deflation in the North Sea: implications of the sequence stratigraphic evidence. In *Geological Society, London, Petroleum Geology Conference series* (Vol. 4, No. 1, pp. 337-345). Geological Society of London.
- Vollset, J. and Doré, A. G. (eds.) 1984: A revised Triassic and Jurassic lithostratigraphic nomenclature for the Norwegian North Sea. NPD-Bulletin No. 3, 53 pp.
- Weimer, P., Slatt, R. M., (2007). Petroleum geology of deepwater settings. AAPG Studies in Geology, vol. 57, American Association of Petroleum Geologists, Tulsa, 816 pp.
- Wheeler, H. E. (1958). Time-stratigraphy. *AAPG Bulletin*, 42(5), 1047-1063.
- Ziegler, P. A. (1988). Evolution of the Arctic-North Atlantic and the Western Tethys: A visual presentation of a series of Paleogeographic-Paleotectonic maps. *AAPG memoir*, 43, 164-196.
- Ziegler, P. A. (1990). Geological atlas of western and central Europe. Geological Society of London.